1-1-2013

Development of Degradable Renewable Polymers and Stimuli-Responsive Nanocomposites

Ersan Eyiler

Development of degradable renewable polymers and stimuli-responsive nanocomposites

By

Ersan Eyiler

A Dissertation
Submitted to the Faculty of
Mississippi State University
in Partial Fulfillment of the Requirements
for the Degree of Doctor of Philosophy
in Chemical Engineering
in the Swalm School of Chemical Engineering

Mississippi State, Mississippi

August 2013

Development of degradable renewable polymers and stimuli-responsive nanocomposites

By

Ersan Eyiler

Approved:

Keisha B. Walters Associate Professor and Graduate Coordinator Chemical Engineering (Dissertation Director)	Edwin A. Lewis Professor Chemistry (Committee Member)
Priscilla J. Hill Associate Professor Chemical Engineering (Committee Member)	Hossein Toghiani Associate Professor Chemical Engineering (Committee Member)
Billy B. Elmore Associate Professor Chemical Engineering (Committee Member)	Royce O. Bowden Interim Dean of the Bagley College of Engineering

Name: Ersan Eyiler

Date of Degree: August 17, 2013

Institution: Mississippi State University

Major Field: Chemical Engineering

Major Professor: Dr. Keisha B. Walters

Title of Study: Development of degradable renewable polymers and stimuli-responsive nanocomposites

Pages in Study: 164

Candidate for Degree of Doctor of Philosophy

The overall goal of this research was to explore new living radical polymerization methods and the blending of renewable polymers. Towards this latter goal, polylactic acid (PLA) was blended with a new renewable polymer, poly(trimethylene-malonate) (PTM), with the aim of improving mechanical properties, imparting faster degradation, and examining the relationship between degradation and mechanical properties. Blend films of PLA and PTM with various ratios (5, 10, and 20 wt %) were cast from chloroform. Partially miscible blends exhibited Young's modulus and elongation-to-break values that significantly extend PLA's usefulness. Atomic force microscopy (AFM) data showed that incorporation of 10 wt% PTM into PLA matrix exhibited a Young's modulus of 4.61 GPa, which is significantly higher than that of neat PLA (1.69 GPa). The second part of the bioplastics study involved a one-week hydrolytic degradation study of PTM and another new bioplastic, poly(trimethylene itaconate) (PTI) using DI water (pH 5.4) at room temperature, and the effects of degradation on crystallinity and mechanical properties of these films were examined by differential scanning calorimetry (DSC) and AFM. PTI showed an increase in crystallinity with

degradation, which was attributed to predominately degradation of free amorphous regions. Depending on the crystallinity, the elastic modulus increased at first, and decreased slightly.

Both bulk and surface-tethered stimuli-responsive polymers were studied on amine functionalized magnetite (Fe_3O_4) nanoparticles. Stimuli-responsive polymers studied, including poly(N-isopropylacrylamide) (PNIPAM), poly(2-(dimethylamino)ethyl methacrylate) (PDMAEMA), and poly(itaconic acid) (PIA), were grafted via surface-initiated aqueous atom transfer radical polymerization (SI-ATRP). Both Fourier transform infrared spectroscopy (FTIR) and x-ray photoelectron spectroscopy (XPS) spectroscopies showed the progression of the grafting. The change in particle size as a function of temperature was measured using dynamic light scattering (DLS). Once the PIA was grafted from the Fe_3O_4 nanoparticles for 13 h, the PIA thickness was around 13 nm. After the PNIPAM was grafted for 6 h, the stimuli-responsive nanocomposites with a lower critical solution temperature (LCST) of 32 °C exhibited a particle size of 236 nm. Moreover, a variety of stimuli-responsive bulk block copolymers were synthesized. The stimuli-responsive nanocomposites could be good candidates as drug carriers for the targeted and controllable drug delivery.

DEDICATION

To my angel, my mother, Gulhan Eyiler.

ACKNOWLEDGEMENTS

In general, I would like to thank everyone who I love and who loves me. A special gratitude is owed to my advisor, Dr. Keisha Walters, for all her guidance, support, sleepless nights, and 24/7 effort over the past four years and Dr. Keith Walters.

Over the four years, I have had wonderful friends in our research group, PolySEL, and I would like to thank old and new group members: Mat Rowe, Erick Vasquez, Zach Wynne, Ashley Wynne, Caitlin Naske, Emily Smith, Maryam Dadgarmoghaddam, and Dr. I-Wei Chu. I will never forget the AIChE conference memories and sleepless Swalm nights with my 'buddy' Erick. I also want to thank the undergraduate researchers, especially Jasmine Young and Jack Stogner in our group and the other graduate students in the department. Of course, I want to express gratitude to all Swalm faculty and staff, especially Dr. Elmore for his 'hi', encouragement and endless pizza offers. In addition, I appreciate my committee members, Dr. Edwin Lewis, Dr. Hossein Toghiani, and Dr. Priscilla J. Hill for their time and effort.

Of course, a special 'thank you' to my family and friends, and their help, encouragement, and love are priceless and inexpressible.

Thank you…

TABLE OF CONTENTS

LIST OF TABLES

LIST OF FIGURES

CHAPTER I

INTRODUCTION

This dissertation is comprised of two polymer topics: (1) the blending and degradation of bioplastics and (2) the synthesis of stimuli-responsive polymers (SRPs) in bulk and surface-grafted from magnetic nanoparticles. Each of these topics is presented and discussed separately here and throughout the dissertation. This chapter is dedicated to providing a context for the research efforts presented.

1.1 Properties of renewable bioplastics

Plastics are good substitutes for metal, paper, and glass, if they demonstrate suitable energy savings, weight savings, and/or durability. (Note that 'plastic' is being used here as a layperson's term for polymeric materials.) In recent years, plastics have been by weight the most used material worldwide. In 2010, 31 million tons of plastic waste were generated with only 8.2 wt% being recycled [1]. Traditional plastics have very long degradation times. So the low level of recycling points towards a big environmental problem that needs solutions. This work described efforts towards the development of renewable and/or degradable plastics.

Renewable polymers, known as bioplastics, are biodegradable polymeric materials. In recent years, biodegradable polymers from both renewable resources and petroleum resources have attracted increasing attention. Renewable resources have the

potential to be an alternative of petroleum resources to sustain the development of technology economically and ecologically. A biodegradable polymer obtained from renewable resources, can be called a green polymer. The life cycle of a biodegradable polymer is represented in Figure 1.1.

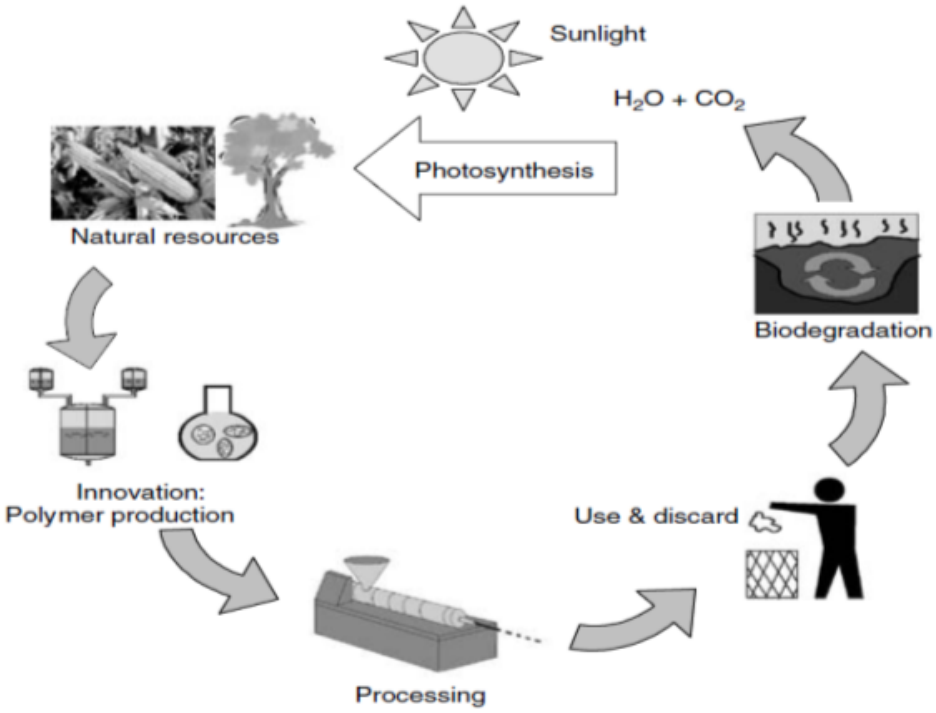

Figure 1.1 Life cycle of biodegradable polymers in the environment [2].

1.1.1 Polylactic acid (PLA)

The most common biodegradable polymer is polylactide (or polylactic acid, PLA), which is a linear aliphatic thermoplastic polyester [2]. Polyhydroxyalkanoates, poly(glycolic acid), polysaccharides, vegetable-derived polymers, and poly(orthester) are other examples of biodegradable polymers [2]. These polymers span a range of

physicochemical properties, cost, and degradation rates, and have the potential to compete with petroleum-based plastics in terms of properties and cost.

1.1.2 Poly(trimethylene malonate) (PTM) and poly(trimethylene itaconate) (PTI)

Biorefineries that produce multiple products, including higher-value chemicals as well as fuels and power, have become significant because this development can help to reduce fossil fuels dependence. For this reason, in 2004, the U.S. Department of Energy (DOE) identified 12 building block chemicals derived from sugars that can serve as key feedstocks for future biorefineries due to their functionality, availability, toxicity, and possible derivatives [3]. These chemicals and their derivatives have the potential to be biomonomers used for production of renewable polymers. These 12 building block chemicals (or chemical groups) are listed in Table 1.1.

Table 1.1 Sugar-derived building block chemicals as determined by the US DOE [3].

1) 1,4 succinic, fumaric, and malic acid	7) 2,5 furan dicarboxylic acid
2) 3-hydroxy propionic acid	8) aspartic acid
3) glucaric acid	9) glutamic acid
4) itaconic acid	10) levulinic acid
5) 3-hydroxybutyrolactone	11) glycerol
6) sorbitol	12) xylitol and arabinitol

In a recent study by Rowe and Walters, several monomers were selected from the DOE 12 building blocks list and used to produce two renewable polymers, or bioplastics [4]. One of these, poly(trimethylene malonate) (PTM), belongs to the Polyhydroxyalkanoates (PHA) family and exhibited the same tendencies to hydrolytically

degrade as seen in other PHAs. PTM was synthesized from 1,3-propane diol and malonic acid to produce a linear copolymer. Hydrolytic degradation of PTM was examined under variable pH conditions. A novel branched/cross-linked, unsaturated polyester was made by the copolymerization of itaconic acid (IA) and 1,3-propanediol (PDO) to make poly(trimethylene itaconate) (PTI). The polymer backbone of PTI contains ester bonds that are susceptible to hydrolysis, but the specific factors that may influence PTI degradation are unknown. In general, molecular weight (Mw) and crystallinity have been shown to have the largest impact on polyester degradation [5]. The degradation in an amorphous polymer could happen quickly since water attacks the weakly-packed segments more easily [5].

1.1.3 Blends of bio-based polymers

Poly(esters) have shown the most promise for commercialization and replacement of petroleum-based polymers, especially with the development of poly(lactic acid) (PLA), poly(glycolic acid) (PGA), and poly(ε-caprolactone) (PCL). In the 1960s and 1970s, PGA was the first bio-compatible and hydrolytically degradable synthetic polymers and was commercialized as a dissolvable suture material [6]. This advance spurred research into other bio-compatible polymers and into other applications for these polymers. However, performance issues, such as poor thermal stability and brittleness, were encountered with PLA and PGA [7]. To overcome the thermal and mechanical short comings of PLA, PGA, and PCL, polymeric blends and copolymers of these with one another and also with other polymers were used to modulate the properties, and have shown varying degrees of success [8-9]. Simoes et al. used PCL with PLA to prepare

blends, and the results showed that PCL behaved as a plasticizer to PLA with a better flexibility and ductility [9].

1.2 Synthesis of stimuli-responsive polymers via ATRP

1.2.1 Living/controlled polymerizations

Modern polymer research and advanced material applications were focused on macromolecular engineering that covers polymers with well-defined compositions, molecular weight, architectures and functionalities [10]. Block, star and graft copolymers are a few examples of these kind of polymers that have a significance role in membrane technology, nanotechnology, drug delivery systems, and thermoplastic elastomers [10].

Numerous polymerization techniques have been used for the production of commercial polymers. Among these techniques, free-radical polymerization is the most widely used process from the viewpoint of industrial production and applications [11]. This technique is easy to apply due to its versatility, and leads to polymers with high molecular weight under mild reaction conditions [10]. However, the main limitations with this technique are the poor control over the molecular weight, molecular weight distribution, end-functionalities and macromolecular architecture. The unavoidable fast radical termination is the main reason for these limitations. Recently, several living/control radical polymerization (CRP) processes have been developed to overcome these limitations. The term of 'living' indicates that a polymerization proceeds without the occurrence of termination [10]. Some well-defined polymers produced by CRPs are represented in Figure 1.2.

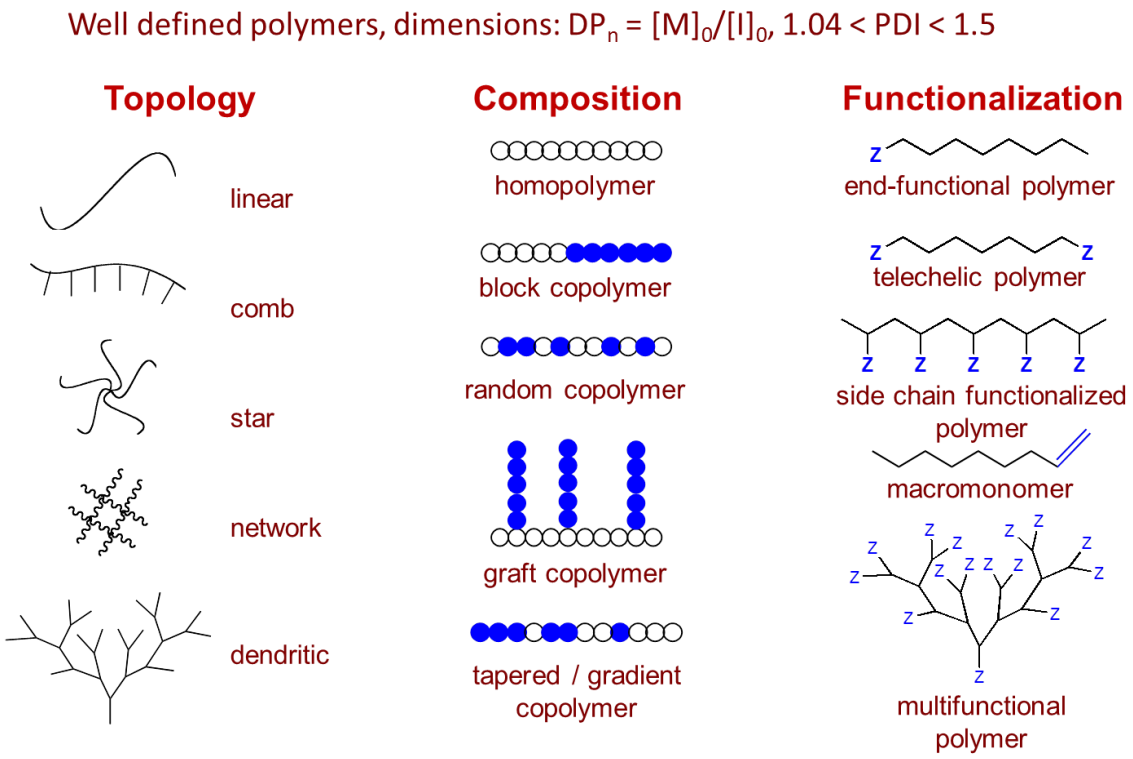

Figure 1.2 Well-defined polymers produced by living/radical polymerization techniques [10].

1.2.2 Atom transfer radical polymerization (ATRP)

Atom transfer radical polymerization (ATRP), reversible addition-fragmentation chain transfer polymerization (RAFT) and single electron transfer (SET-LRP) are just a few examples of types of living radical polymerization (LRP) method. Among these LRP methods, ATRP is the most promising method due to its ability to use a broad range of monomers and its tolerance to solvents and impurities. In addition, ATRP is an excellent robust method to control the uniform and precise chemical composition and architecture of polymers.

1.2.3 Stimuli-responsive polymers

Stimuli-responsive polymers have attracted interest for a few decades. There are many different types of these "smart" polymeric materials, and many have been inspired by nature. The external stimulus can be a change in temperature, pH, salt, light, magnetic field, etc.; however in surveying the literature, only a few types of these have been extensively studied [12-15]. Furthermore, most of the studies of responsive polymers were related to biomedical fields due to the potential for these soft materials to match or mimic the dynamic materials found in living systems. In fact, smart polymeric materials can be designed to adapt their properties in response to conditions and interactions with specific biomacromolecules found in the body, so that they can be used in the applications of drug delivery, diagnostics, sensing, and separations.

Magnetic nanoparticles (MNPs) consisting of cores made of iron oxides, etc. can be controlled and targeted to a specific area using magnetic field. Grafting of a biocompatible polymer from MNPs can provide benefits to MNPs in terms of shielding from the surrounding environment and functionality by attaching carboxyl groups, biotin, avidin, carbodiimide and other molecules [16-18]. When the magnetic nanoparticles are retained at the target area in the body by external magnetic fields, stimuli-responsive polymers can be used to release the drug via external stimuli that can be a change in temperature, pH, etc. [19]. These magnetic nanocomposites have major advantages over the normal, non-targeted drug delivery systems including reduction of the associated side effects and the drug dosage.

1.3 Research objectives

In Chapters 2 and 3, the goal is to investigate of mechanical properties of renewable bioplastics and bioplastic blends. The improvement in the mechanical properties of the bioplastics by blending with other bioplastics and the influence of the hydrolytic degradation on the elastic modulus of the bioplastics in nanoscale by atomic force microscopy (AFM) were examined. Blends of PLA and PTM or PTI prepared via solvent casting have been investigated. The thermal properties were studied as well to determine the miscibility. In addition, in the degradation study of PTM and PTI produced by our group, elastic modulus was monitored as a function of degradation time (100 to 10000 min) in DI water to determine changes.

In Chapters 4-6, the overall goal is to develop stimuli responsive polymers either as bulk polymers or grafted from magnetic nanoparticles using ATRP to provide for well-controlled architectures. The research objectives include the synthesis and characterization of various thermo- and pH-responsive polymers. First, chemical analysis is performed to confirm whether polymerizations are successful or not, and then, the response ability is examined.

In Chapter 4, the synthesis and characterization of homopolymer and block copolymer structures containing N-isopropylacrylamide (NIPAM), 2-(dimethylamino)ethyl methacrylate (DMAEMA), itaconic acid (IA), and/or styrene are described. Chemical, physical, and thermal analyses of the bulk block copolymers by FTIR, DLS, and TGA are discussed. Chapter 5 attempts to summarize the research findings on grafting of pH- and thermoresponsive block copolymers containing itaconic acid (IA) and N-isopropylacrylamide (NIPAM) from iron oxide (Fe_3O_4) magnetic

nanoparticles (MNP) via aqueous SI-ATRP. Analysis of chemical composition, structure, size, thermal behavior and morphology of the modified MNPs by FTIR, XPS, DLS, TGA, and TEM are presented. In Chapter 6, grafting of pH- and thermo-responsive polymers containing N-isopropylacrylamide (NIPAM) and 2-(dimethylamino)ethyl methacrylate (DMAEMA) from iron oxide (Fe_3O_4) magnetic nanoparticles (MNP) via aqueous SI-ATRP are introduced. The thermo-responsiveness of the modified MNPs is shown.

1.4 References

1. *Municipal Solid Waste Generation, Recycling, and Disposal in the United States:Facts and Figures for 2010*; United States Environmental Protection Agency: 2011.

2. Mohanty, A. K.; Misra, M.; Drzal, L. T., *Natural fibers, biopolymers, and biocomposites*. CRC Press: 2005.

3. Werpy, T.; Petersen, G.; Aden, A.; Bozell, J.; Holladay, J.; White, J.; Manheim, A.; Eliot, D.; Lasure, L.; Jones, S. *Top Value Added Chemicals From Biomass. Volume 1-Results of Screening for Potential Candidates From Sugars and Synthesis Gas*; DTIC Document: 2004.

4. Rowe, M. D.; Walters, K. B. In *Synthesis and Characterization of Bioplastics from Polyfunctional Renewable Monomers*, ANTEC - Society of Plastics Engineers (SPE), Chicago, IL, June 22-24; Chicago, IL, **2009**.

5. El-Hadi, A.; Schnabel, R.; Straube, E.; Müller, G.; Henning, S., "Correlation between degree of crystallinity, morphology, glass temperature, mechanical properties and biodegradation of poly (3-hydroxyalkanoate) PHAs and their blends," *Polymer Testing*, **2002**, 21, 665-674.

6. Chu, C., "Hydrolytic degradation of polyglycolic acid: tensile strength and crystallinity study," *Journal of Applied Polymer Science*, **1981**, 26, 1727-1734.

7. Quynh, T. M.; Mitomo, H.; Yoneyama, M.; Hien, N. Q., "Properties of radiation-induced crosslinking stereocomplexes derived from poly (L-lactide) and different poly (D-lactide)," *Polymer Engineering & Science*, **2009**, 49, 970-976.

8. Oyama, H. T.; Tanaka, Y.; Kadosaka, A., "Rapid controlled hydrolytic degradation of poly (l-lactic acid) by blending with poly (aspartic acid-< i> co</i>-l-lactide)," *Polymer Degradation and Stability*, **2009**, 94, 1419-1426.

9. Simões, C. L.; Viana, J. C.; Cunha, A. M., "Mechanical properties of poly(ε-caprolactone) and poly(lactic acid) blends," *Journal of Applied Polymer Science*, **2009**, 112, 345-352.

10. Qiu, J.; Charleux, B.; Matyjaszewski, K., "Controlled/living radical polymerization in aqueous media: homogeneous and heterogeneous systems," *Progress in polymer science*, **2001**, 26, 2083-2134.

11. Moad, G.; Solomon, D. H., *The chemistry of radical polymerization*. Elsevier Science Limited: 2006, 1-9.

12. Jiang, J.; Tong, X.; Morris, D.; Zhao, Y., "Toward photocontrolled release using light-dissociable block copolymer micelles," *Macromolecules*, **2006**, 39, 4633.

13. Dai, S.; Ravi, P.; Tam, K. C., "pH-Responsive polymers: synthesis, properties and applications," *Soft Matter*, **2008**, 4, 435-449.

14. André, X.; Zhang, M.; Müller, A. H. E., "Thermo- and pH-Responsive Micelles of Poly(acrylic acid)-block-Poly(N,N-diethylacrylamide)," *Macromolecular Rapid Communications*, **2005**, 26, 558-563.

15. Wang, D.; Wu, T.; Wan, X.; Wang, X.; Liu, S., "Purely salt-responsive micelle formation and inversion based on a novel schizophrenic sulfobetaine block copolymer: structure and kinetics of micellization," *Langmuir*, **2007**, 23, 11866-11874.

16. Koneracká, M.; Kopčanský, P.; Antalík, M.; Timko, M.; Ramchand, C. N.; Lobo, D.; Mehta, R. V.; Upadhyay, R. V., "Immobilization of proteins and enzymes to fine magnetic particles," *Journal of Magnetism and Magnetic Materials*, **1999**, 201, 427-430.

17. Mehta, R. V.; Upadhyay, R. V.; Charles, S. W.; Ramchand, C. N., "Direct binding of protein to magnetic particles," *Biotechnology Techniques*, **1997**, 11, 493-496.

18. Koneracká, M.; Kopčanský, P.; Timko, M.; Ramchand, C. N.; de Sequeira, A.; Trevan, M., "Direct binding procedure of proteins and enzymes to fine magnetic particles," *Journal of Molecular Catalysis B: Enzymatic*, **2002**, 18, 13-18.

19. Alexiou, C.; Arnold, W.; Klein, R. J.; Parak, F. G.; Hulin, P.; Bergemann, C.; Erhardt, W.; Wagenpfeil, S.; Lubbe, A. S., "Locoregional cancer treatment with magnetic drug targeting," *Cancer Research*, **2000**, 60, 6641-6648.

CHAPTER II

MECHANICAL PROPERTIES OF POLY(LACTIC ACID) AND POLY(TRIMETHYLENE MALONATE) BLENDS

2.1 Abstract

Polytrimethylene malonate (PTM) was synthesized from 1,3-propane diol and malonic acid to produce a linear copolymer. Blend films of poly(lactic acid) (PLA) and PTM were prepared by solvent casting. Differential scanning calorimetry (DSC) and thermogravimetric (TGA) analyses were used to show shifted phase transitions corresponding to PTM content in blend films indicating that the blends were partially miscible. Morphology and mechanical analyses of the PLA/PTM blend films were performed by atomic force microscopy (AFM)-peak force QNM mode. The elastic modulus, adhesion, and roughness maps of the neat PLA and blend films were investigated. With increasing PTM content, the DMT modulus of the blend films unexpectedly increased.

2.2 Introduction

Thermoformability, energy and weight savings, and durability of polymers make them ideal substitutes for metal, paper, and glass. Since 1976 polymers have been by weight the most heavily utilized material globally [1]. But petroleum-based polymers lack the sustainability of renewable plastics. With increased concern for the environment

and the increased cost of petroleum feedstock, 'green' polymers—those developed from biomass-based resources and degradable—are being sought out as alternatives to petroleum-based polymers. Renewable (bio)plastics are produced from biomass-derived monomers, and often can be biologically and/or hydrolytically degraded. Products based on recycled and renewable resources are entering the market as toys, packaging materials, clothing, and other products [1-6].

There are several types of hydrolytically degradable polymers, including poly(anhydrides), poly(orthoesters), poly(depsipeptides), poly(ether esters), and poly(esters), that are currently being researched as replacements for non-hydrolytically degradable petroleum-based polymers [7]. Poly(esters) have shown the most promise for commercialization and replacement of petroleum-based polymers, especially with the development of poly(lactic acid) (PLA), poly(glycolic acid) (PGA), and poly(ε-caprolactone) (PCL). In the 1960s and 1970s, PGA was the first bio-compatible and hydrolytically degradable synthetic polymer and was commercialized initially as a dissolvable suture material [8]. This advance spurred research into other bio-compatible polymers and into other applications for these polymers. However, performance issues, such as poor thermal stability and brittleness, were encountered with PLA and PGA [9-10]. To overcome the thermal and mechanical short comings of PLA, PGA, and PCL, polymeric blends and copolymers of these together and also with other polymers were examined to modulate the properties with varying degrees of success [7, 9-14]. In the past 10 years, interest has increased in bio-based polymer materials—either naturally occurring or synthetic—and their methods of degradation as demonstrated by an order of magnitude increase in publications since 2000.

Poly(trimethylene malonate) (PTM), developed as part of this study, belongs to the PHA family and exhibits the same tendencies to hydrolytically degrade as observed in other PHAs. In this study, 'green' polymer films made from blends of poly(lactic acid) (PLA) and PTM were prepared by solvent casting. Thermal and mechanical properties of these PLA/PTM films were investigated.

2.3 Experimental section

2.3.1 Materials

PLA resin (PLA 4042D) was purchased from NatureWorks LLC. The PLA pellets were translucent with a density of 1.24 g/mL. Malonic acid (MA, 99%) and chloroform (98%) were used as received from VWR. 1,3-Propane diol (PDO, 98%), $AlCl_3$ (98%), and diethyl ether (>99%) were used as received from Sigma-Aldrich. Poly(trimethylene malonate) (PTM) copolymers were synthesized via melt polycondensation as previously described [15].

2.3.2 Methods

2.3.2.1 Copolymerization of PDO-MA

Polymerizations were run in 100 mL round bottom flask at 25 torr. PDO and MA were charged to the reaction flask at a 1:1 molar ratio and a 100:1 monomer to catalyst ($AlCl_3$) ratio. The flask was then immediately placed into an oil bath, and the polymerizations were carried out at 155 °C for 4 h [15].

2.3.2.2 Polymer separation

When the reactions were complete, excess monomer and catalyst were removed by dissolving the reaction product in chloroform. This chloroform solution was then

poured into diethyl ether. The polymer precipitated out of solution and was removed by filtration using Whatman (grade 40) filter paper. This separation process was repeated until no additional polymer precipitated. The filtered polymer was then dried in a vacuum oven at 15 torr and 20 °C for 24 h and weighed.

2.3.2.3 Preparation of blend films

The PLA resin was dried in a convection oven at 80 °C overnight prior to use. PLA and PTM were dissolved separately in chloroform at the concentration of 5% w/w. The solutions were stirred for 12 h at room temperature. PTM was then added to PLA to form final concentrations of 5, 10, and 20% w/w. Each PLA-PTM solution was cast into a glass Petri dish, and a lid was placed on top with one side lifted in order to allow for slow solvent evaporation. The cast films were dried at room temperature for 24 h and then vacuum dried at room temperature for 48 h.

2.3.3 Characterization

2.3.3.1 Thermogravimetric analysis (TGA)

A TA Instruments Q-600 simultaneous DSC/TGA (SDT) was used to characterize the thermal stability of PLA and PLA/PTM blend films with the TA Universal Analysis 2000 software (v4.7A). The 5 mg samples were analyzed from room temperature to 400 °C at a rate of 10 °C/min under a 50 mL/min nitrogen purge.

2.3.3.2 Differential scanning calorimetry (DSC)

A TA Instruments Q-2000 modulated DSC (mDSC) was used for thermal analysis of PLA and PLA/PTM blend films with the TA Universal Analysis 2000 software (v4.7A). The blend film samples weighing 5 mg were first heated from 40 to 200 °C at a

rate of 10 °C/min, and then held for 5 min to eliminate the thermal history. Subsequently, they were cooled to - 50 °C, and heated again from – 90 °C to 200 °C at a rate of 10 °C/min under 50 mL/min of nitrogen purge. The glass transition temperature (T_g), melting temperature (T_m) and melting enthalpy (ΔH_m) of the PLA and PLA/PTM blend films were determined from the exotherms, and the degree of crystallinity (X_m) was calculated with the following equation [16]:

$$X_m\ (\%) = \frac{\Delta H_m - \Delta H_{cc}}{\Delta H_0 * W_f} * 100 \qquad (2.1)$$

where ΔH_m is the melting enthalpy of PLA in the blends, ΔH_{cc} is the cold crystallization enthalpy of PLA, ΔH_0 is the melting enthalpy of the 100 % crystalline PLA, and W_f is the weight fraction of PLA in the blends. For PLA, the 100 % crystalline melting enthalpy was taken to be 93 J/g [16]. The average values of three samples at a minimum are presented.

2.3.3.3 Atomic force microscopy (AFM)

In this study, a new AFM mode called 'PeakForce QNM' was used on a Dimension Icon AFM to map the mechanical properties of the bioplastic blend samples. Using Peak Force Tapping™, damage to the tip and sample can be minimized by directly controlling the forces applied to the tip and using forces lower than those generally used in tapping mode. This better control ensures the tip-sample contact area is as small as possible [17].

During tapping, the AFM generates force curves for each pixel on the sample surface and converts them to the force-separation plots that give some of the major mechanical properties such as elastic modulus, adhesion, dissipation, and deformation.

Figure 2.1 shows the force-separation curve describing the mechanical quantities during a single peak force tapping.

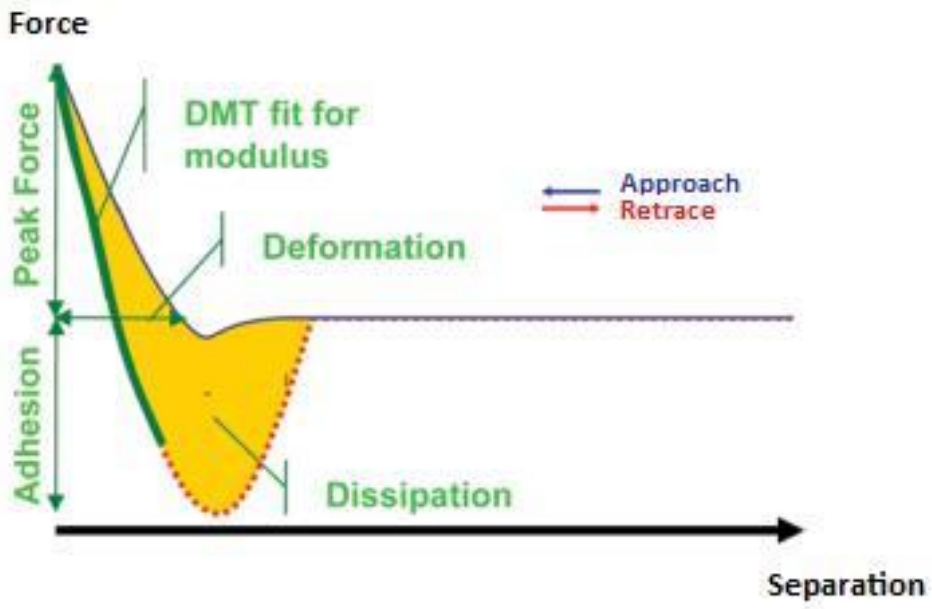

Figure 2.1 Force-separation curve to obtain the mechanical properties of the sample. Figure adapted from [17].

The Derjaguin-Muller-Toporov (DMT) model can be used to fit the retract curve in order to estimate the reduced modulus, E* [17]. The DMT model uses Eqn. 2.2 with the relationship between modulus and forces given as:

$$E^* = \frac{3}{4}(F - F_{adh}) / \sqrt{R(d - d_0)^3} \quad (2.2)$$

where E* is the reduced elastic modulus of the sample, R is the tip radius, ($F-F_{adh}$) is the difference between the relative forces of the tip and adhesion during the tapping, and ($d-d_0$) is the sample deformation. The Young's modulus of the sample (E_s), can be

calculated directly from the reduced modulus by using the known Poisson's ratio of the sample:

$$E^* = \left[\frac{1-\nu_s{}^2}{E_s} + \frac{1-\nu_{tip}^2}{E_{tip}}\right]^{-1} \quad (2.3)$$

where E_s is the Young's modulus of the sample, E_{tip} is the modulus of the tip, and ν_s and ν_{tip} are the Poisson's ratios of the sample and the tip, respectively. Here, the elastic modulus of the tip (E_{tip}) can be assumed infinite [17].

AFM PeakForce Quantitative Nanomechanical (QNM) measurement mode was performed on a Dimension ICON AFM using a RTESPA probe with 10 nm tip radius to map the topography and mechanical properties of the bioplastic blend samples. PLA/PTM blend samples were attached onto the metal AFM pan using adhesive tape. The scanning rate was < 1 Hz and the scan size was 5 x 5 μm (512 x 512 pixels). The peak-force set-point and the Poisson's ratio were set to 3.0 μN and 0.3, respectively. AFM images were analyzed with NanoScope Analysis software (v1.40).

2.3.3.4 Mechanical analysis

Tensile tests were carried out to measure the mechanical properties of the PLA and PLA/PTM blend films. The tests were performed on an Instron 5869 electro-mechanical universal testing machine with a 50 kN load cell in accordance with ASTM D882-10. The rectangular specimen samples (50 x 5 x 0.40 mm) were stored in ambient conditions. A crosshead speed of 6 mm/min and an initial distance between grips of 35 mm were used. The three specimens of each sample were tested, and the average values are presented.

2.3.3.5 Scanning electron microscopy (SEM)

The surfaces of PLA and PLA/PTM blend films were studied by a JEOL JSM-6500F field emission scanning electron microscope (FE-SEM) coupled with energy dispersive spectrometry (EDS) at 15 kV. The films were mounted onto the metal pan using adhesive tape, and then an EMS 150T ES coater was used to sputter the film surfaces with 5 nm of platinum to reduce electrostatic charging.

2.4 Results and discussion

2.4.1 Copolymerization of PDO-MA

Melt polycondensation of PDO-MA was successful using aluminum chloride as the catalyst along with vacuum and stirring under mild reaction conditions. A yield of ~78±5 wt.% was obtained at the reaction conditions of 155 °C and 4 h, but the product had a bimodal Mw of ~1.4 and ~34 kDa. The resulting polymer, polytrimethylene malonate (PTM), is a linear polymer composed of ester and ether backbone bonds. The glass transition temperature, -57 °C, makes it useful for specialty applications or as a plasticizer [15].

2.4.2 Thermal properties

The thermal behavior of the solvent-cast films of PLA, PTM, and PLA/PTM blends was analyzed by DSC, and the data are summarized in Table 2.1. The second heating thermograms are shown in Figure 2.2. Neat amorphous PTM has a glass transition of -57 °C. Neat PLA cast film has a single melting temperature of 140 °C, and a glass transition of 40 °C. A very weak crystallization of the neat PLA was observed, and its crystallization temperature was around 113 °C. A single glass transition

temperature of the blend films can indicate the miscibility of the two polymers. The glass transition temperature of the blends was decreased with addition of PTM into PLA matrix that can be explained with PTM's plasticizer behavior. In Figure 2.2, for PLA/PTM blends, a double peak melting point appeared around 135 °C and 144 °C. The double melting peak can be caused by heterogeneous nucleation effect of a plasticizer indicating two different crystalline structures. The melting temperatures of PLA film were shifted and increased slightly by blending with PTM. Besides, the cold crystallization peak became narrower and decreased by an increase in PTM content, even was bimodal at 20 % of PTM. Such a crystallization change was reported by Pillin et al. and Wu et al. [18, 19]. They observed that there was a strong decrease in crystallization temperature for plasticized PLA.

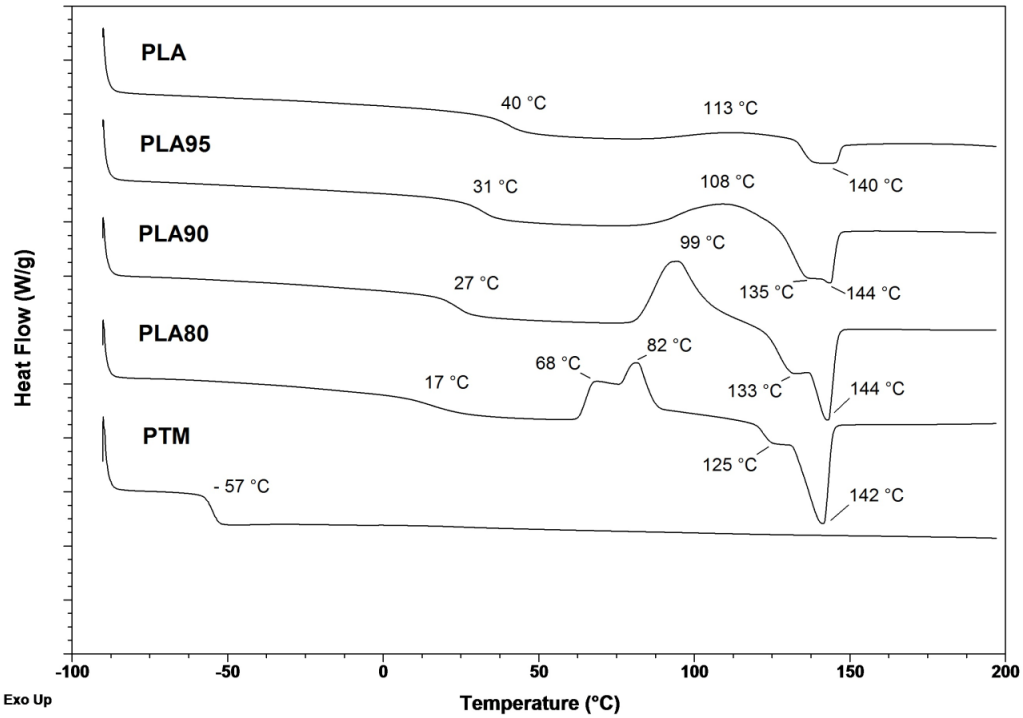

Figure 2.2 DSC thermograms of PLA, PTM and PLA/PTM blend films from the second heating cycle.

Table 2.1 Thermal analysis data of PLA, PTM and PLA/PTM blend films.

PLA Weight Fraction	$T_{5\%}$ (°C)	T_{max} (°C)	T_g (°C)	T_{cc1} (°C)	T_{cc2} (°C)	T_{m1} (°C)	T_{m2} (°C)	ΔH_m (J/g)	ΔH_{cc} (J/g)	X_m (%)	X_{mf} (%)
1.00	332	360	40	113	-	140	-	5.0	3.8	1.3	21.0
0.95	305	346	31	108	-	135	144	17.0	13.2	4.2	19.9
0.90	295	345	27	99	-	133	144	24.5	22.6	2.3	19.6
0.80	276	338	17	68	82	125	142	22.7	17.9	6.6	19.3
0.00	210	340	-57	-	-	-	-	-	-	-	

The degree of crystallinity for PLA and the PLA/PTM blends was determined using Eqn. 2.1 and are listed in Table 2.1. The melting enthalpy (ΔH_m) from the second heating cycle was used to find the crystallinity of each sample. The degree of crystallinity

(X_m) was 1.3 % for neat PLA and 4.2 % for a PLA/PTM blend with 5 wt% of PTM. The degree of crystallinity of cast PLA film increased with increasing PTM content. This may indicate that PTM serves as a nucleating agent. The findings of DSC analysis that PTM has simultaneously served as a plasticizer and a nucleating agent of PLA, may be related to the bimodal Mw distribution observed in the PTM sample. The degree of crystallinity (X_{mf}) was also calculated from the first heating cycle. It showed higher values than that from the second heating and decreased slightly with PTM addition.

Thermal stability of solution cast PLA and PLA/PTM blend films was investigated by TGA. In Table 2.1, the temperature where 5% weight loss is attained ($T_{5\%}$) and the maximum working temperature where 50 wt.% loss occurs (T_{max}) are both listed for each sample. Thermal stability of PLA/PTM blends cast from chloroform was found to be lower than that of PLA. Thermal degradation temperatures of $T_{5\%}$ and T_{max} for neat PLA films were 332 °C and 360 °C, respectively, and were similar to those of PLA resin. It seemed that thermal stability of neat PLA was not affected by the solvent casting process.

2.4.3 Nanomechanical properties

In this study, nanomechanical properties of neat PLA and PLA/PTM blends were investigated by atomic force microscopy (AFM) PeakForce QNM. By AFM, both qualitative and quantitative topographical and nanomechanical information can be obtained. Figure 2.3 shows height (topography) maps of the neat PLA and PLA/PTM blends. The crystalline structure of neat PLA is observed in Figure 2.3; the crystalline phase is brighter, and the amorphous phase is darker. In PLA/PTM blend films, the crystalline structure became less apparent as the ratio of PTM increased. PTM addition to

the PLA matrix also made the blend film surfaces rougher. The average AFM RMS roughness value for neat PLA film was 2.34±1.09 nm, and then it increased with PTM addition to 9.20±3.99 nm at 5%, 31.08±9.76 nm at 10%, and 33.45±8.53 nm at 20%, respectively. At 20 wt.% PTM, the PLA/PTM blend film had a maximum height of 206 nm. In addition to increased roughness, the addition of PTM resulted in higher adhesion in the blend films, as confirmed by AFM. The mean adhesion force increased significantly from 2.67 nN for neat PLA to 51.9 nN for PLA blended with 20 wt% PTM.

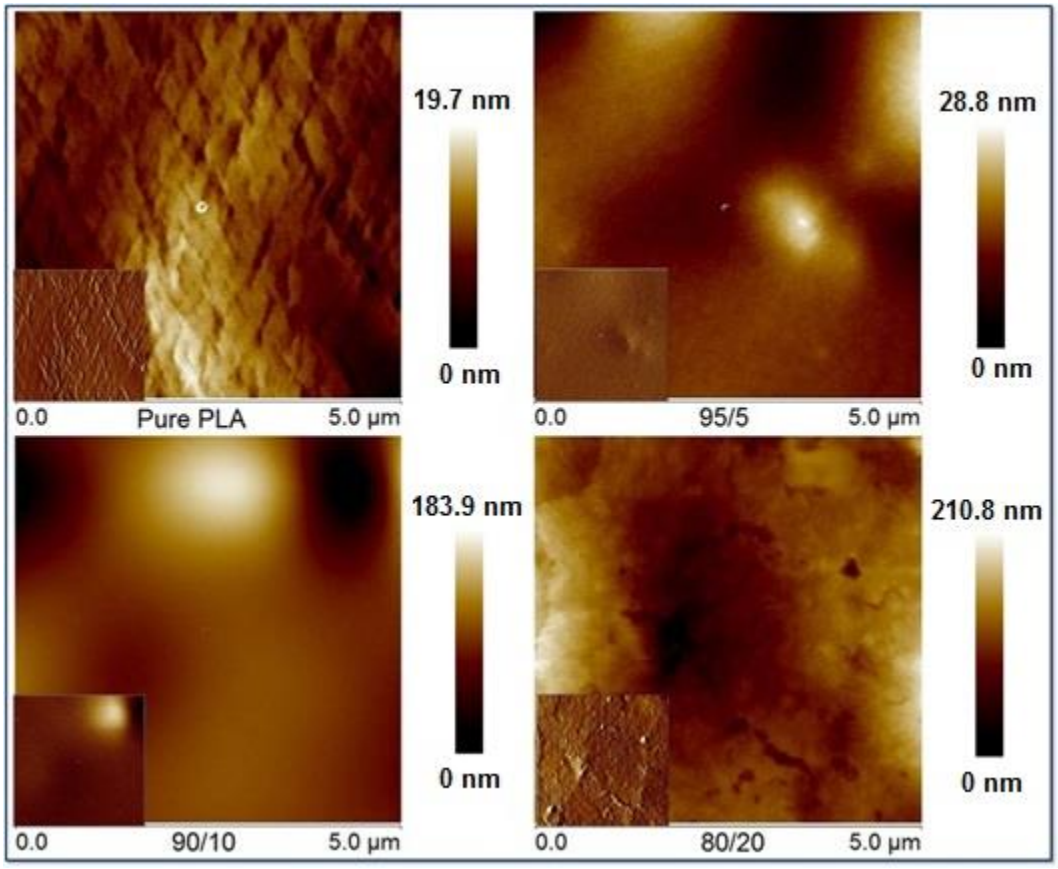

Figure 2.3 Topographical AFM maps (5×5 μm^2) of neat PLA and PLA/PTM blends with z-axis (height) scales. The insets are peak force error images, which are the force signal error at each pixel location, and show rapid changes in surface morphology. With increasing PTM content, the crystallinity decreased and the roughness increased.

Peak Force QNM-DMT modulus maps (5×5 μm^2) of the neat PLA and PLA/PTM cast blend films are shown in Figure 2.4. The tensile modulus of extruded neat PLA films provided by NatureWorks was 3.3 GPa [20]. In this work, average DMT modulus of the neat PLA films was measured to be 2.5 GPa +/- 0.7 GPa. High modulus areas with lighter colors are visible in the PLA crystalline structure while the darker areas are representative of low modulus of amorphous phase. The 95/5 PLA/PTM blend (with 5 wt % PTM) is similar to the neat PLA, and has a smooth surface with a uniform modulus. As the amount of PTM was increased from 5 to 10 wt %, dark, low modulus areas can be seen in the PLA matrix. The regions are shaped from ovoids to a linear "tiger paw" stripes and have a very low modulus of 47 MPa indicating only PTM (or empty voids) is present. The light areas with a modulus of approximately 8.05 GPa are much harder than the neat PLA surface, and this may be ascribed to the higher number of ester bonds in the blends. The modulus maps of the 80/20 PLA/PTM blend films (with PTM content of 20 wt%) is similar to that obtained for the blend with 10 wt% PTM. The PTM domains are a significant portion of the surface and lower the average DMT modulus to 5.54 GPa (Table 2.2). AFM-Peak Force QNM analysis was also performed on PLA/PTM blend films at 90 °C to investigate the impact of elevated temperature on modulus. The results show that the moduli of all blends are significantly lower at 90 °C versus room temperature decrease (Table 2.2).

Table 2.2 Average elastic modulus (E) of PLA, PTM and PLA/PTM blend films (5×5 μm^2).

PLA Weight Fraction	DMT Modulus (GPa) at 25 °C	DMT Modulus (GPa) at 90 °C
1.00	2.52±0.24	-
0.95	2.89±0.48	1.27±0.02
0.90	7.21±0.37	1.31±0.04
0.80	4.09±0.56	1.50±0.38
0.00	0.007	-

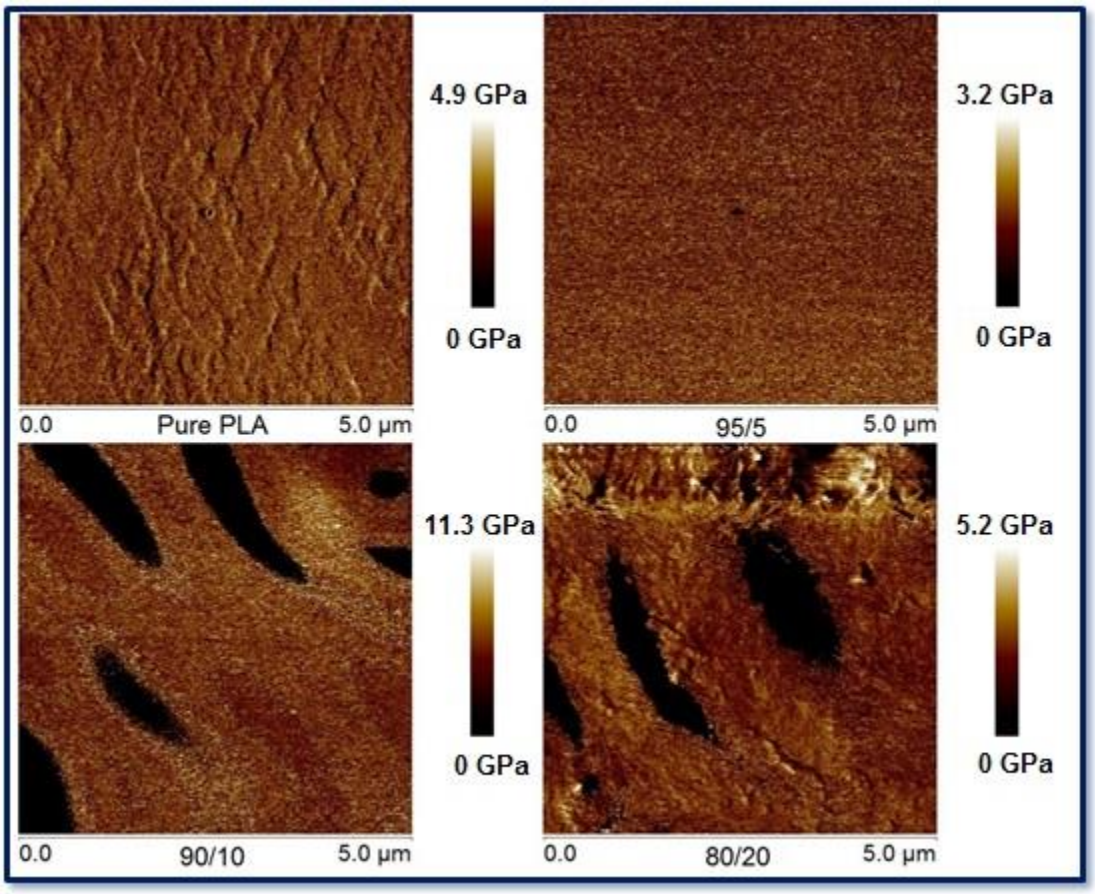

Figure 2.4 AFM DMT modulus maps (5×5 μm^2) of neat PLA and PLA/PTM blends.

2.4.4 Tensile properties

After the AFM study, the macro-scale mechanical properties of PLA and PLA/PTM blend films were studied to investigate the effect of PTM on the tensile strength, strain at break, and Young's modulus. Results are shown in Figure 2.5 and Table 2.3. Table 2.3 shows that PLA/PTM blend films have a significant increase in Young's modulus and tensile strength than that of neat PLA films. The largest Young's modulus measured for this set of PLA/PTM films was with the incorporation of 10 wt. % PTM. Because of the phase separation observed, the Young's modulus decreased by 36 % as PTM content was increased from 10 to 20 wt%. Therefore, the Young's modulus results are correlated with the miscibility of PLA and PTM. Another important mechanical property, strain at break, can be observed in the stress-strain curves (Figure 2.5). Strain at break increased with the increase of the PTM wt% in the blends, and 5 wt% was found to be the optimum level that gave the strain at break of 107.69 % which was about 7-fold of the neat PLA films. So, incorporation of PTM into PLA at leveled below 20 wt. % increased key mechanical properties; however, at a 20 wt. % loading of PTM, the PTM phase segregation starts to cause negative impacts.

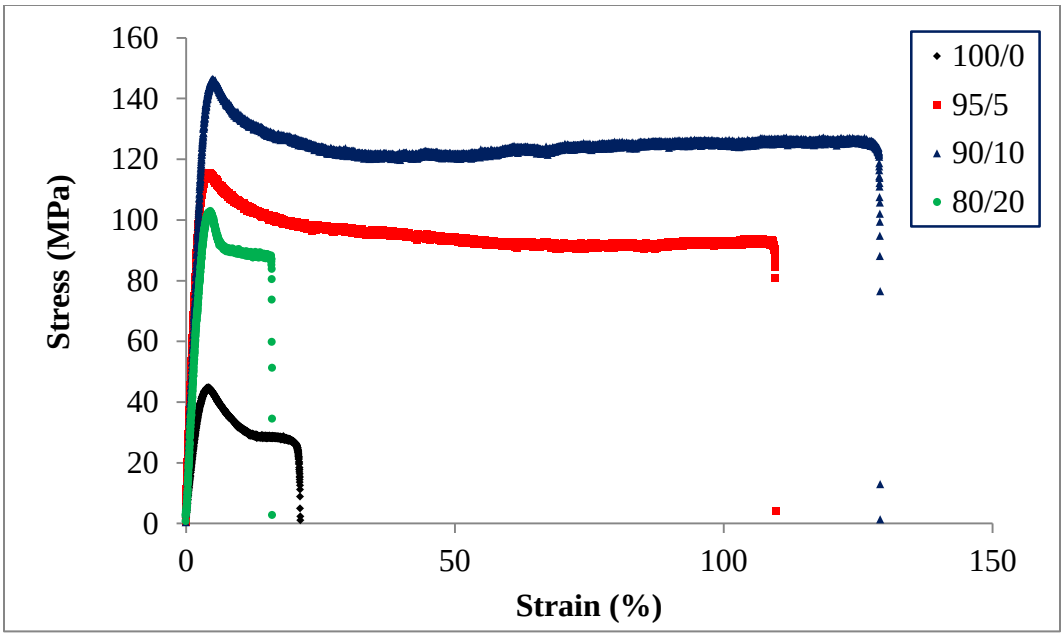

Figure 2.5 Stress-strain curves of PLA and PLA/PTM blend films.

Incorporation of PTM also increased the tensile strength and showed the same trend as was observed for the Young's modulus values. A maximum average value of 105.61 MPa was obtained at 10 wt% PTM. This is highly notable, as PTM is a soft and waxy amorphous linear copolymer with an elastic modulus of around 7 MPa. It was anticipated that PTM would behave as a plasticizer for PLA, and reduce PLA's Young's modulus but increase its strain at break. However, incorporation of PTM into the PLA matrix improved PLA's mechanical properties until a miscibility/solubility limit was reached.

Table 2.3 Summary of the mechanical properties of PLA and PLA/PTM blend films.

PLA Weight Fraction	Tensile Strength (MPa)	Strain at Break (%)	Young's modulus (GPa)
1.00	21.20±8.74	15.59±4.69	1.69±0.60
0.95	83.24±8.48	107.69±6.42	4.01±0.12
0.90	105.61±19.76	81.49±16.53	4.61±0.72
0.80	71.79±23.27	13.37±2.75	2.96±0.90

2.4.5 Scanning electron microscopy (SEM)

The 'as cast' surfaces of the neat PLA and PLA/PTM blend films were observed with SEM (Figure 2.6) that looks at these samples at a different length scale than the AFM images. The neat PLA surface was smooth. Incorporation of PTM into the PLA resulted in apparent empty voids on the surfaces of all blend films that was also confirmed by EDS. The well-dispersed PTM in the blend films with 5 and 10 wt % PTM seemed to confirm the partial miscibility of the two bioplastics as mentioned in AFM study. The diameter of the empty voids in PLA/PTM blends became larger with increasing PTM bulk content from 10 to 20 wt %. It can be clarified with the gas permeability of PTM during the slow drying.

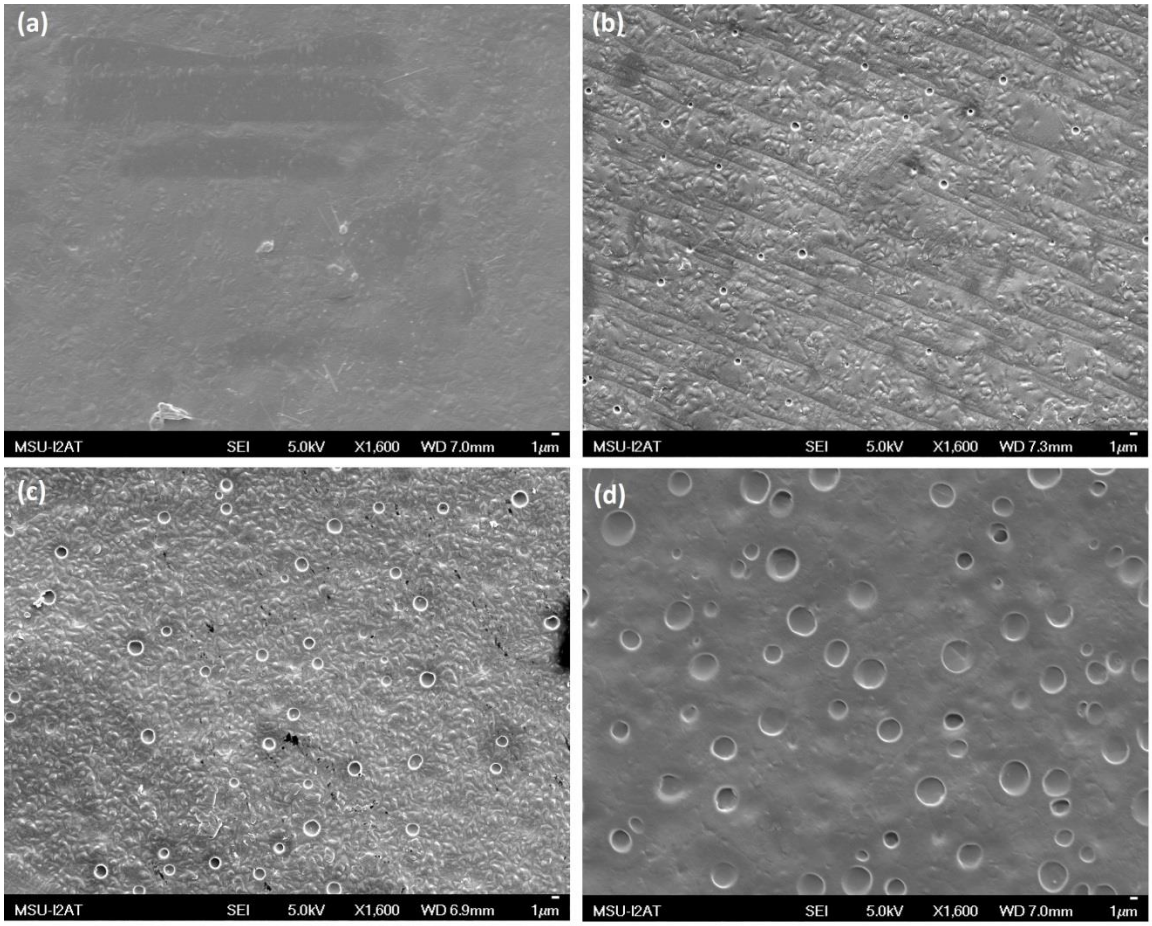

Figure 2.6 SEM micrographs of the surfaces of solution cast (a) PLA, (b) 95/5 PLA/PTM blend, (c) 90/10 PLA/PTM blend, and (d) 80/20 PLA/PTM blend films.

SEM was also used to analyze the fracture surface morphology of the tensile specimens. Figure 2.7 shows the surface micrographs of neat PLA and PLA/PTM blends. A typical tensile fracture surface of PLA is shown in Figure 2.7a, which had straight cracks indicating brittle fracture of PLA [21]. Incorporation of 5 wt % PTM into PLA significantly influenced the morphology and removed the cracks as shown in Figure 2.7b. The smooth fractured surface confirmed the miscible nature of PLA and PTM and the plasticization behavior of PTM. The increase in elasticity was shown before in the AFM

section. In the micrographs of the blends with 10 wt % and 20 wt % PTM, defect cavities were observed with different sizes depending PTM ratio. The presence of these empty microvoids may be caused by debonding and/or gas bubbles during the slow drying. These microvoids can cause high tensile strength by consuming more energy during the fracture [22] as seen in tensile study.

Figure 2.8(a-d) shows SEM micrographs of the tensile fractured side surfaces. A number of small cleavage planes are observed in Figure 2.8a, corresponding a brittle failure. In Figure 2.8(b-c), there were no separate domains of PLA and PTM with spherical shape, which indicates the morphology of miscible polymer blends. The micrograph of the blend with 20 wt % PTM (Figure 2.8d) revealed huge cavitation caused by debonding. Therefore, the low ratio of PTM in the blend is better for the dispersion of PTM in the PLA matrix and avoids the forming of empty voids and phase separation. These results were consistent with the AFM and tensile data.

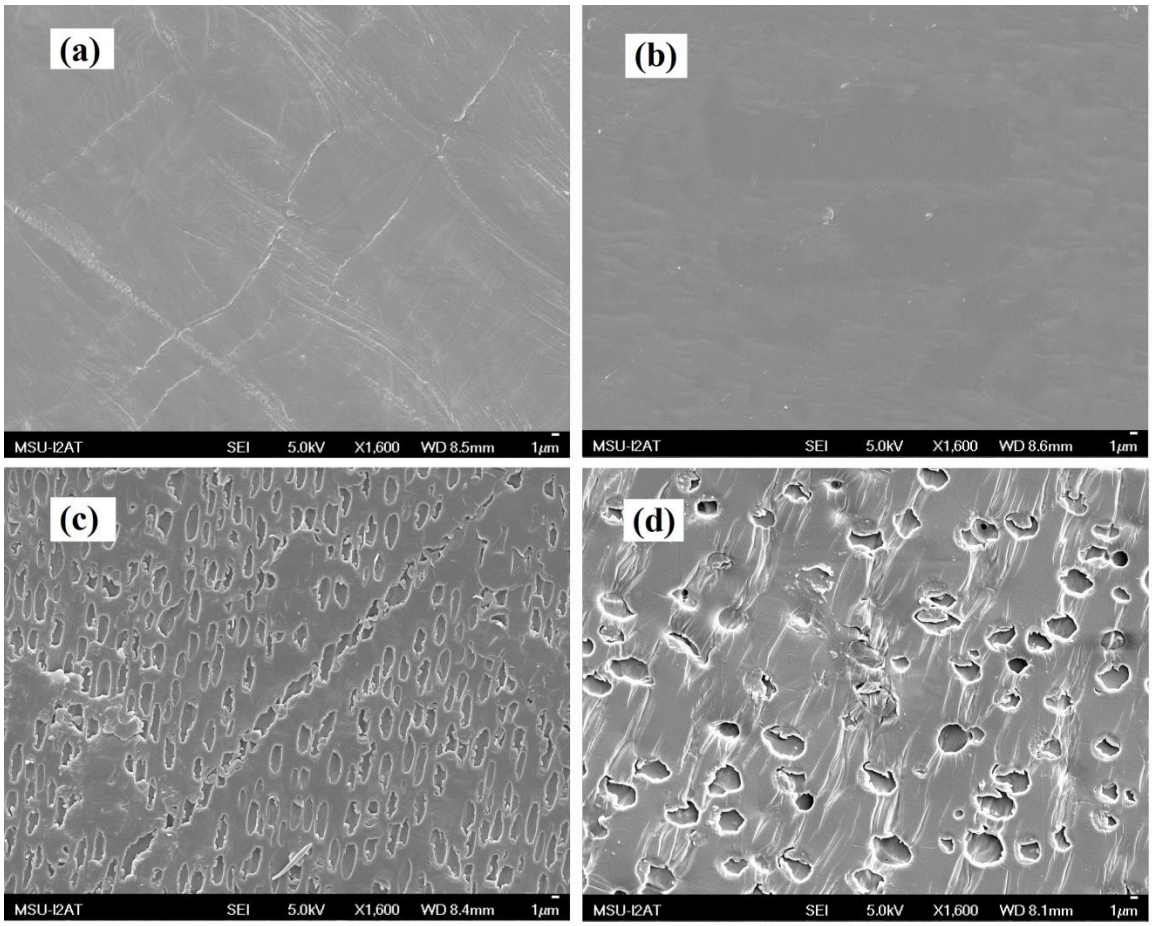

Figure 2.7 SEM micrographs (x1600) of the fracture top surface of tensile specimens of (a) PLA, (b) 95/5 PLA/PTM blend, (c) 90/10 PLA/PTM blend, and (d) 80/20 PLA/PTM blend films.

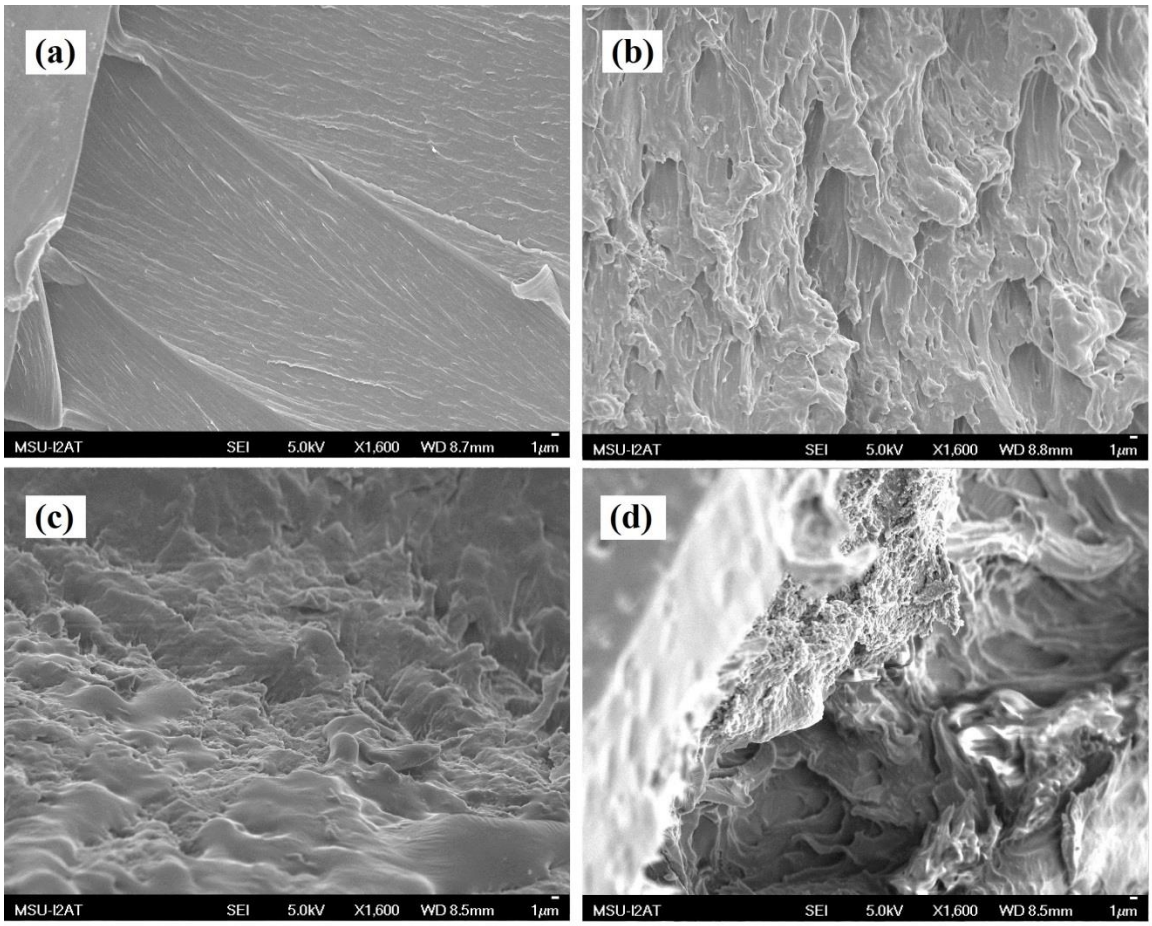

Figure 2.8 SEM micrographs (x1600) of the fracture side surface of tensile specimens of (a) PLA, (b) 95/5 PLA/PTM blend, (c) 90/10 PLA/PTM blend, and (d) 80/20 PLA/PTM blend films.

2.5 Conclusions

PLA and PLA/PTM 'green' blend films were prepared by the solvent-casting method from chloroform. Thermal properties of the blend films were investigated by DSC and TGA. In addition to standard AFM scanning, Peak Force QNM was used to map the morphology and nanomechanical properties. The addition of PTM increased the degree of crystallinity for the blends. The shifting of the melting temperatures of PLA film by blending with PTM and single glass transition temperature for the blends indicate

that the two biodegradable polymers were partially miscible. Addition of PTM gave the blends higher modulus and adhesion than neat PLA films. Phase separation occurred in the blends with PTM content of 10 wt% and 20 wt%, and at 20 wt%, the Young's modulus decreased significantly, but was still higher than neat PLA. These biopolymer blends give promising mechanical properties, and can be used in biomedical, food, and specialty packaging applications due to their anticipated biocompatibility.

2.6 Acknowledgements

A portion of this work was performed through the Sustainable Energy Research Center at Mississippi State University (MSU) and supported by the US Department of Energy under award number DE-FG3606GO86025. We are grateful to the MSU Bagley College of Engineering Ph.D. Fellowship program and The Republic of Turkey's Ministry of National Education for financial support. Thermal characterization and atomic force microscopy instrumentation was available for this effort through support of the National Science Foundation [CBET-0933493 and CBET-0923474]. The authors gratefully acknowledge the fruitful research discussion and equipment access with Drs. Hossein Toghiani and Judy Schneider. AFM and SEM work was performed by Dr. I-Wei Chu at MSU's I2AT (Institute for Imaging & Analytical Technologies).

2.7 References

1. Mapleston, P., "New Technologies for a greener industry Industry," *Plastics engineering*, **2008**, 64, 10-15.

2. Stewart, R., "Going Green: Eco-Friendly Materials and Recycling on Growth Paths," *Plastic Engineering*, **2008**, 64, 17-23.

3. Robinson, G., "Biofocals," *Waste Management World*, **2007**, 77-83.

4. Pandey, J. K.; Ahn, S.; Lee, C. S.; Mohanty, A. K.; Misra, M., "Recent advances in the application of natural fiber based composites," *Macromolecular Materials and Engineering*, **2010**, 295, 975-989.

5. Inman, H., "Who Said Potato? Starch-based thermoplastics," *Plastics engineering*, **2010**, 66, 42-44.

6. Keshavarz, T.,; Roy, I., "Polyhydroxyalkanoates: bioplastics with a green agenda," *Current opinion in microbiology*, **2010**, 13, 321-326.

7. Neffe, A. T.; Tronci, G.; Alteheld, A.; Lendlein, A., "Controlled Change of Mechanical Properties during Hydrolytic Degradation of Polyester Urethane Networks," *Macromolecular Chemistry and Physics*, **2010**, 211, 182-194.

8. Chu, C. C., "Hydrolytic Degradation of Polyglycolic Acid: Tensile Strength and Crystallinity Study," *Journal of Applied Polymer Science*, **1981**, 26, 1727-1734.

9. Quynh, T. M.; Mitomo, H.; Yoneyama, M.; Hien, N. Q., "Properties of Radiation-Induced Crosslinking Stereocomplexes Derived from Poly(L-Lactide) and Different Poly(D-Lactide)," *Polymer Engineering and Science*, **2009**, 49, 970-976.

10. Shirahase, T.; Komatsu, Y.; Tominaga, Y.; Asai, S.; Sumita, M., "Miscibility and Hydrolytic Degradation in Alkaline Solution of Poly(L-Lactide) and Poly(Methyl Methacrylate) blends," *Polymer*, **2006**, 47, 4829-4844.

11. Catiker, E.; Gumusderelioglu, M.; Guner, A., "Degradation of PLA, PLGA homo- and Copolymers in the Presence of Serum Albumin: A Spectroscopic Investigation," *Polymer International*, **2000**, 49, 728-734.

12. Hill, S. P.; de Oca, H. M.; Klein, P. G.; Ward, I. M.; Rose, J.; Farrar, D., "Dynamic Mechanical Studies of Hydrolytic Degradation in Isotropic and Oriented Maxon B," *Biomaterials*, **2006**, 27, 3168-3177.

13. Hoglund, A.; Odelius, K.; Hakkarainen, M.; Albertsson, A.-C., "Controllable Degradation Product Migration from Cross-Linked Biomedical Polyester-Ethers through Predetermined Alterations in Copolymer Composition," *Biomacromolecules*, **2007**, 8, 2025-2032.

14. Oyama, H. T.; Tanaka, Y.; Kadosaka, A., "Rapid Controlled Hydrolytic Degradation of Poly(L-Lactic Acid) by Blending with Poly(Aspartic Acid-co-L-Lactide)," *Polymer Degradation and Stability*, **2009**, 94, 1419-1426.

15. Rowe, M.D.; Walters, K.B. "Synthesis and Characterization of Bioplastics from Polyfunctional Renewable Monomers," Proceedings of ANTEC – Society of Plastics Engineers (SPE), Chicago, IL, June 22-24, 2009, 67, 508-512.

16. Simoes, C.; Viana, J.; Cunha, A., "Mechanical properties of poly (ε-caprolactone) and poly (lactic acid) blends," *Journal of Applied Polymer Science*, **2009**, 112, 345-352.

17. Pittenger, B.; Erina, N.; Su, C., "Quantitative mechanical property mapping at the nanoscale with PeakForce QNM," *Application Note Veeco Instruments Inc*, **2010**.

18. Pillin, I.; Montrelay, N.; Grohens, Y., "Thermo-mechanical characterization of plasticized PLA: Is the miscibility the only significant factor?," *Polymer* **2006,** 47, 4676-4682.

19. Wu, W.; Tian, H.; Xiang, A., "Influence of Polyol Plasticizers on the Properties of Polyvinyl Alcohol Films Fabricated by Melt Processing," *Journal of Polymers and the Environment*, **2012**, 20, 63-69.

20. NatureWorks LLC, "Technical data sheet of NatureWorks® PLA polymer 4042D," www.natureworksllc.com, accessed 03/05/2012.

21. Todo, M.; Takayama, T., "Improvement of mechanical properties of Poly (l-lactic acid) by blending of lysine triisocyanate," *J Mater Sci*, **2007**, 42, 4712-4715.

22. Prolongo, S. G.; Campo, M.; Gude, M. R.; Chaos-Morán, R.; Ureña, A., "Thermo-physical characterisation of epoxy resin reinforced by amino-functionalized carbon nanofibers," *Composites Science and Technology*, **2009**, 69, 349-357.

CHAPTER III

EFFECTS OF HYDROLYTIC DEGRADATION ON THE MECHANICAL PROPERTIES OF RENEWABLE BIOPLASTICS: POLY(TRIMETHYLENE MALONATE) AND POLY(TRIMETHYLENE ITACONATE)

3.1 Abstract

Hydrolytic degradation of two renewable copolymers, poly(trimethylene malonate) (PTM) and poly(trimethylene itaconate) (PTI), was performed in aqueous solutions adjusted to pH values ranging from approximately 5.5 to 11. Elastic modulus was monitored as a function of degradation time (100 to 10000 min) in DI water to determine changes. The influence of the degradation on the elastic modulus of these bioplastics was examined by a new atomic force microscopy (AFM) mode. After degradation for one week, the degree of crystallinity had significantly increased, and the elastic modulus of PTI had decreased by 58 %. PTM was found to be hygroscopic. Due to significant swelling and uneven surfaces—in both the dry and wet state—PTM samples could neither be easily imaged nor its nanomechanical properties evaluated by AFM. Differential scanning calorimetry (DSC) and thermogravimetric (TGA) analyses were used to show shifted phase transitions depending on the degradation.

3.2 Introduction

With increased concern for our environment and the increased cost of petroleum feedstock, 'green' polymers are being sought from biomass-based resources as an alternative to petroleum-based polymers. Products based on recycled and renewable resources are entering the market as toys, packaging materials, clothing, and other products [1-4]. There are several types of hydrolytically degradable polymers currently being researched as replacements for non-hydrolytically degradable petroleum-based polymers, including poly(anhydrides), poly(orthoesters), poly(depsipeptides), poly(ether esters), and poly(esters) [5]. Poly(esters) have shown the most promise for commercialization and replacement of petroleum-based polymers, especially with the development of poly(lactic acid) (PLA), poly(glycolic acid) (PGA), and poly(ε-caprolactone) (PCL). In the 1960s and 1970s, PGA was the first bio-compatible and hydrolytically degradable synthetic polymers and was commercialized as a dissolvable suture material [6]. This advance spurred research into other bio-compatible polymers and into other applications for these polymers. However, performance issues, such as poor thermal stability and brittleness, were encountered with PLA and PGA [7-8]. To overcome the thermal and mechanical short comings of PLA, PGA, and PCL, polymeric blends and copolymers of these with one another and also with other polymers were used to modulate the properties, and have shown varying degrees of success [5, 7, 8-12]. In the past 10 years, interest has increased in bio-based polymeric materials—either naturally occurring or synthetic—and their methods of degradation as demonstrated by a 14-fold increase in publications since 2000.

Two renewable copolymers, poly(trimethylene malonate) (PTM) and poly(trimethylene itaconate) (PTI), have been produced with ester bonds incorporated into the polymer backbone to facilitate hydrolytic and/or enzymatic degradation. PTM was synthesized from 1,3-propane diol and malonic acid to produce a linear copolymer. PTI was synthesized from 1,3-propane diol and itaconic acid to produce a branched and possibly cross-linked copolymer [13]. A study into the hydrolytic degradation of these renewable polymers in aqueous solutions that had been adjusted to pH values from ~5.5 to 11 has previously been detailed [13]. Weight change was monitored as a function of degradation time (10 to 10000 min) to determine if solubilization and/or degradation occurred. To summarize, final weight loss varied from 20 to 37 wt% for PTM and from 7 to 21 wt% for PTI as a function of aging time and initial solution pH. Hydrolytic degradation is expected to change the mechanical properties of these bioplastic materials. In this study, the effect of hydrolysis on the mechanical properties is examined at the nanoscale by atomic force microscopy (AFM).

3.3 Experimental section

3.3.1 Materials

Malonic acid (MA, 99%), itaconic acid (IA, 99%) and chloroform (98%) were used as received from VWR. 1,3-Propane diol (PDO, 98%), $AlCl_3$ (98%), and diethyl ether (>99%) were used as received from Sigma-Aldrich. Potassium hydroxide (KOH, 99%) was purchased from Fisher Scientific. Poly(trimethylene malonate) (PTM) and poly(trimethylene itaconate) (PTI) were produced as described previously [13].

3.3.2 Methods

3.3.2.1 Copolymerization of PDO-MA

Polymerizations were performed in a 100 mL round bottom flask at 25 torr. For PTM and PTI, PDO and MA or PDO and IA, respectively, were fed at a 1:1 molar ratio using a 100:1 monomer to catalyst ($AlCl_3$) ratio. The flask was then immediately placed into an oil bath with the reactions performed at 155 °C for the samples in this study. The polymerizations were carried out for 4 h for PDO-MA and 16 h for PDO-IA [13].

3.3.2.2 Polymer separation

When the reactions were completed, excess monomer and catalyst were removed by dissolving the reaction product in chloroform. This chloroform solution was then poured into diethyl ether. The polymer precipitated out of solution and was removed by filtration using Whatman (grade 40) filter paper. This separation process was repeated until no additional polymer precipitated. The filtered polymer was then dried in a vacuum oven at 15 torr and 20 °C for 24 h and weighed.

3.3.2.3 Compression molding PTM

PTM (PDO-MA, 155 °C, 4 h) was compression molded into a 12 cm x 12 cm x 0.159 cm sheet using a Carver 15 ton hydraulic press at 6.9 MPa and 30 °C for 10 min. The sheet was cut into 1 cm x 0.318 cm x 0.318 cm coupons. For each coupon, dimensions and weight were recorded and then each coupon was placed into an individual vial.

3.3.2.4 PTI grinding

PTI was ground by hand into a powder using a mortar and pestle until all particles could easily sift through 18 x 18 mesh stainless steel wire cloth. FTIR and GPC analyses were performed on the PTI samples both before and after grinding. No impact was observed on the Mw or chemical structure of the samples due to grinding.

3.3.2.5 Hydrolytic degradation

For the PTM hydrolysis experiment, samples were initially placed under vacuum at room temperature and 25 torr for 24 h to remove excess water. Vials were then prepared containing one compression molded PTM coupon along with 10 mL DI water (measured 5.4 pH), pH 7 KOH, pH 9 KOH, or pH 11 KOH aqueous solutions. One set of sample vials contained no liquid and was used as an 'air' control, to take into account any changes due to non-hydrolytic aging. All sample vials were then sealed and placed into a 25 °C water bath for 10, 100, 1000, or 10000 min.

For each PTI sample, 0.75 g of PTI powder was placed into a 16 mL clear glass vial and 10 mL of the aqueous solutions listed above were added. One set of PTI samples had no solution added as an 'air' control. The sealed vials were placed into a 25 °C water bath for 100, 1,000, or 10000 min.

At each pre-designated time, samples were removed from solution, gently blotted with a KimWipe®, and the wet weights recorded. They were then vacuum dried (25 torr) at room temperature for 24 h and then dry sample weights were recorded. All degradation samples were run in triplicate.

3.3.3 Characterization

3.3.3.1 Thermogravimetric analysis (TGA)

A TA Instruments Q-600 simultaneous DSC/TGA (SDT) instrument with the TA Universal Analysis 2000 software (v4.7A) was used to assess the thermal stability of the degraded PTI samples. The 5 mg samples were analyzed from room temperature to 600 °C at a rate of 10 °C/min under 50 mL/min of nitrogen purge.

3.3.3.2 Differential scanning calorimetry (DSC)

A TA Instruments Q-2000 modulated DSC (mDSC) with the TA Universal Analysis 2000 software (v4.7A) was used for thermal analysis of the degraded PTI samples. The 5 mg samples were heated from 40 to 200 °C at a rate of 10 °C/min under 50 mL/min of nitrogen purge. The cold crystallization temperature (T_{cc}), melting temperature (T_m) and melting enthalpy (ΔH_m) of the degraded PTI samples were determined from the exotherms, and the degree of crystallinity (X_m) was not calculated since the melting enthalpy for 100% crystalline PTI is unknown.

3.3.3.3 Atomic force microscopy (AFM)

In this study, a new AFM mode known as “PeakForce QNM” was used on a Dimension Icon AFM to map the mechanical properties of the bioplastic samples. By using Peak Force Tapping™, damage to the tip and sample can be minimized by directly controlling the forces applied to the tip and using forces lower than those generally used in tapping mode. This method also allows for better control of the maximum force (Peak Force) on the tip as it ensures the tip-sample contact area is as small as possible [14].

During the tapping, the AFM generates force curves for each pixel on the sample surface and converts them to the force-separation plots that give some of the major mechanical properties such as elastic modulus, adhesion, dissipation, and deformation. Figure 3.1 shows the force-separation curve describing the mechanical quantities during a single peak force tapping.

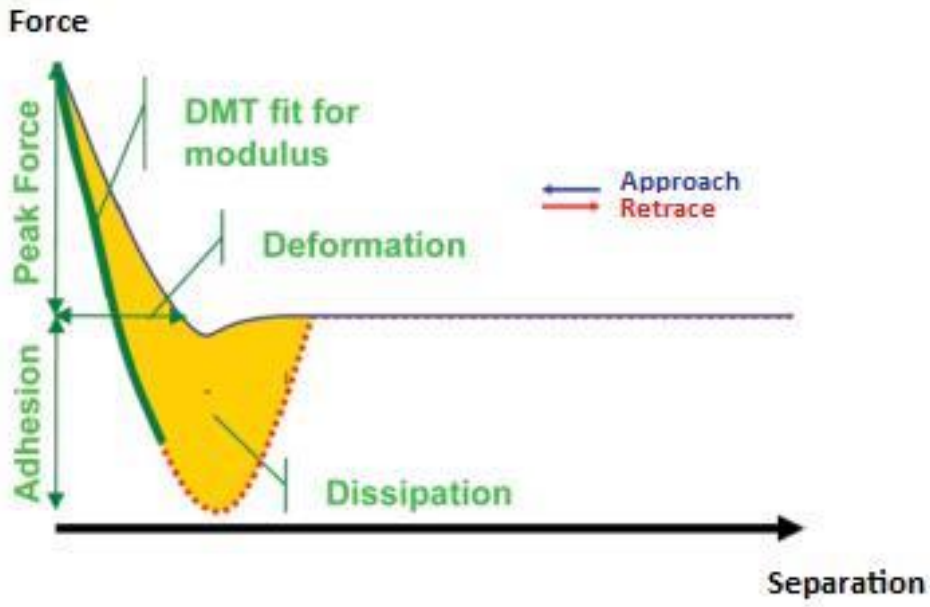

Figure 3.1 Force-separation curve to obtain the mechanical properties of the sample. Figure adapted from [14].

The Derjaguin-Muller-Toporov (DMT) model can be used to fit the retract curve in order to estimate the reduced modulus, E* [14]. The DMT model uses Eqn. 3.1 with the relationship between modulus and forces given as

$$E* = \frac{3}{4}(F - F_{adh}) / \sqrt{R(d - d_0)^3} \quad (3.1)$$

where E* is the reduced elastic modulus of the sample, R is the tip radius, ($F-F_{adh}$) is the difference between the relative forces of the tip and adhesion during the tapping, and ($d-d_0$) is the sample deformation. The most common elastic modulus, Young's modulus of the sample (Es), can be calculated directly from the reduced modulus by using the known Poisson's ratio of the sample

$$E^* = \left[\frac{1-\nu_s{}^2}{E_s} + \frac{1-\nu_{tip}^2}{E_{tip}}\right]^{-1} \quad (3.2)$$

where Es is the Young's modulus of the sample, E_{tip} is the modulus of the tip, and ν_s and ν_{tip} are the Poisson's ratios of the sample and the tip, respectively. Here, the elastic modulus of the tip (E_{tip}) can be assumed infinite [14].

First, the appropriate cantilever was selected based on the sample type and calibrated to measure its sensitivity, spring constant, and radius; a TAP525A probe with tip radius of 10 nm was used. All mechanical analyses of PTI as a function of the hydrolytic degradation were performed in air at ambient temperature. PTI samples were attached onto the metal AFM pan using adhesive tape. The scanning rate was less than 1 Hz and 512 x 512 pixels were used for 5 x 5 μm scans. The peak-force set-point and the Poisson's ratio were set to 3.0 μN and 0.3, respectively. After the Peak Force Tapping™ was performed, the AFM images were analyzed with the NanoScope Analysis software version 1.40.

3.4 Results and Discussion

3.4.1 Copolymerization of PDO-MA and PDO-IA

Melt polycondensation of PDO-MA (to form PTM) and PDO-IA (to form PTI) was successful under mild reaction conditions. PDO-MA was not difficult to extract and

purify using chloroform and ether. PDO-IA did present some difficulties in extraction using chloroform due to the branching and/or cross-linking present.

3.4.2 Hydrolytic degradation

A hydrolytic degradation study was performed on the renewable polymers PTM and PTI in aqueous solutions adjusted to pH values from ~5.5 to 11. During the degradation, the diffusion of acidic monomers and oligomers into the solution caused the pH of all solution to become acidic (~ pH 3.4). Weight change was monitored as a function of degradation time (10 to 10000 min) to determine if solubilization and/or degradation was occurring. Final weight loss varied from 20 to 37 wt% for PTM and from 7 to 21 wt% for PTI as a function of aging time and initial solution pH. DI water (pH 5.4, the lowest value in this study) had the highest degradation rate and is hypothesized to be due to the lack of K+ ions to inhibit carbonyl protonation or to stabilize the carboxylate anions formed during hydrolysis [13].

3.4.3 Thermal properties

The thermal behavior of the neat (non-degraded, 0 min) and degraded PTI samples was analyzed by DSC. The data are presented in Table 3.1, and the heating thermograms are shown in Figure 3.2. Second heating was attempted to erase the thermal history; however, the samples did not recrystallize, so only the first scans were used to determine the transition temperatures. Neat PTI had a cold crystallization temperature of 159 °C and a double melting temperature of 159 °C and 214 °C. Wang et al. reported a bimodal melting behavior of polyethylene produced by intercalated silicate with nickel diimine complex [15]. They also concluded that the polymers with low melting point and

high molecular weight were firstly produced through a “chain walking” mechanism and followed by formation of polymer with high melting point and low molecular weight. PTI produced in this study by melt polycondensation did show a bimodal Mw of 1 kDa with 1.78 PDI and 38 kDa with 1.71 PDI. This bimodal molecular weight distribution can result in the bimodal melting behavior.

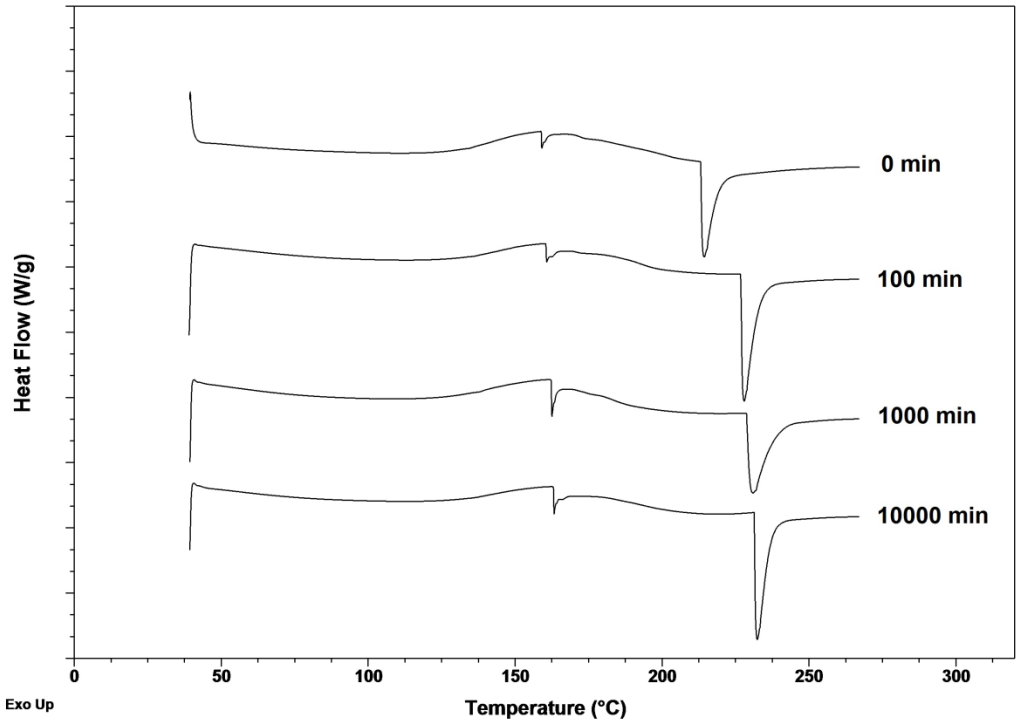

Figure 3.2 DSC thermograms of PTI after 0, 100, 1000, and 10,000 min of degradation showing phase transitions.

Table 3.1 Thermal analysis data of PTI sample as a function of degradation time.

Degradation Time (min)	$T_{5\%}$ (°C)	T_{max} (°C)	T_{cc} (°C)	T_{m1} (°C)	T_{m2} (°C)	ΔH_m (J/g)
0	186	382	159	159	214	20.6
100	208	384	160	161	228	28.0
1000	209	386	162	163	231	26.7
10000	223	386	162	163	232	25.6

In addition, the cold crystallization temperature and melting temperatures of the PTI both increased as a function of the degradation time. The increase in the second melting peak position was more significant (an upward shift of 18 °C) while the cold crystallization temperature only shifted by 3 °C. The increase in the melting points can be attributed to the scission of the ester bonds in the polymer chain. The initial degradation in the amorphous phase could happen quickly since water attacks the weakly-packed segments more easily. This resulted in an increase in chain mobility, and thus new, more organized crystalline regions occurred. As a result, this behavior called "cleavage-induced crystallization" [16], could increase the melting point of semi-crystalline PTI during the degradation [17].

Since the melting enthalpy for 100% crystalline PTI was unknown, the degree of crystallinity (X_m) was not calculated. Therefore, the total melting enthalpies were used to monitor PTI's crystallinity. In general, the crystallinity of PTI tended to increase with the degradation. Again, this could be explained by the behavior of semi-crystalline polymers, such as PTI, undergoing partial degradation of the amorphous phase, as was previously described. Even though the crystallinity decreased gradually from 100 min until 10000 min, it was still higher than that of neat PTI. In another study, Vasanthan and Gezer [18]

investigated the crystallinity changes of as-cast PLLA films with degradation, and concluded that a degradation of restricted amorphous phase may cause an increase in crystallinity. Such an increased crystallinity induced by the chain segmental motion may be a serious drawback when semi-crystalline polymers are used in biomedical applications as an implant material because this re-crystallinization can slow down the hydrolytic degradation of the material in the body [19].

The thermal stability of PTI and degraded PTI samples was investigated by TGA. Table 3.1 presents these results including $T_{5\%}$ (5% weight loss) and T_{max} (50% weight loss) of the PTI samples. Neat PTI thermal degradation temperatures, $T_{5\%}$ and T_{max}, were 186 °C and 382 °C, respectively. One would expect that the thermal stability would decrease eventually when the degradation is carried out. From the GPC study done previously [13], it was suggested that the amorphous phase and small crystalline structures could be readily degraded or diffused out of PTI in the first 100 min, and the larger crystals did not experience degradation until 1000 min. That is why the thermal stability of PTI samples shifted to higher temperatures with the hydrolytic degradation. A similar thermal decomposition behavior for semi-crystalline polymers was also reported by Olewnik et al. [17].

3.4.4 Nanomechanical properties

In previous work, DI water with a pH of 5.4 had the highest degradation rate for PTI [13]. In this study, mechanical testing of PTI as a function of the hydrolytic degradation time in DI water was performed. The goal was that the chemical and physical changes in PTI can be related to the mechanical properties.

By atomic force microscopy both qualitative and quantitative topography and micromechanical information can be obtained. Figures 3.3, 3.4, and 3.5 show height (topography), DMT modulus, and adhesion maps for neat PTI and PTI samples degraded in DI water (pH 5.4) for different degradation times. Surface roughness of the samples increased with degradation time. The average AFM RMS roughness value for neat PTI is 16.17±4.03 nm, and then it did not increase significantly with degradation until 10000 min. The average RMS roughness for 100 and 1000 min degradation were 16.07±3.65 nm and 10.63±1.14 nm, respectively. At 10000 min, the degraded PTI has a average height of 21.47±4.11 nm. In addition to increased roughness, the degradation of PTI resulted in higher adhesion. The mean adhesion force increased from 23.67±0.62 nN for neat PTI to 34.57±2.55 nN for PTI degraded for 10000 min.

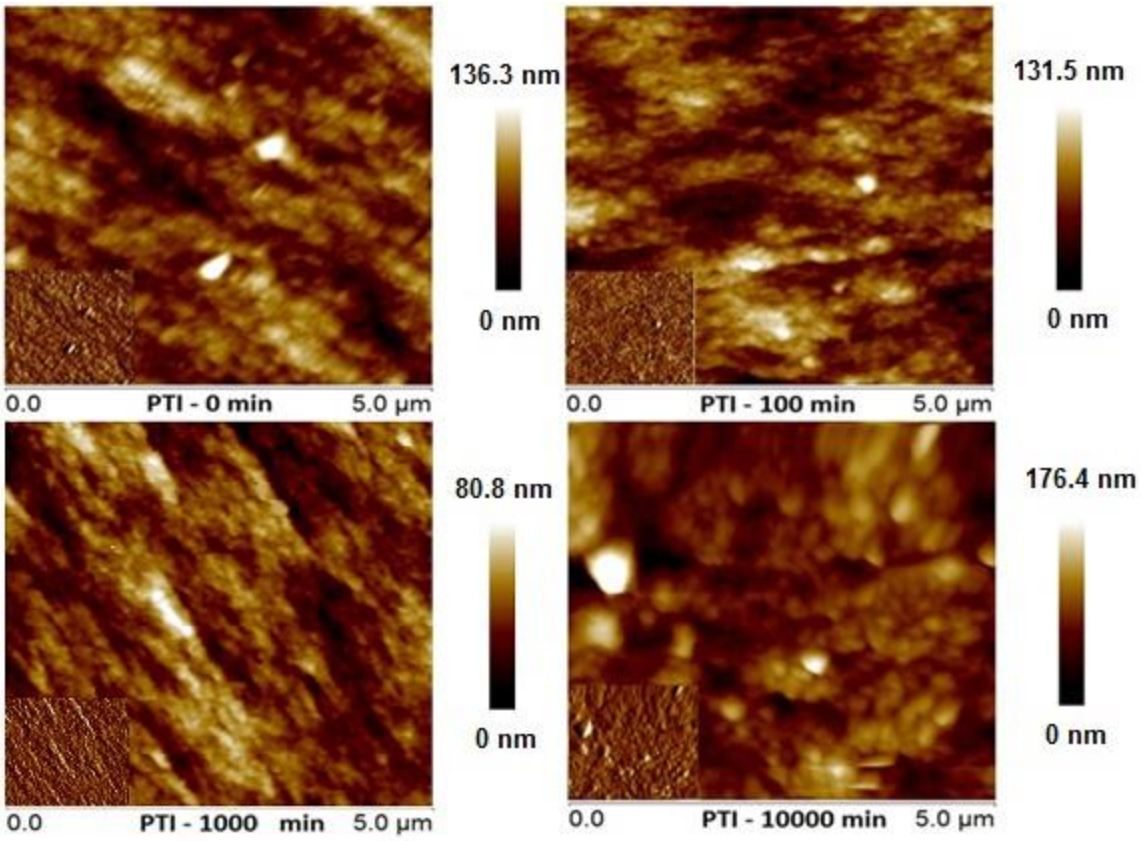

Figure 3.3 AFM topographical maps (5×5 μm^2) of neat PTI and PTI degraded for 100 min, 1000 min, and 10000 min.

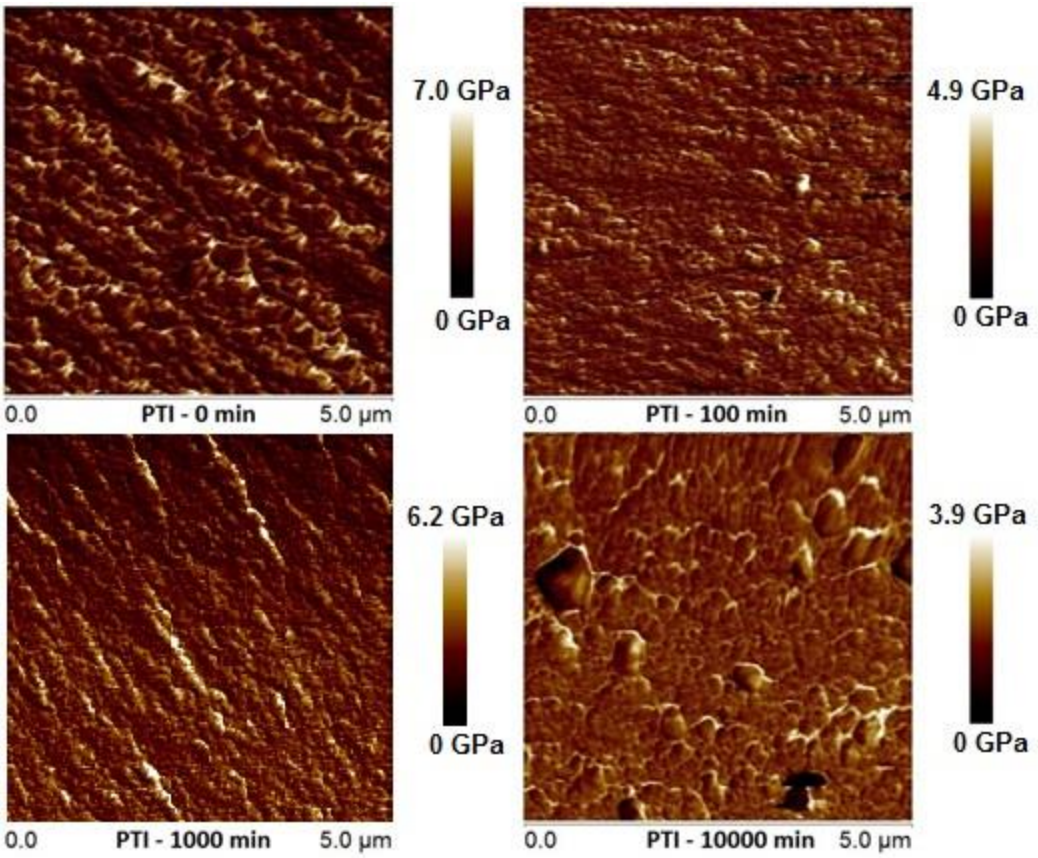

Figure 3.4 AFM DMT modulus maps (5×5 μm^2) of neat PTI and PTI degraded for 100 min, 1000 min, and 10000 min.

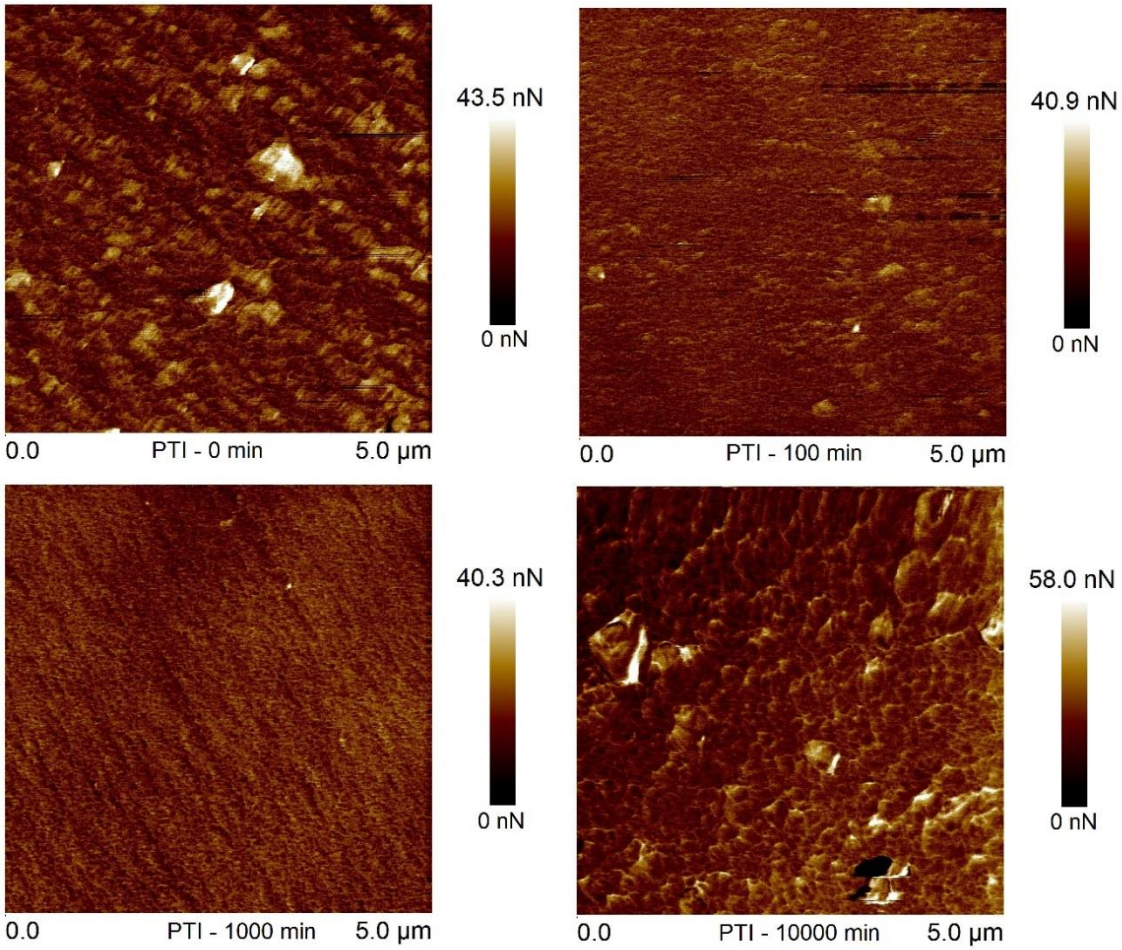

Figure 3.5 AFM adhesion maps (5×5 μm^2) of neat PTI and PTI degraded for 100 min, 1000 min, and 10000 min.

The effect of the hydrolytic degradation on the elastic modulus of PTI is shown in Figures 3.4 and 3.6. High modulus areas with lighter colors are visible in the PTI crystalline structure while the darker areas are representative of low modulus of amorphous phase. According to the DMT modulus values, the neat PTI sample had an average surface modulus of 4.3 GPa. During hydrolytic degradation, the DMT modulus initially increased and then decreased significantly after 10000 min of degradation time. Castilla-Cortázar et al. reported a similar trend; as degradation proceeded, Young's

modulus of poly(ε-caprolactone) (PCL) networks increased at first and decreased slightly after week 38 of degradation in water and PBS [20]. After 10000 min, the mean modulus of the degraded PTI sample was 1.8 GPa, a 58 % decrease in modulus from the neat PTI sample. During the hydrolytic degradation, PTI demonstrated decreases in sample mass and molecular weight along with chemical changes such as the hydrolysis of backbone chain segments [13]. These physical and chemical changes during degradation are significant factors in the loss of elastic modulus for the semi-crystalline PTI bioplastic [6, 21-22].

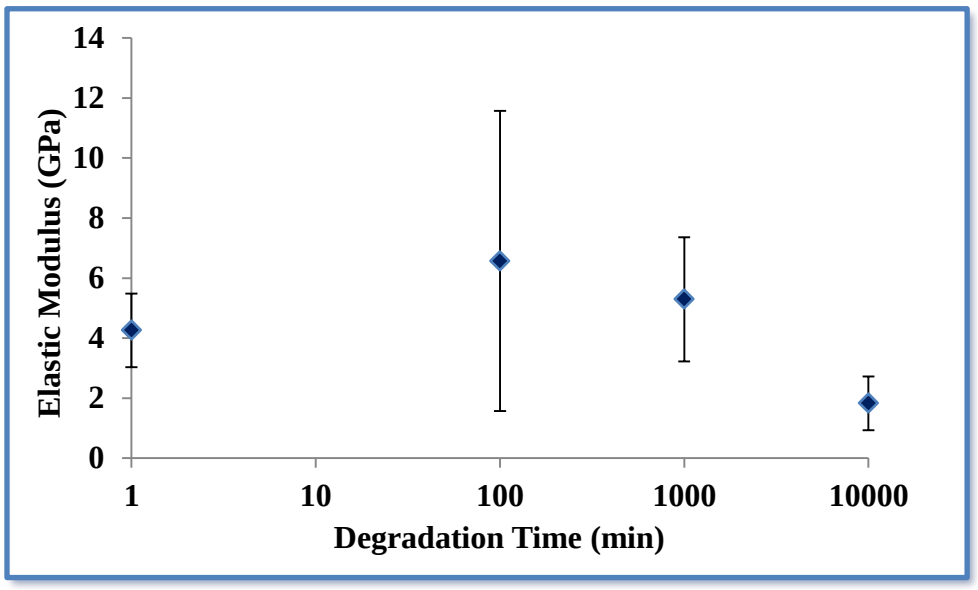

Figure 3.6 Elastic modulus of the neat and hydrolytically degraded PTI samples as a function of degradation time.

Unfortunately, PTM was able to be scanned only once as it required a specific AFM tip that was available only during a vendor demonstration. In this single AFM

experiment, PTM was found to be very soft with an elastic modulus of 7 MPa (Fig. 3.7). The degraded PTM samples were gel-like and not suitable for AFM imaging.

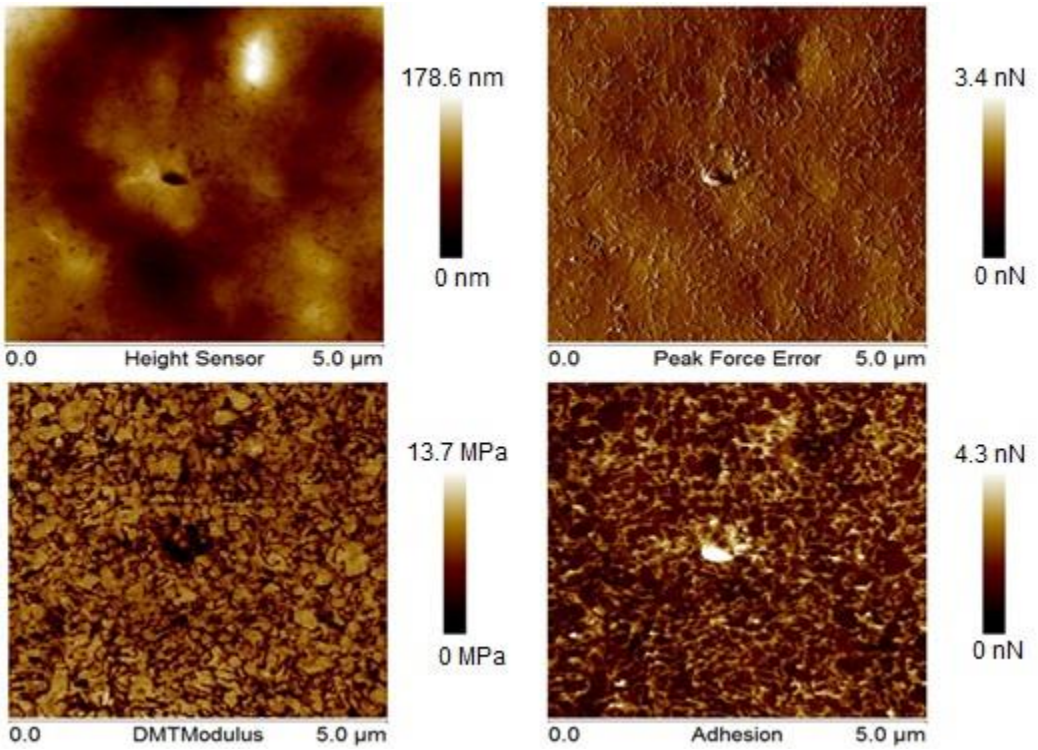

Figure 3.7 Neat PTM AFM maps (5×5 μm^2).

3.5 Conclusions

PTM and PTI hydrolytic degradation was performed at 25 °C for up to 10000 min with pH 7, 9, 11 KOH/DI water solutions and DI water (pH 5.4). Although the solutions used for degradation started at discrete pH values, all of the solutions decreased in pH to a value of ~3.4 after 100 min of degradation. This pH decrease is due to the release of acidic monomer and oligomers. At this relatively low pH, the ester hydrolysis degradation mechanism should be dominant for all of the test solutions.

Significant hydrolytic degradation weight losses have been demonstrated for PTM and PTI. Maximum weight losses of 50 and 21 wt%, respectively, were measured over one week. Morphology and micro/nano mechanical testing of PTM and PTI samples degraded in DI water (pH 5.6) were examined using AFM. Difficulties were encountered in using AFM with the PTM samples due to its soft and sticky nature—especially after degradation, uneven surface, and hygroscopic behavior. Therefore, extensive mechanical property testing using AFM was performed on only the PTI samples.

During the hydrolytic degradation, the PTI samples showed major changes in their morphology, thermal properties, and mechanical properties, especially after 10000 min. It was found that the melting temperatures and thermal stability of PTI could be influenced by change in crystallinity. The elastic modulus of degraded PTI samples decreased linearly as a function of the degradation time. PTI is a semi-crystalline copolymer, and in the non-crystalline regions, the chain segments can be broken to smaller segments. This led to molecular weight loss during degradation and caused a reduction in the elastic modulus.

3.6 Acknowledgements

A portion of this work was performed through the Sustainable Energy Research Center at Mississippi State University and supported by the US Department of Energy under award number DE-FG3606GO86025. The AFM, DSC, and TGA work were made possible through the National Science Foundation [CBET-0923474; CBET-0933493]. MSU's Bagley College of Engineering Ph.D. Fellowship and The Republic of Turkey's Ministry of National Education are also acknowledged for financial support.

Undergraduate researchers Mitch Wall, Erin Smith, Zach Wynne, and Philip Jamison assisted on this project and their efforts are appreciated.

3.7 References

1. Mapleston, P., "New Technologies for a Greener Industry," *Plastic Engineering*, **2008**, 11-15.

2. Stewart, R., "Going Green: Eco-Friendly Materials and Recycling on Growth Paths", *Plastic Engineering*, **2008**, 17-23.

3. Robinson, G., "Biofocals", *Waste Management World*, **2007**, 77-83.

4. Tullo, A. H., "World Chemical Outlook: United States", *Chemical and Engineering News*, **2008**, 16-19.

5. Neffe, A. T., Tronci, G. Alteheld, A. Lendlein, A., "Controlled Change of Mechanical Properties during Hydrolytic Degradation of Polyester Urethane Networks," *Macromolecular Chemistry and Physics*, **2010**, 211, 182-194.

6. Chu, C. C., "Hydrolytic Degradation of Polyglycolic Acid: Tensile Strength and Crystallinity Study," *Journal of Applied Polymer Science*, **1981**, 26, 1727-1734.

7. Quynh, T. M., Mitomo, H., Yoneyama, M., Hien, N. Q., "Properties of Ratiation-Induced Crosslinking Sterocomplexes Derived from Poly(L-Lactide) and Different Poly(D-Lactide)," *Polymer Engineering and Science*, **2009**, 970-976.

8. Shirahase, T., Komatsu, Y., Tominaga, Y., Asai, S., Sumita, M., "Miscibility and Hydrolytic Degradation in Alkaline Solution of Poly(L-Lactide) and Poly(Methyl Methacrylate) blends," *Polymer*, **2006**, 47, 4829-4844.

9. Catiker, E., Gumusderelioglu, M., Guner, A., "Degradation of PLA, PLGA homo- and Copolymers in the Presence of Serum Albumin: A Spectroscopic Investigation," *Polymer International*, **2000**, 49, 728-734.

10. Hill, S. P., de Oca, H. M., Klein, P. G., Ward, I. M., Rose, J., Farrar, D., "Dynamic Mechanical Studies of Hydrolytic Degradation in Isotropic and Oriented Maxon B," *Biomaterials*, **2006**, 27, 3168-3177.

11. Hoglund, A., Odelius, K., Hakkarainen, M., Albertsson, A.-C., "Controllable Degradation Product Migration from Cross-Linked Biomedical Polyester-Ethers through Predetermined Alterations in Copolymer Composition," *Biomacromolecules*, **2007**, 8, 2025-2032.

12. Oyama, H. T., Tanaka, Y., Kadosaka, A., "Rapid Controlled Hydrolytic Degradation of Poly(L-Lactic Acid) by Blending with Poly(Aspartic Acid-co-L-Lactide)," *Polymer Degradation and Stability*, **2009**, 94, 1419-1426.

13. Rowe, M.D.; Eyiler, E.; Walters, K.B., “pH and Time Dependent Hydrolytic Degradation of Bioplastics from Renewable Monomers,” *SPE-ANTEC Tech. Papers*, **2011**, 69, 306-311.

14. Pittenger, B.; Erina, N.; Su, C., "Quantitative mechanical property mapping at the nanoscale with PeakForce QNM," *Application Note Veeco Instruments Inc*, **2010**.

15. Wang, Q.; Liu, P., "Dual bimodal polyethylene prepared by intercalated silicate with nickel diimine complex," *Journal of Polymer Science Part A: Polymer Chemistry*, **2005**, 43, 5506-5511.

16. Brito, Y.; Sabino, M.; Ronca, G.; Müller, A., "Changes in crystalline morphology, thermal, and mechanical properties with hydrolytic degradation of immiscible biodegradable PPDX/PCL blends," *Journal of Applied Polymer Science*, **2008**, 110, 3848-3858.

17. Olewnik, E.; Czerwiński, W.; Nowaczyk, J., "Hydrolytic degradation of copolymers based on l-lactic acid and bis-2-hydroxyethyl terephthalate," *Polymer degradation and stability*, **2007**, 92, 24-31.

18. Vasanthan, N.; Gezer, H., "Thermally induced crystallization and enzymatic degradation studies of poly (L-lactic acid) films," *Journal of Applied Polymer Science*, **2013**, 127, 4395-4401.

19. Auras, R. A.; Lim, L.-T.; Selke, S. E.; Tsuji, H., *Poly (lactic acid): synthesis, structures, properties, processing, and applications*. Wiley: 2011; Vol. 10, 121-123.

20. Castilla-Cortázar, I.; Más-Estellés, J.; Meseguer-Dueñas, J. M.; Escobar Ivirico, J. L.; Marí, B.; Vidaurre, A., "Hydrolytic and enzymatic degradation of a poly(ε-caprolactone) network," *Polymer Degradation and Stability*, **2012**, 97, 1241-1248.

21. Sabino, M. A.; González, S.; Márquez, L.; Feijoo, J. L., "Study of the hydrolytic degradation of polydioxanone PPDX," *Polymer Degradation and Stability*, **2000**, 69, 209-216.

22. Sabino, M.; Sabater, L.; Ronca, G.; Müller, A., "The effect of hydrolytic degradation on the tensile properties of neat and reinforced poly (p-dioxanone)," *Polymer Bulletin*, **2002**, 48, 291-298.

CHAPTER IV

SYNTHESIS OF STIMULI-RESPONSIVE BLOCK COPOLYMERS BY ATRP

4.1 Abstract

A variety of homopolymers and block copolymers were synthesized from one or more of these polymers: PNIPAM, PDMAEMA, PS, and PIA. Chemical analysis of these polymers was performed using ATR-FTIR and DLS. TGA analysis was used to investigate thermal stability, degradation, and the relative size/distribution of the 'blocks' in the block copolymers. By optimizing the polymerization conditions, the cloud point temperature of PDMAEMA/PNIPAM block copolymers can be tailored to fall within the 30-37 °C physiological temperature range, suggesting PDMAEMA/PNIPAM block copolymers may be good candidates for drug delivery and other biomedical applications.

4.2 Introduction

Stimuli-responsive polymers are 'smart' materials that show a measurable change in their properties with environmental stimuli such as temperature, pH, light, magnetic field, moisture, etc. This stimuli responsive behavior can be utilized in a wide range of applications, including "smart" drug delivery, biomedical materials, and even textiles. Moreover, in some cases, several stimuli have been combined to tune the properties of the responsive polymers in manifold ways.

Modern polymer research and advanced material applications are focused on macromolecular engineering including polymers with well-defined compositions, molecular weights, architectures, tailored responsiveness to external stimuli, and multifunctionality [1]. For this purpose, numerous polymerization techniques have been used. Among these techniques, free-radical polymerization is the most common process in industrial production and commercial applications [2]. This technique is versatile, and leads to polymers with high molecular weight under mild reaction conditions [1]. However, the main limitations with this technique are poor control over molecular weight, broad molecular weight distribution, end-functionalities and macromolecular architecture. The unavoidable fast radical termination is the main reason for these limitations. In the last decade, several living/controlled radical polymerization (L/CRP) processes have been developed to overcome these limitations [1]. Atom transfer radical polymerization (ATRP), reversible addition-fragmentation chain transfer polymerization (RAFT) and single electron transfer (SET-LRP) are just a few examples of the living radical polymerization (LRP) method. Among these LRP methods, ATRP is the most promising method due to its applicability to a broad range of monomers and its tolerance to solvents and impurities. In addition, ATRP excels as a robust LRP method to control the molecular weight, precise chemical composition and architecture of polymers.

Poly(N-isopropylacrylamide) (PNIPAM) is one of the most studied thermoresponsive polymers with a lower critical solution temperature (LCST) around 32 °C that makes it suitable for use in targeted and controlled release applications of drugs [3]. At temperatures lower than the LCST, PNIPAM is completely soluble in water. Above the LCST, the polymer become insoluble and aqueous solutions of PNIPAM

become cloudy. It was reported that this phase transition is attributed to the interactions of hydrogen bonds between amide groups and water due to the increase molecular movements of water at higher temperatures [4]. The temperature of such a transition can be adjusted by copolymerization with another monomer. Another well-studied stimuli responsive polymer is poly(2-(dimethylamino)ethyl methacrylate) (PDMAEMA) that displays dual thermo- and pH-responsiveness. PDMAEMA also has been shown to have potential in antibacterial, hemostatic, and anticancer applications [5]. The other responsive polymer synthesized in this study is pH-responsive polyitaconic acid (PIA). PIA is a weak biopolyelectrolyte with two carboxylic acid groups, each with a different pKa value. However, only a few studies on PIA have been performed due to its insolubility in common organic solvents except methanol [6].

In this study, homopolymer and block copolymer structures containing N-isopropylacrylamide (NIPAM), 2-(dimethylamino)ethyl methacrylate (DMAEMA), itaconic acid (IA), and/or styrene were synthesized and examined. Chemical composition, structure, size, and thermal behavior of the bulk block copolymers were analyzed by FTIR, DLS, and TGA.

4.3 Experimental section

4.3.1 Materials

N-isopropylacrylamide (NIPAM) (Aldrich, ≥99%), 2-(dimethylamino) ethyl methacrylate (DMAEMA) (Aldrich, 98%), itaconic acid (Acros, 99+%), styrene (Sigma-Aldrich, ≥99%), tris[2-(dimethylamino)ethyl]amine (Me_6TREN) (Aldrich), ethyl α-bromoisobutyrate (EBIB) (Aldrich, 98%), 2,2-bipyridyl (bpy) (Sigma-Aldrich, ≥99%), copper(I) bromide (Sigma-Aldrich, 98%), copper(I) chloride (Sigma-Aldrich, 97%),

neutral alumina (Acros Organics), THF (anhydrous, Sigma-Aldrich, ≥99.9%), toluene (anhydrous, Sigma-Aldrich, 99.8%), 2-propanol (anhydrous, Sigma-Aldrich, 99.5%), anisole (anhydrous, Sigma-Aldrich, 99.7%), sodium hydroxide (Sigma-Aldrich, ≥98%), diethyl ether (Fisher), petroleum ether (Sigma-Aldrich, ACS reagent), and water (HPLC grade) were used as received without further purification.

4.3.2 Methods

4.3.2.1 Homopolymerization of itaconic acid (IA)

First, the Schlenk tube equipped with a magnetic stir bar was purged with N_2. At the same time, a 1 M solution of itaconic acid (IA) (1.301 g, 10 mmol) was prepared using 10 mL HPLC water and then the monomer was deprotonated by adjusting the pH to 7 using NaOH. Depending on a given reaction, either 2,2-bipyridyl (bpy) (31.24 mg, 0.4 mmol) or Me_6TREN (53.45 µL, 0.2 mmol) was then added as the ligand, and the mixture was sonicated for 10 min. Three freeze-pump-thaw cycles were used to degas the mixture and remove dissolved oxygen. Finally, either Cu(I)Br (14.3 mg, 0.1 mmol) (for bpy) or Cu(I)Cl (9.9 mg, 0.1 mmol) (for Me_6TREN) was quickly added to the frozen mixture, and two additional freeze-pump-thaw cycles followed. The mixture was sonicated again for 10 min and then the polymerization was carried out at room temperature under N_2 atmosphere for 25 h for bpy and 26 h for Me_6TREN. The polymerization was stopped by exposure to air. The solution subsequently was dried in a rotary evaporator. The residual was dissolved in THF and precipitated into acetone, followed by drying in a vacuum oven at 50 °C overnight.

4.3.2.2 Block copolymerization of styrene and N-isopropylacrylamide (NIPAM) to form PS-b-PNIPAM

To polymerize bulk polystyrene using ATRP, first a Schlenk flask equipped with a magnetic stir bar was purged with N_2. Then a 2 M solution of styrene (4.166 g, 40 mmol) and anisole (20 mL) was added, along with PMDETA (83.5 µL, 0.4 mmol), and sonicated for 10 min. Three freeze-pump-thaw cycles followed to degas the mixture and remove dissolved oxygen. Finally, Cu(I)Br (28.7 mg, 0.2 mmol) and EBIB (29.4 µL, 0.2 mmol) were added quickly to the frozen mixture, and two additional freeze-pump-thaw cycles were completed. After another 10 min sonication, the flask was immersed into a pre-heated oil bath at 110 °C and the mixture allowed to stir for 6 h under inert atmosphere. After the polymerization, the solution was precipitated into ice-cold methanol, and then dried under vacuum at room temperature overnight. Note that the polymerization solution was not intentionally quenched to protect the reactive bromine radical.

Addition of a PNIPAM block to the PS homopolymer was performed using a similar polymerization scheme as described previously, except the free radical is present now on the PS chain terminus. NIPAM (1.132 g, 10 mmol) and dichloromethane (10 mL) were charged to a Schlenk flask containing the PS-Br macroinitiator (100 mg) and a magnetic stir bar. After three freeze-pump-thaw cycles, 2,2-bipyridyl (bpy) (15.6 mg, 0.1 mmol) and Cu(I)Br (7.2 mg, 0.05 mmol) were added quickly. The Schlenk flask was then degassed again with two additional freeze-pump-thaw cycles, followed by a sonication for 10 min. The mixture was stirred at room temperature for 12 h under inert atmosphere, and then the polymerization was stopped by exposure to air. The solution subsequently was diluted with THF and passed through a neutral alumina column to remove the

catalyst. The solution was precipitated into ice-cold methanol, and then dried under vacuum at 40 °C.

4.3.2.3 Block copolymerization of styrene and 2-(dimethylamino)ethyl methacrylate (DMAEMA) to form PS-b-PDMAEMA

First, a Schlenk flask equipped with a magnetic stir bar was purged with N_2. At the same time, a 2 M solution of styrene (4.166 g, 40 mmol) and anisole (20 mL) was prepared and added to the mixture to the flask along with PMDETA (83.5 µL, 0.4 mmol). The mixture was sonicated for 10 min and then three freeze-pump-thaw cycles were used to degas the mixture and remove dissolved oxygen. Finally, Cu(I)Br (28.7 mg, 0.2 mmol) and EBIB (29.4 µL, 0.2 mmol) were added quickly to the frozen mixture, and two additional freeze-pump-thaw cycles followed. After another 10 min sonication, the mixture was immersed into a pre-heated oil bath at 110 °C, and stirred for 6 h under inert atmosphere. After the polymerization, the solution was precipitated into ice-cold methanol, and then dried under vacuum at room temperature overnight.

DMAEMA (1.572 g, 10 mmol) and anhydrous THF (10 mL) were charged to the Schlenk flask containing the PS-Br macroinitiator (100 mg) and magnetic stir bar. After three freeze-pump-thaw cycles, 2,2-bipyridyl (bpy) (15.6 mg, 0.1 mmol) and Cu(I)Br (7.2 mg, 0.05 mmol) were added quickly. The Schlenk flask was then degassed again with two additional freeze-pump-thaw cycles, followed by sonication for 10 min. The mixture was place into an oil bath at 50 °C and stirred for 14 h under nitrogen atmosphere. The polymerization was stopped by exposure the tube to air. The solution subsequently was diluted with THF and passed through a neutral alumina column to remove the catalyst.

The solution was precipitated into ice-cold methanol, and then dried in a vacuum oven at 40 °C.

4.3.2.4 Block copolymerization of 2-(dimethylamino) ethyl methacrylate (DMAEMA) and N-isopropylacrylamide (NIPAM) to form PDMAEMA-b-PNIPAM

First, a Schlenk flask equipped with a magnetic stir bar was purged with N_2. At the same time, 2 M solution of DMAEMA (6.288 g, 40 mmol) and anhydrous 2-propanol/HPLC water (3:1, v/v, total volume 20 mL) was prepared and was added to the flask along with 2,2-bipyridyl (bpy) (62.5 mg, 0.4 mmol). The mixture was sonicated for 10 min and then three freeze-pump-thaw cycles were used to degas the mixture and remove dissolved oxygen. Finally, Cu(I)Br (28.7 mg, 0.2 mmol) and EBIB (29.4 µL, 0.2 mmol) were added quickly to the frozen mixture, and two additional freeze-pump-thaw cycles followed. After another 10 min sonication, the mixture was immersed into a pre-heated oil bath at 50 °C, and stirred for 14 h under inert atmosphere. After the polymerization, the solution was dried in a rotary evaporator. The sample was then dissolved in methanol, followed by precipitation into petroleum ether, and then dried under vacuum at room temperature overnight.

NIPAM (1.132 g, 10 mmol) and anhydrous 2-propanol/HPLC water (3:1, v/v, total volume 10 mL) were charged to a Schlenk flask containing the PDMAEMA-Br macroinitiator (138 mg) and a magnetic stir bar. After three freeze-pump-thaw cycles, 2,2-bipyridyl (bpy) (15.6 mg, 0.1 mmol) and Cu(I)Br (7.2 mg, 0.05 mmol) were quickly added. The Schlenk flask was then degassed again with two freeze-pump-thaw cycles, followed by a 10 min sonication. The mixture was stirred at room temperature for 17 h under inert atmosphere. The polymerization was stopped by exposure to air. The solution

was subsequently dried in a rotary evaporator. The residue was dissolved in THF and passed through a neutral alumina column to remove the catalyst, followed by precipitation into diethyl ether, and then dried in a vacuum oven at 40 °C.

4.3.3 Characterization

The polymer modified-magnetic nanoparticles were characterized by ATR-FTIR spectroscopy using a dry air-purged Thermo Electron 6700 instrument with a mercury-cadmium-telluride (MCT) detector and a KBr beam splitter. A MIRacle-ATR (Pike Technologies) with ZnSe/diamond crystal was used to collect spectra over the wavenumber range of 800-4000 cm^{-1} with the resolution of 4 cm^{-1} and 256 scans. Samples were directly placed as solids onto the ZnSe/diamond crystal.

A ZetaPALS analyzer (Brookhaven Instruments Corporation, BIC) with a laser wavelength of 659 nm was used to measure the mean particle size and size distributions of the block copolymers in water. Particle size was measured at a 90° angle. Prior to measurements, the samples were sonicated for 10 min and then allowed to stabilize in the cuvette for 10 min prior to data collection. A total of 3 measurements (5 min per measurement) were carried out for particle size determination using the effective diameter. BIC Particle Solutions software (v2.0) was utilized for data collection and analysis.

A TA Instruments Q-600 simultaneous DSC/TGA (SDT) with the TA Universal Analysis 2000 software (v4.7A) was used to assess the thermal stability of polymers and determine the homopolymer ratio of the block copolymers. The samples were analyzed from room temperature to 600 °C at a rate of 10 °C/min under 50 mL/min of nitrogen purge.

A Waters gel permeation chromatography (GPC) with RI detector, 4E and 5E (polystyrene-divinylbenzene, 4.6 x 300 mm) Styragel® columns, and THF as the effluent at 0.3 mL/min was used to determine molecular weights and polydispersities. GPC was calibrated with 10-point polystyrene standards.

4.4 Results and discussion

The successful polymerization of itaconic acid was further confirmed by FTIR spectroscopy (Fig. 4.1). The spectrum of itaconic acid (IA) monomer shows two sharp peaks at 1682 cm^{-1} and 1622 cm^{-1} due to C=O and C=C stretching vibrations, respectively. The IA peak at 1436 cm^{-1} represents C-O stretching of the carboxylate anion (COO^{-}). In the spectra of PIA using either bpy or Me_6TREN as the ligand, two strong carboxylate anion stretching peaks can be seen clearly at 1569 and 1397 cm^{-1} [7]. The absorbance around 1234 cm^{-1} corresponds to the C-O stretching of the carboxylic acid. It was expected that a characteristic carboxylic acid peak for PIA appeared around 1735 cm^{-1}. According to Sankhe et al., the absence could be explained by the anionic form of the acid sites [7]. The TGA curve of PIA had single stage thermal decomposition starting around 403 °C, and a total of 71 wt% remained at 520 °C (Fig. 4.2).

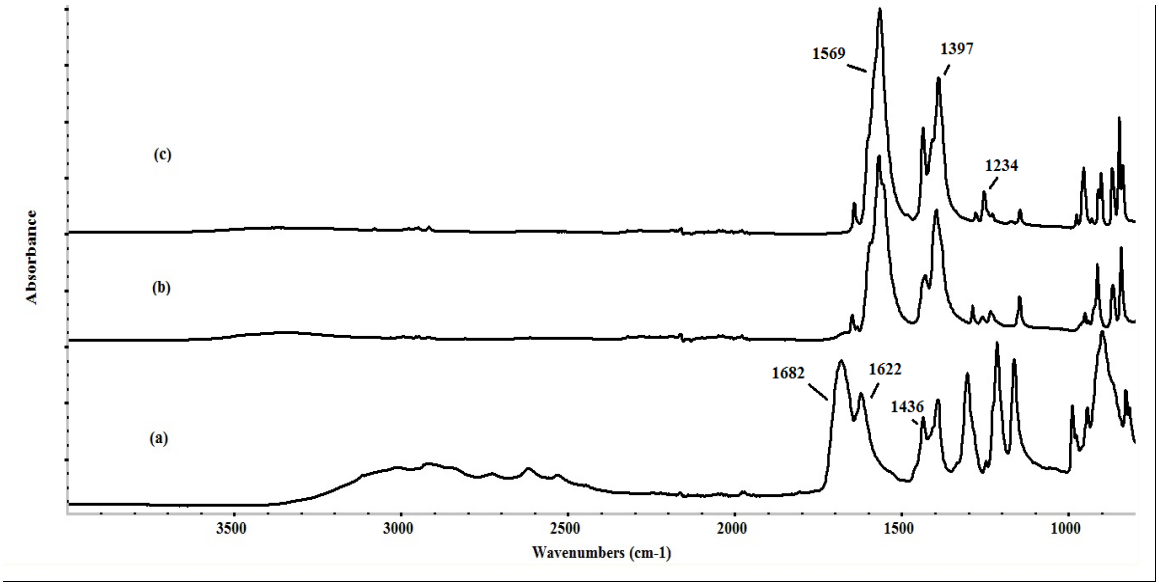

Figure 4.1 FTIR spectra of (a) itaconic acid, (b) PIA using bpy as the polymerization ligand, and (c) PIA using Me_6TREN as the ligand.

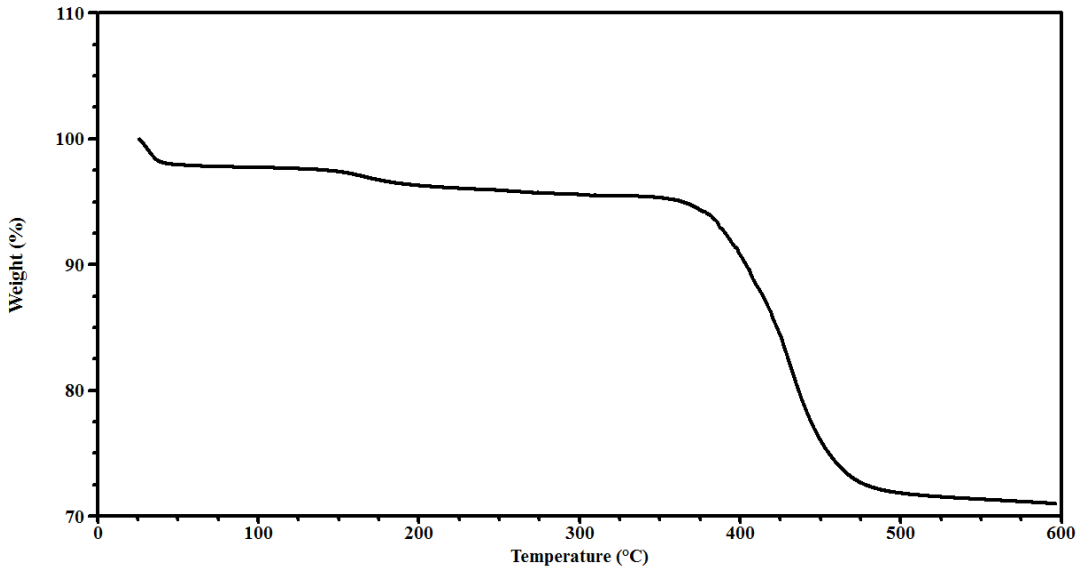

Figure 4.2 TGA trace for PIA polymer synthesized using Me_6TREN as the ligand.

As an example procedure for the copolymerizations, block copolymerization of PS and PNIPAM via ATRP is shown in Figure 4.3. Figure 4.4(a, b) shows the absorbance of styrene monomer and polystyrene, and a sharp peak at 1630 cm^{-1} due to C=C stretching vibration appeared in the spectrum of monomer whereas it is absent in that of polymer. The FTIR spectrum of DMAEMA monomer shows a characteristic peak at 1717 cm^{-1} due to C=O stretching. This characteristic peak was also observed at 1728 cm^{-1} in the spectrum of PS-b-PDMAEMA copolymer.

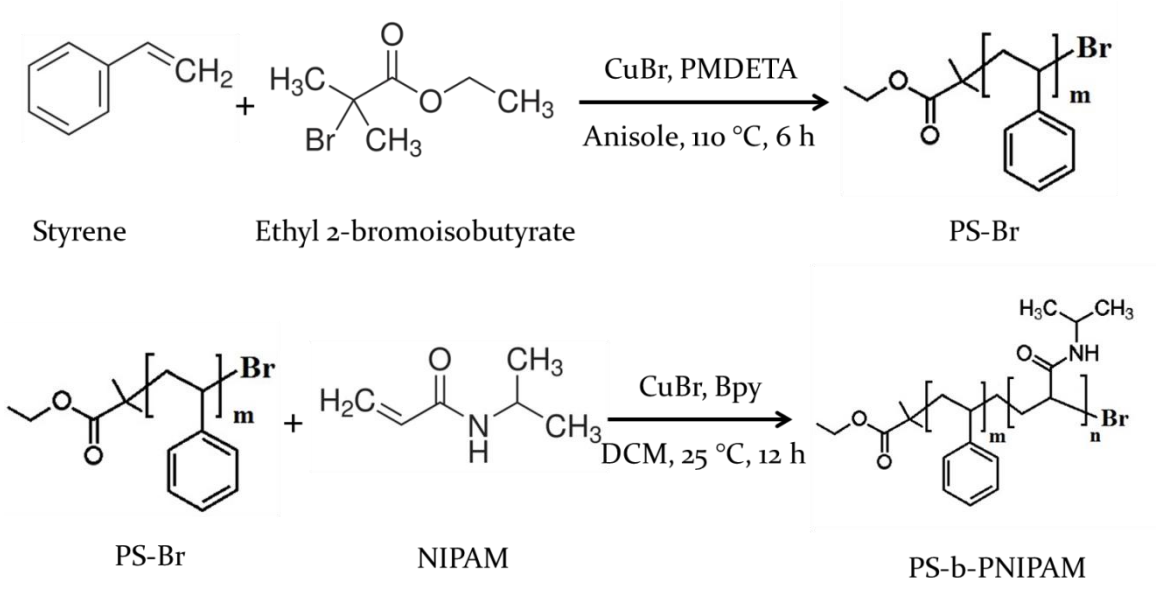

Figure 4.3 Schematic route for the synthesis of PS-PNIPAM copolymer.

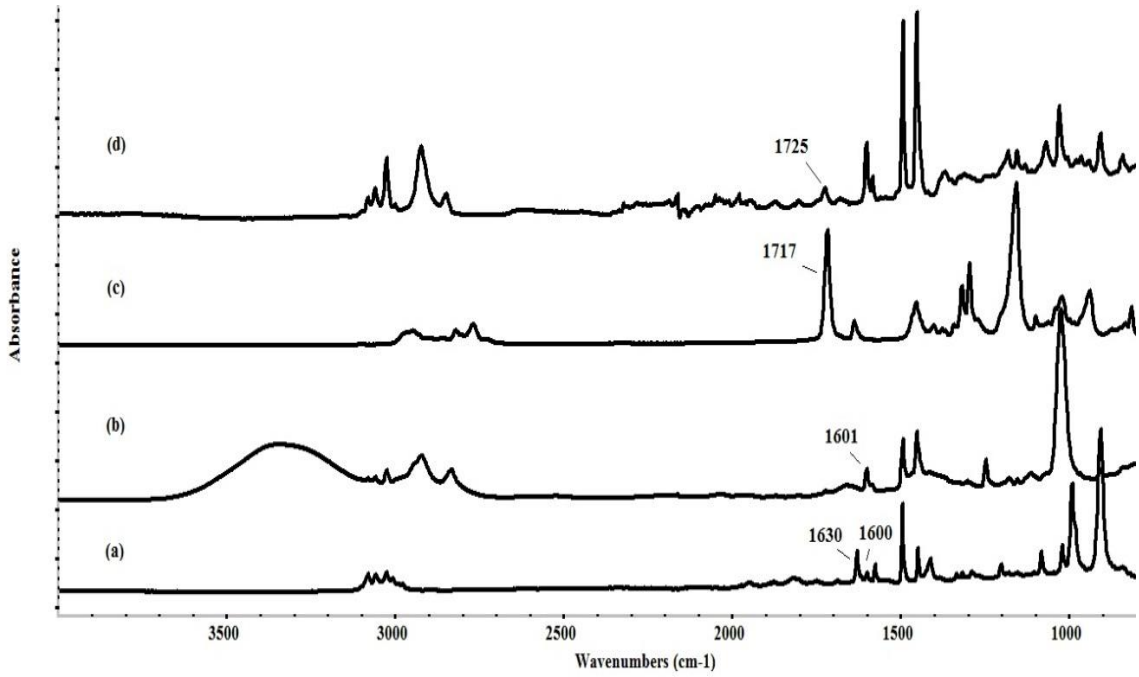

Figure 4.4 FTIR spectra of (a) styrene, (b) PS, (c) DMAEMA, and (d) PS-b-PDMAEMA copolymer.

The thermogravimetric analysis (TGA) curves of the PS, PDMAEMA and PS-b-PDMAEMA were shown in Fig. 4.5. The TGA curve of PS had single stage thermal decomposition starting around 367 °C, with an end weight loss at 430 °C with heating. A typical TGA profile for PDMAEMA was observed [8]. The curve has a double-step degradation where the first step started at 264 °C and the second step at 386 °C. For PS-b-PDMAEMA, a weight loss of around 96 % occurred between 300 and 471 °C, and a total of 2 % remained at 471 °C.

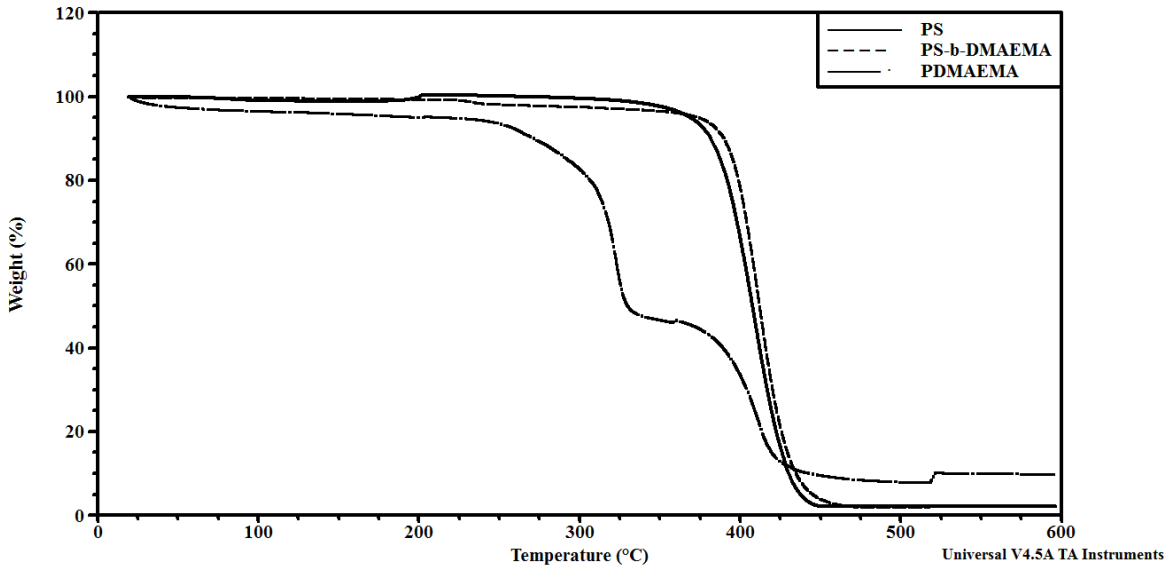

Figure 4.5 TGA traces for PS, PDMAEMA, and PS-b-PDMAEMA copolymer.

Fig. 4.6(a, b) shows the absorbance of styrene monomer and polystyrene, and a sharp peak at 1630 cm^{-1} due to C=C stretching vibration appeared in the spectrum of monomer whereas it is absent in that of the polymer. The FTIR spectrum of NIPAM monomer shows characteristic peaks at 1621, 1656, and 3281 cm^{-1} due to C=C, C=O, and N-H stretching vibrations, respectively. In the spectrum of PS-b-PNIPAM copolymer, the characteristic peaks of PNIPAM at 1635 cm^{-1} and 1513 cm^{-1} correspond to the C=O stretching of amide secondary and N-H stretching of amide secondary, respectively, that indicated the successful copolymerization of styrene and NIPAM.

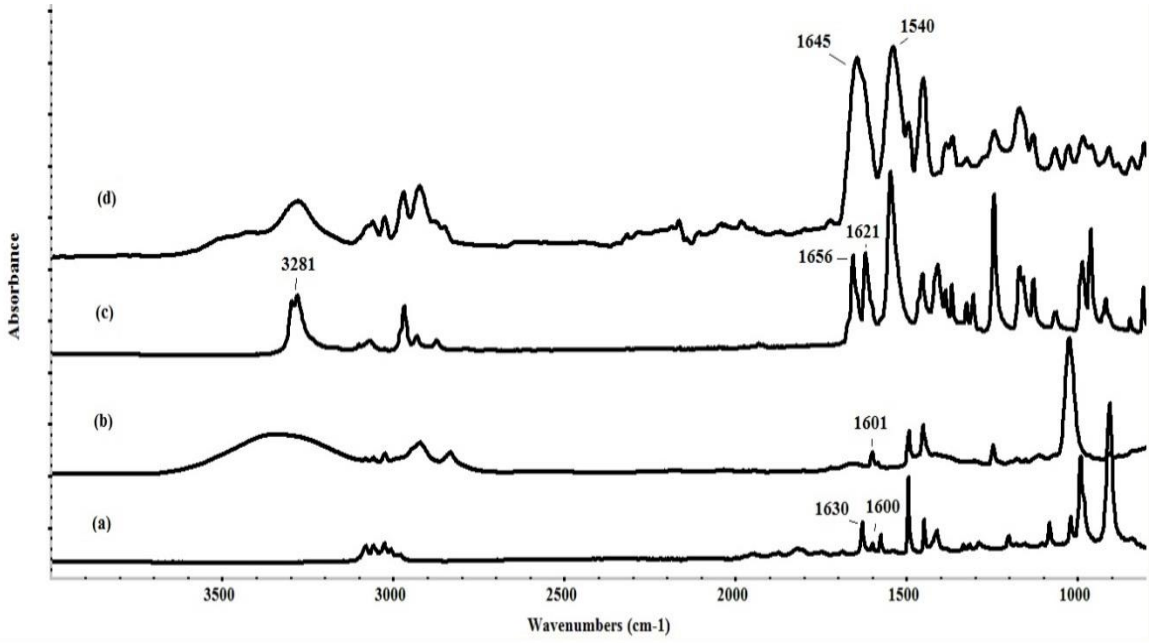

Figure 4.6 FTIR spectra of (a) styrene, (b) PS, (c) NIPAM, and (d) PS-b-PNIPAM copolymer.

The thermogravimetric analysis (TGA) curves of the PS and PS-b-PNIPAM are shown in Fig. 4.7. The TGA curve of PS had single stage thermal decomposition starting around 367 °C, with an end weight loss at 430 °C with heating. It is hard to determine the weight loss fractions of PS and PNIPAM separately by TGA since both polymers degrade thermally in the same temperature range. However, the total weight loss of both polymers can be obtained. For PS-b-PNIPAM, a weight loss of around 87 wt% occurred between 300 and 460 °C, and a total of 2 wt% remained at 460 °C.

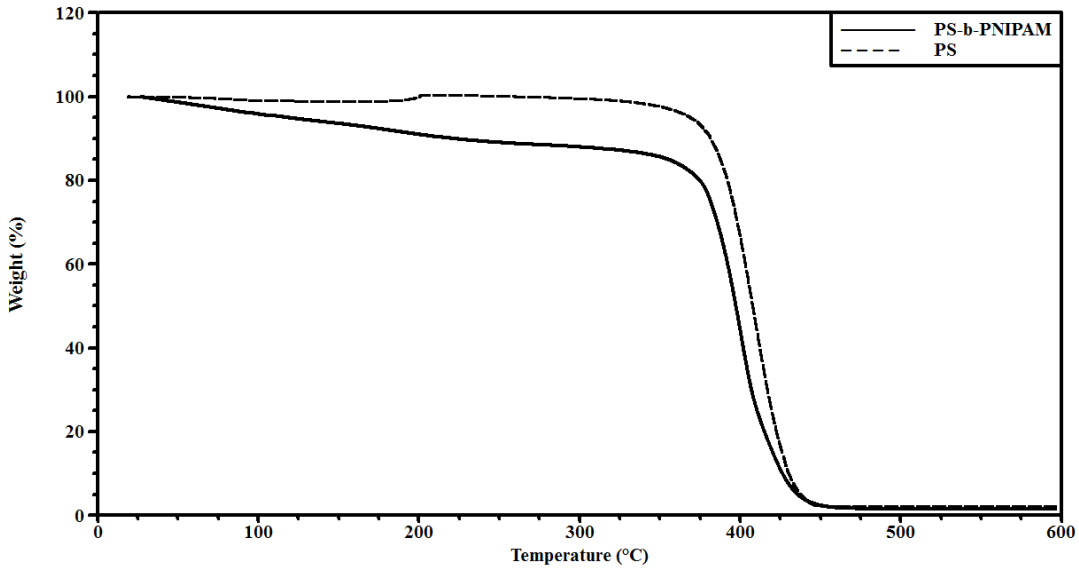

Figure 4.7 TGA traces for PS and PS-b-PNIPAM copolymer.

Fig. 4.8 shows the absorbance of DMAEMA monomer and PDMAEMA, and a sharp peak at 1717 cm^{-1} due to C=O stretching vibration appeared in both spectrum of monomer and that of the polymer. The FTIR spectrum of NIPAM monomer shows characteristic peaks at 1621, 1656, and 3281 cm^{-1} due to C=C, C=O, and N-H stretching vibrations, respectively. In the spectrum of PDMAEMA-b-PNIPAM copolymer, the characteristic peaks of PNIPAM at 1640 cm^{-1} and 1536 cm^{-1} correspond to the C=O stretching of amide secondary and N-H stretching of amide secondary, respectively, that indicated the successful copolymerization of DMAEMA and NIPAM.

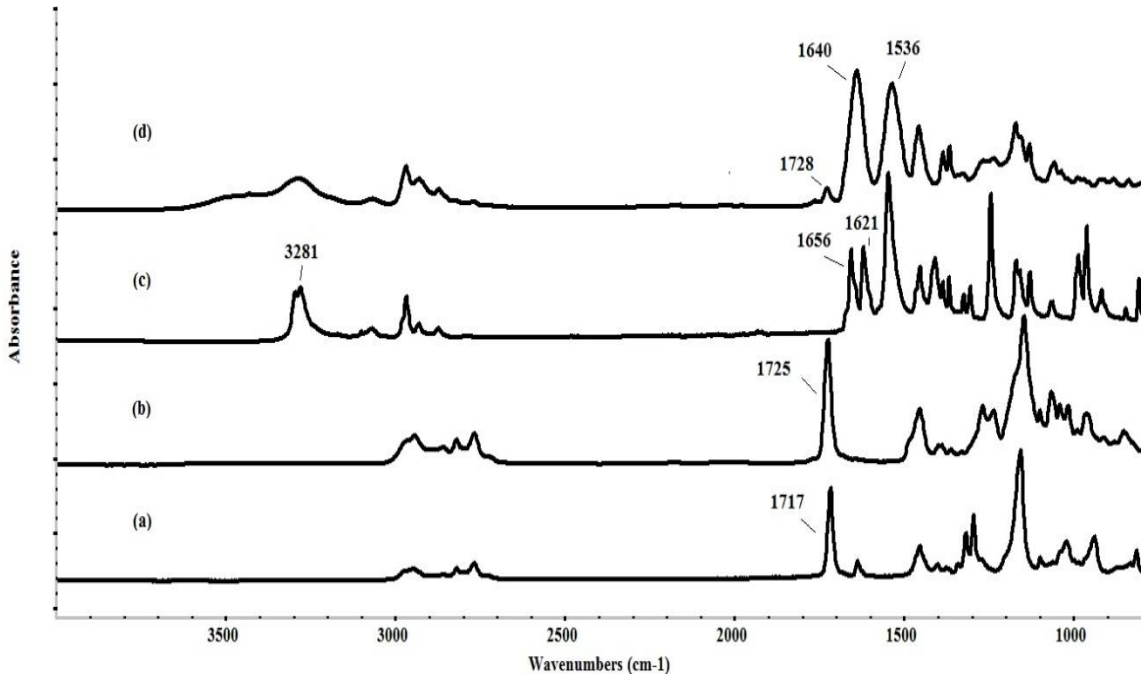

Figure 4.8 FTIR spectra of (a) DMAEMA, (b) PDMAEMA, (c) NIPAM, and (d) PDMAEMA-b-PNIPAM copolymer.

The DLS measurements were performed to obtain the size distributions of PDMAEMA-b-PNIPAM copolymers in water and their thermoresponsive behavior (Fig. 4.9). It is well known that the PNIPAM has a LCST at 32 °C. It was reported that this phase transition is attributed to the interactions of hydrogen bonds between amide groups and water due to the thermal movement of water at higher temperatures [4]. On the other hand, PDMAEMA in aqueous solution has a LCST around 40 °C depending on the polymer composition, concentration and molecular weight and also pH. The DLS measurements were conducted from 25 °C to 46 °C. Fig 4.8 shows the change in the average hydrodynamic diameter (D_h) of the copolymers as a function of the temperature. From 25 to 31 °C, no significant change in the size was observed, and the phase transition took place around 37 °C that is higher than the LCST of pure PNIPAM (32 °C).

The D_h of PDMAEMA-b-PNIPAM at 25 °C was found as 115 nm, and it increased about 1440 times of that at 25 °C to 165,452 nm at 46 °C. This huge increase indicates large micelle formed in the solution due to hydrophobic attractive forces. Xiong et al. studied the thermo-responsive properties of polyampholyte PDMAEMA-b-PAA at different pHs and found that at high pHs, the DMAEMA segments collapsed to form the core of micelles due to the hydrophobic property of the de-protonized DMAEMA upon heating [9].

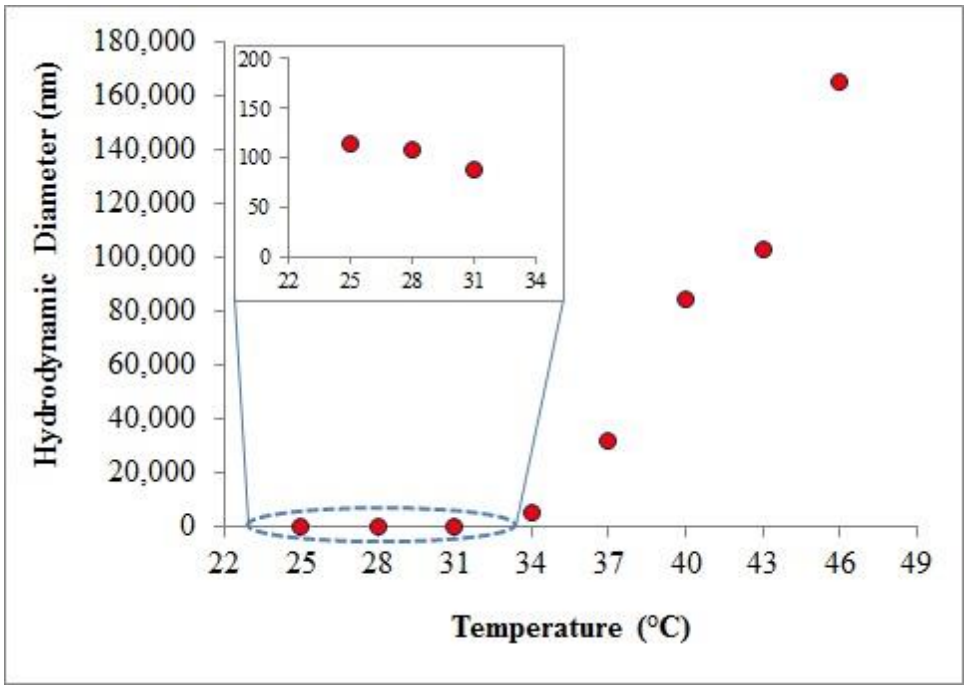

Figure 4.9 Temperature dependence of hydrodynamic diameter of the PDMAEMA-b-PNIPAM copolymers.

The thermogravimetric analysis (TGA) curves of the PDMAEMA and PDMAEMA-b-PNIPAM are shown in Fig. 4.10. The curve of PDMAEMA has a two-step degradation where the first step starting at 264 °C and the second step at 386 °C. It is

hard to determine the weight loss fractions of PDMAEMA and PNIPAM separately by TGA since both polymers degrade thermally in the same temperature range. However, the total weight loss of both polymers can be obtained. For PDMAEMA-b-PNIPAM, a weight loss of around 80 % occurred between 270 and 440 °C, and a total of 5 % remained at 440 °C.

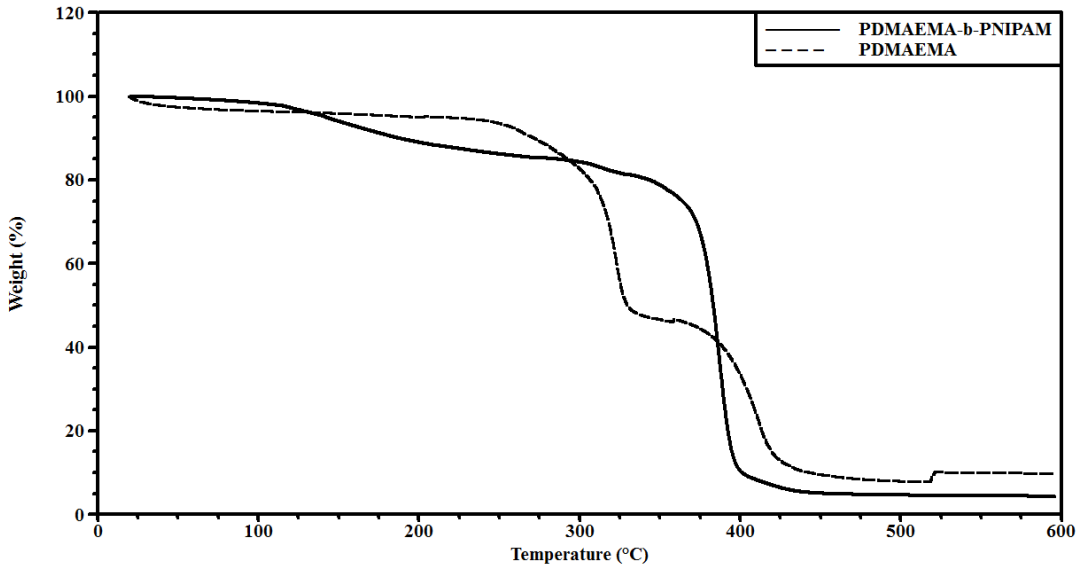

Figure 4.10 TGA traces for PDMAEMA and PDMAEMA-b-PNIPAM copolymer.

The average molecular weights of polymerized homo- and co-polymers were estimated by gel permeation chromatography (GPC) using 10-point PS standards. As shown in Table 4.1, the weight-average molecular weight (Mw) and polydispersity index (PDI) of PS was found to be 13992 Da and 1.10, respectively. The low PDI indicated a contolled/living polymerization. The block copolymers, PS-*b*-PDMAEMA and PS-*b*-PNIPAM had 13648 and 151558 Da Mw and 1.21 and 1.19 PDI, respectively. Mw of

PDMAEMA and PDMAEMA-*b*-PNIPAM showed that major part of the block copolymer was consisted of PNIPAM. PIA had 774 Da Mw over 25 h.

Table 4.1 Molecular weights of homo- and copolymers.

Polymers	Solvent	Temp. (˚C)	Time (h)	Mw	Mn	PDI
PS	Anisole	110	6	13992	12741	1.10
PS-*b*-PDMAEMA	THF	50	14	13648	11300	1.21
PS-*b*-PNIPAM	DCM	25	12	151558	127262	1.19
PDMAEMA	H_2O/PrOH	50	14	907	638	1.42
PDMAEMA-*b*-PNIPAM	H_2O/PrOH	25	17	50667	42699	1.19
PIA	H_2O/PrOH	25	25	774	589	1.31

4.5 Conclusions

The synthesis of stimuli-responsive homo- and diblock copolymers via ATRP that can be used in applications required stimuli responsive behavior were studied. A variety of thermo-responsive block copolymers consisting of PNIPAM, PDMAEMA, and PS and PIA homopolymer were prepared via ATRP. The polymers were characterized by FTIR, DLS, and TGA. The LCST of polymers varied with the polymer composition. In particular, these thermo-responsive copolymers can be used in smart drug delivery devices and other biomedical applications that required a stimuli responsive behavior on a substrate surface.

4.6 Acknowledgements

The Republic of Turkey's Ministry of National Education is acknowledged for financial support. TGA and DLS measurements were made possible by financial support by the National Science Foundation [CBET-0933493; EPS-1006883]. The authors

gratefully acknowledge undergraduate researchers Jasmine Young and Jack Stogner for their assistance in the lab.

4.7 References

1. Qiu, J.; Charleux, B.; Matyjaszewski, K., "Controlled/living radical polymerization in aqueous media: homogeneous and heterogeneous systems," *Progress in polymer science*, **2001**, 26, 2083-2134.

2. Moad, G.; Solomon, D. H., The chemistry of radical polymerization. Elsevier Science Limited: 2006, 1-9.

3. (a) Zhang, J. L.; Srivastava, R. S.; Misra, R. D. K., "Core−Shell Magnetite Nanoparticles Surface Encapsulated with Smart Stimuli-Responsive Polymer: Synthesis, Characterization, and LCST of Viable Drug-Targeting Delivery System," *Langmuir*, **2007**, 23, 6342-6351; (b) Reynolds, A. F.; Hilt, J. Z., "Poly(n-isopropylacrylamide)-based hydrogel coatings on magnetite nanoparticles via atom transfer radical polymerization," *Nanotechnology*, **2008**, 19, 175101.

4. (a) Akiyama, Y.; Shinohara, Y.; Hasegawa, Y.; Kikuchi, A.; Okano, T., "Preparation of novel acrylamide-based thermoresponsive polymer analogues and their application as thermoresponsive chromatographic matrices," *Journal of Polymer Science Part A: Polymer Chemistry*, **2008**, 46, 5471-5482; (b) Aqil, A.; Vasseur, S.; Duguet, E.; Passirani, C.; Benoît, J.-P.; Jérôme, R.; Jérôme, C., "Magnetic nanoparticles coated by temperature responsive copolymers for hyperthermia," *Journal of Materials Chemistry*, **2008**, 18, 3352-3360.

5. Yancheva, E.; Paneva, D.; Maximova, V.; Mespouille, L.; Dubois, P.; Manolova, N.; Rashkov, I., "Polyelectrolyte Complexes between (Cross-linked) N-Carboxyethylchitosan and (Quaternized) Poly[2-(dimethylamino)ethyl methacrylate]: Preparation, Characterization, and Antibacterial Properties," *Biomacromolecules*, **2007**, 8, 976-984.

6. Marvel, C. S.; Shepherd, T. H., "Polymerization Reactions of Itaconic Acid and Some of Its Derivatives," *The Journal of Organic Chemistry*, **1959**, 24, 599-605.

7. Sankhe, A. Y.; Husson, S. M.; Kilbey, S. M., "Effect of Catalyst Deactivation on Polymerization of Electrolytes by Surface-Confined Atom Transfer Radical Polymerization in Aqueous Solutions," *Macromolecules*, **2006**, 39, 1376-1383.

8. Roy, D.; Knapp, J. S.; Guthrie, J. T.; Perrier, S., "Antibacterial cellulose fiber via RAFT surface graft polymerization," *Biomacromolecules*, **2007**, 9, 91-99.

9. Xiong, Z.; Peng, B.; Han, X.; Peng, C.; Liu, H.; Hu, Y., "Dual-stimuli responsive behaviors of diblock polyampholyte PDMAEMA-b-PAA in aqueous solution," *Journal of colloid and interface science*, **2011**, 356, 557-565.

CHAPTER V

MAGNETIC NANOPARTICLES SURFACE MODIFIED WITH DUAL-STIMULI RESPONSIVE BLOCK COPOLYMERS

5.1 Abstract

Superparamagnetic iron oxide (Fe_3O_4) nanoparticles were modified with a pH and temperature responsive block copolymer, polyitaconic acid-*block*-poly(N-isopropylacrylamide) (PIA-*b*-PNIPAM), via surface-initiated aqueous atom transfer radical polymerization (SI-ATRP). Neat and modified MNPs were characterized using ATR-FTIR, XPS, and TEM to discern morphology and chemical composition. DLS and TGA analyses were used to obtain the size distribution and phase transitions in response to temperature and the grafting percentage, respectively. These Fe_3O_4-PIA-PNIPAM nanocomposites have a magnetic core surrounded by a polymer 'shell' that contains contain amphiphilic stimuli responsive blocks. These nanocomposites could be used for separations, data coding, and as delivery vehicles; for example, in biomedical applications these multifunctional nanocomposites could be used for hyperthermic heating, (magnetofection) carrier for therapeutics, proteins, antigens, and DNA, and/or magnetic field flow fractionation.

5.2 Introduction

Nanotechnology has attracted much attention due to its demonstrated improvements to electronic [1], optical [2], magnetic [3], mechanical, and thermal properties, and the opportunities to develop new nano-scale materials and technologies. Nanoparticles (NPs) are ubiquitous, and there are many examples of naturally occurring nanoparticles. Engineered nanoparticles have been produced to have unique dimensions and often with well-defined surface structures and functionality. Among the various nanoparticle types, iron oxide nanoparticles are ideal candidates for applications that benefit from the combination of high specific surface area and superparamagnetism [4]. In addition, magnetic nanoparticles can be targeted to the specific area and separated by external magnets, depending on the particle size and system geometry.

One focus of modern polymeric advanced material research is macromolecular engineering including synthesizing polymers with well-defined compositions, molecular weights, architectures, tailored responsiveness to external stimuli, and multifunctionality [5]. Block, star and graft copolymers are a few examples of these kind of polymers that have a significance role in membrane technology, nanotechnology, drug delivery systems, and thermoplastic elastomers [5]. Numerous polymerization techniques have been used; among these, free-radical polymerization is the most common in industrial production and commercial applications [6]. This technique is versatile, and leads to polymers with high molecular weight under mild reaction conditions [5]. However, the main limitations with this technique, mainly due to unavoidable fast radical termination, are the poor control over molecular weight, broad molecular weight distribution, low degree of end-functionality, and lack of control over the macromolecular architecture.

Atom transfer radical polymerization (ATRP) is a promising method due to its applicability to a broad range of monomers and solvents. In addition, ATRP excels as a robust LRP method to control the molecular weight, precise chemical composition and architecture [5].

The development of biorefineries that produce multiple products, including higher-value chemicals as well as fuels and power, has become significant because this development can help to reduce fossil fuels dependence. For this reason, in 2004, The U.S. Department of Energy (DOE) identified 12 building block chemicals derived from sugars that can serve as key feedstocks for future biorefineries due to their functionality, availability, toxicity, and possible derivatives [7]. These chemicals and their derivatives have potential to be biomonomers used for production of biopolymers. Among these identified building blocks, itaconic acid (IA), generally produced by fungal fermentation of carbonhydrates [8], is one of the most promising and flexible biomonomers [7]. pH-responsive polyitaconic acid (PIA) is a weak polyelectrolyte with two carboxylic acid groups, each with a different pKa value. However, only a few studies on PIA have been performed due to its insolubility in common organic solvents except methanol [9].

Poly(N-isopropylacrylamide) (PNIPAM) is one of the most studied thermoresponsive polymers to be used at the targeted and controlled release applications of drugs due to its lower critical solution temperature (LCST) around 32 °C [10-11]. At temperatures lower than the LCST, PNIPAM is completely soluble in water. Above the LCST, the polymer becomes insoluble and aqueous solutions of PNIPAM become cloudy. It was reported that this phase transition is attributed to the interactions of hydrogen bonds between amide groups and water due to the increase molecular

movements of water at higher temperatures [12-13]. The LCST can be adjusted by copolymerization with another monomer.

In this study, we present the surface-initiated (SI) polymerization of a pH- and thermoresponsive block copolymer from iron oxide (Fe_3O_4) magnetic nanoparticles (MNP) via aqueous SI-ATRP. The block copolymer formed contains a pH-sensitive polyitaconic acid (PIA) block and a thermo-responsive poly(N-isopropylacrylamide) (PNIPAM) block. Chemical composition, structure, size, thermal behavior and morphology of the Fe_3O_4-PIA-PNIPAM were analyzed by FTIR, XPS, DLS, TGA, and TEM.

5.3 Experimental section

5.3.1 Materials

Magnetic iron oxide (Fe_3O_4) nanoparticles with a nominal diameter of 200 nm were produced by Chemicell (Berlin, Germany) with amine functional groups already present on the nanoparticle periphery. N-isopropylacrylamide (NIPAM) (Aldrich, ≥99%), itaconic acid (Acros, 99+%), 2,2-bipyridyl (bpy) (Sigma-Aldrich, ≥99%), 2-bromopropionyl bromide (Aldrich, 97%), triethylamine (TEA) (Sigma-Aldrich, ≥99.5%), copper(I) bromide (Sigma-Aldrich, 98%), toluene (anhydrous, Sigma-Aldrich, 99.8%), 2-propanol (anhydrous, Sigma-Aldrich, 99.5%), sodium hydroxide (Sigma-Aldrich, ≥98%), and water (HPLC grade) were used as received without further purification.

5.3.2 Methods

5.3.2.1 Immobilization of Br-initiator on magnetic nanoparticles

First, 1 mL aqueous solution of an amine functionalized Fe_3O_4 nanoparticles (~25 mg) were added into a Schlenk flask, and then dried under vacuum. Under N_2 atmosphere, 5 mL of triethylamine (83.6 µl, 0.6 mmol)/anhydrous toluene solution was added into the Schlenk flask at ~ 0 °C. After 1-2 minutes, 5 mL of 2-bromopropionyl bromide (52.4 µl, 0.5 mmol)/anhydrous toluene solution was charged dropwise to the Schlenk flask, and the mixture was stirred at room temperature overnight under N_2 atmosphere. The bromine-initiated magnetic nanoparticles were then separated using a 1.32 T permanent magnet. After washing with ethanol and sonication three times, the Br-initiated MNPs were dried under vacuum at room temperature.

5.3.2.2 Surface-initiated polymerization of itaconic acid (IA)

First, the Schlenk flask containing the dried Br-initiated MNPs and a magnetic stir bar was purged with N_2. At the same time, 1 M solution of itaconic acid (IA) (2.602 g, 20 mmol) and 15 mL HPLC water was prepared and then deprotonated with NaOH (1.64 g) to adjust to pH 7. 2,2-bipyridyl (bpy) (62.5 mg, 0.4 mmol) and anhydrous 2-propanol (5 mL) were then added to the mixture, and the mixture was sonicated for 10 min. Three freeze-pump-thaw cycles were followed to degas the mixture and remove dissolved oxygen. Finally, Cu(I)Br (28.7 mg, 0.2 mmol) was added quickly during the frozen state of the mixture, and two additional freeze-pump-thaw cycles were followed. After another 10 min sonication, the polymerization was carried out at room temperature for 13 h. under N_2 atmosphere. After the polymerization, the solution was diluted with water. The

PIA-grafted MNPs were then washed with water three times and isolated by magnetic separation followed by drying under vacuum.

5.3.2.3 Surface-initiated block copolymerization of itaconic acid (IA) and N-isopropylacrylamide (NIPAM)

NIPAM (2.263 g, 20 mmol), and anhydrous 2-propanol/HPLC water (3:1, v/v, total volume 20 mL) were charged to the Schlenk flask containing the PIA-grafted magnetic nanoparticles and a magnetic stir bar. After three freeze-pump-thaw cycles, 2,2-bipyridyl (bpy) (62.5 mg, 0.4 mmol) and Cu(I)Br (28.7 mg, 0.2 mmol) were added quickly. The Schlenk flask was then degassed again with two additional freeze-pump-thaw cycles, followed by a 10 min sonication. The mixture was stirred at room temperature for 6 h. under inert atmosphere. The polymerization was stopped by exposure the flask to air, and the PIA-b-PNIPAM-grafted MNPs were separated by magnetic separation. After washing with ethanol and water at least three times to remove any catalyst, unreacted monomer and ungrafted polymers, the nanoparticles were dried under vacuum.

5.3.3 Characterization

The polymer modified-magnetic nanoparticles were characterized by ATR-FTIR spectroscopy using dry air-purged a Thermo Electron 6700 instrument with deuterated triglycine sulfate (DTGS) detector and KBr beam splitter. A MIRacle-ATR (Pike Technologies) with ZnSe/diamond crystal was used to collect spectra over the wavenumber range of 800-4000 cm^{-1} with the resolution of 4 cm^{-1} and 256 scans. Samples were solution cast from THF onto the ZnSe/diamond crystal. Omnic software (v8.1.10) was used to collect and analyze the spectra.

A PHI 1600 Electron Scanning Chemical Analysis (ESCA) instrument (also known as X-ray photoelectron spectroscopy, XPS) with PHI 10-360 spherical detector and achromatic Mg K_α X-ray source (300 W, 15 kV) was used to gather additional information on the chemical composition and repeat unit structure. The spectrum were collected with PHI Surface Analysis Software (Windows version 3.0, copyright 1994, Physical Electronics Inc.) and analyzed with CasaXPS (version 2.2.88). For the XPS sample preparation, one drop of magnetic nanoparticle solutions was cast onto Si wafers and dried under vacuum at room temperature overnight. The samples were run in triplicate, at a minimum.

The morphologies of the nanoparticles were characterized with a JEOL 2100 200 kV transmission electron microscope (TEM). MNPs were dispersed in DI water, sonicated in an ultrasonic bath for 5 min, and then a droplet was deposited on a copper grid. The water was then allowed to dry.

A ZetaPALS analyzer (Brookhaven Instruments Corporation, BIC) with a laser wavelength of 659 nm was used to measure the mean particle size and size distributions of the magnetic nanoparticles in DI water. Particle size was measured at a 90° angle. Prior to measurements, the samples were sonicated for 10 min and then allowed to stabilize in the cuvette for 10 min prior to data collection. A total of 3 measurements (5 min per measurement) were carried out for particle size determination using the mean number diameter. BIC Particle Solutions software (v2.0) was utilized for data collection and analysis.

A TA Instruments Q-600 simultaneous DSC/TGA (SDT) with the TA Universal Analysis 2000 software (v4.7A) was used to access the grafting percentage of PIA and

PNIPAM polymers. The samples were analyzed from room temperature to 800 °C at a rate of 10 °C/min under 50 mL/min of nitrogen purge.

5.4 Results and discussion

The surface modification of the magnetic nanoparticles with PIA and PNIPAM was performed by surface-initiated ATRP (Figure 5.1). The surface modification of the magnetic nanoparticles with PIA and PIA-b-PNIPAM was confirmed by FTIR. ATR-FTIR spectra of the Fe_3O_4-NH_2 (as received), Fe_3O_4-PIA, and Fe_3O_4-PIA-b-PNIPAM are shown in Fig. 5.2. In the spectrum of Fe_3O_4-PIA, two strong carboxylate anion stretching peaks can be seen clearly at 1543 and 1383 cm^{-1} [14]. The absorbance around 1241 cm^{-1} corresponds to the C-O stretching of the carboxylic acid. It is expected that a characteristic carboxylic acid peak for PIA appeared around 1735 cm^{-1}. According to Sankhe et al., the absence could be explained by anionic form of the acid sites [14]. Figure 5.2a shows the spectrum of Fe_3O_4-PIA-b-PNIPAM. The grafting of PNIPAM was confirmed by the characteristic peaks at 1646 and 1557 cm^{-1} that correspond to the C=O stretching of amide secondary and N-H stretching of amide secondary of PNIPAM, respectively.

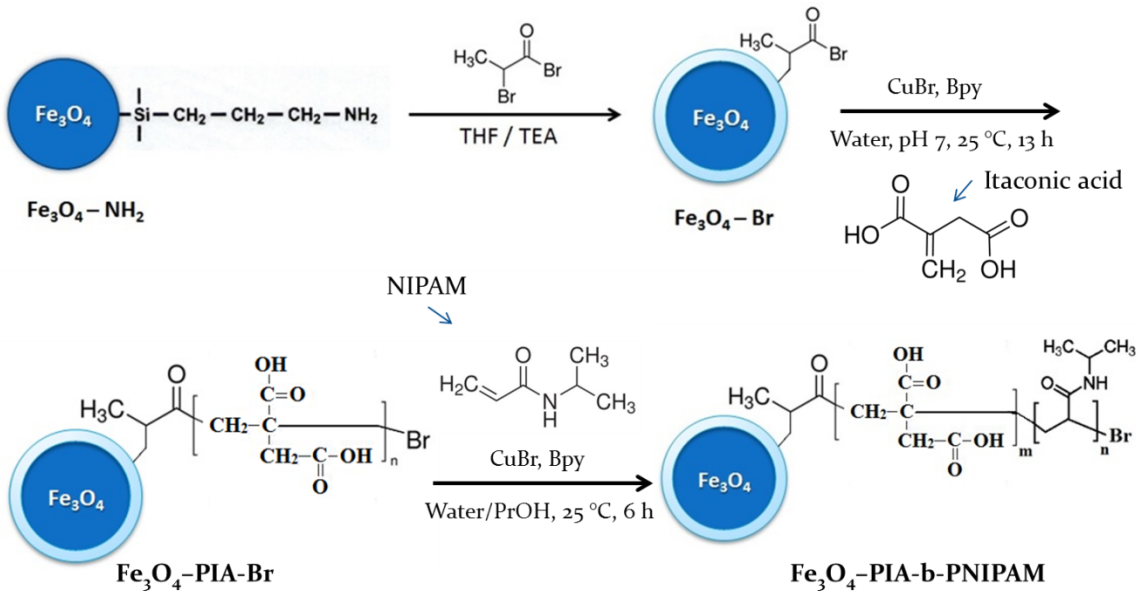

Figure 5.1 Schematic route for the synthesis of Fe_3O_4-PIA-*b*-PNIPAM nanoparticles.

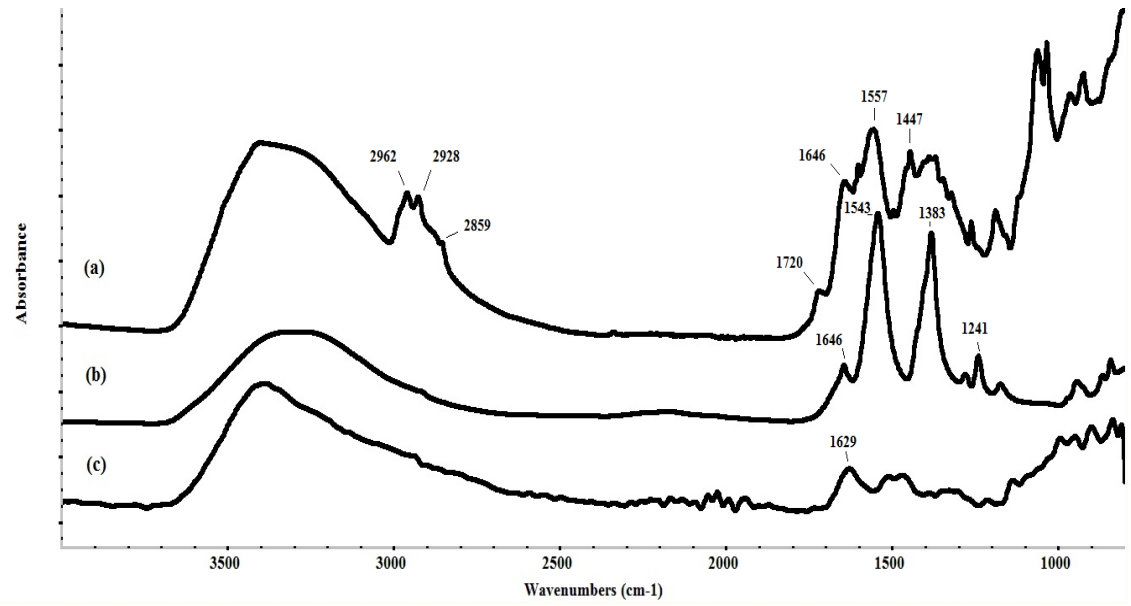

Figure 5.2 FTIR spectra of the Fe_3O_4-PIA-*b*-PNIPAM (a), Fe_3O_4-PIA (b), and Fe_3O_4-NH_2 (c) nanoparticles.

XPS analysis was carried out to characterize the surface composition of Fe_3O_4-PIA-b-PNIPAM. Fig. 5.3 shows representative survey scan spectra of the MNPs before and after the modification, and the atomic percentage of detected elements is presented in Table 5.1. After the surface modification, the atomic concentrations of Fe, O, and Si decreased while that of C increased significantly that indicates the presence of a polymer layer on the MNPs. For XPS, the maximum depth of penetration normal to the surface that photoelectrons are ejected from is approximately 10 nm. Therefore, after the polymer modification the atomic composition mainly consists of elements found in the grafted polymers.

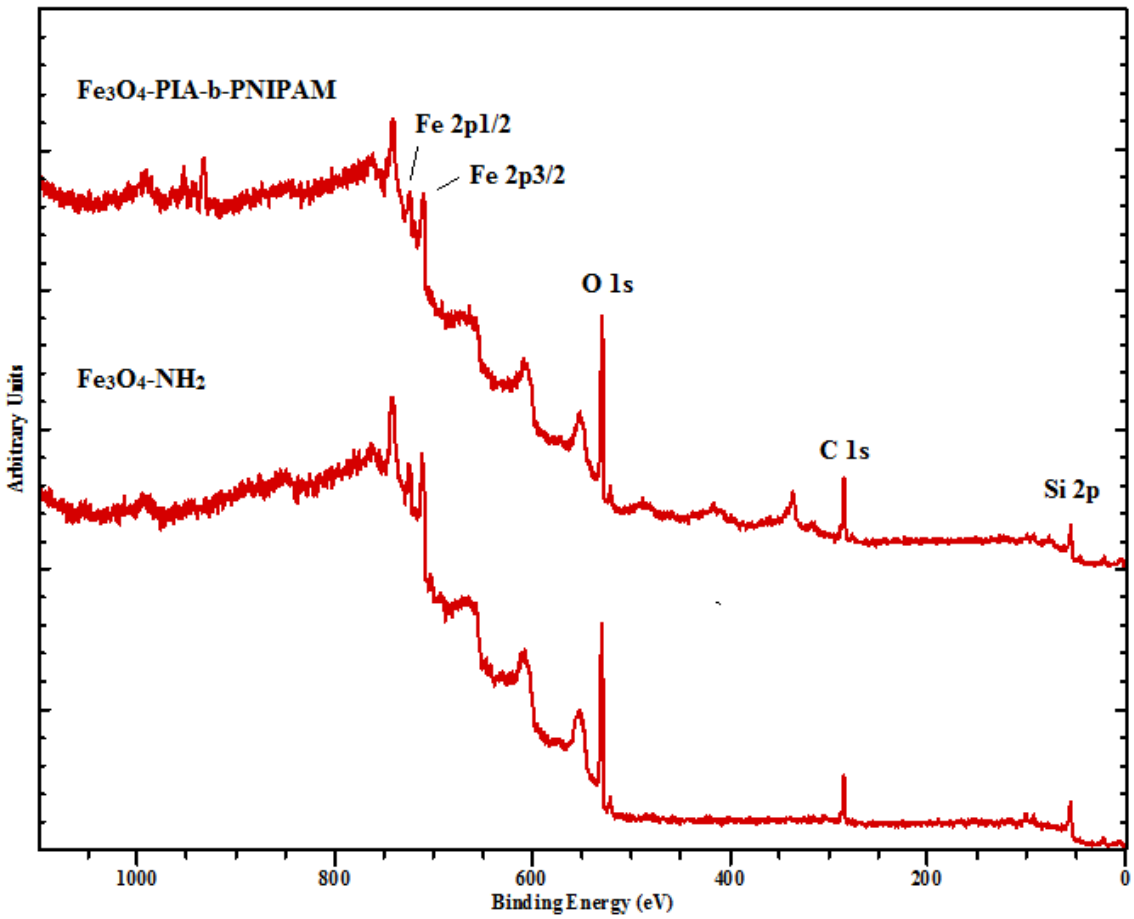

Figure 5.3 XPS survey spectra of the Fe_3O_4-NH_2 and Fe_3O_4-PIA-*b*-PNIPAM magnetic nanoparticles.

Table 5.1 Atomic percentages of the neat and polymer-modified Fe_3O_4 MNPs, as determined by XPS.

Samples	*Fe*	*O*	*C*	*Si*	*O/C*
Fe_3O_4-NH_2	17.7	44.1	29.8	8.4	1.5
Fe_3O_4-PIA-b-PNIPAM	15.0	43.0	38.6	3.4	1.1

DLS measurements were performed to obtain the size distributions of PIA and PNIPAM-modified Fe_3O_4 in water and their thermoresponsive behavior. It is well known

that the PNIPAM has a LCST at 32 °C [10]. It was reported that this phase transition is attributed to the interactions of hydrogen bonds between amide groups and water due to the thermal movement of water at higher temperatures [13]. Therefore, the DLS measurements were conducted from 25 °C to 40 °C. Fig. 5.4 shows the change in the average hydrodynamic diameter (D_h) of the nanoparticles as a function of the temperature. From 25 to 34 °C, a decrease of 20 nm in the size was observed, and the phase transition took place around 32 °C. Besides, the size distribution of nanoparticles became narrower after the modification at 25 and 37 °C (Fig. 5.5).

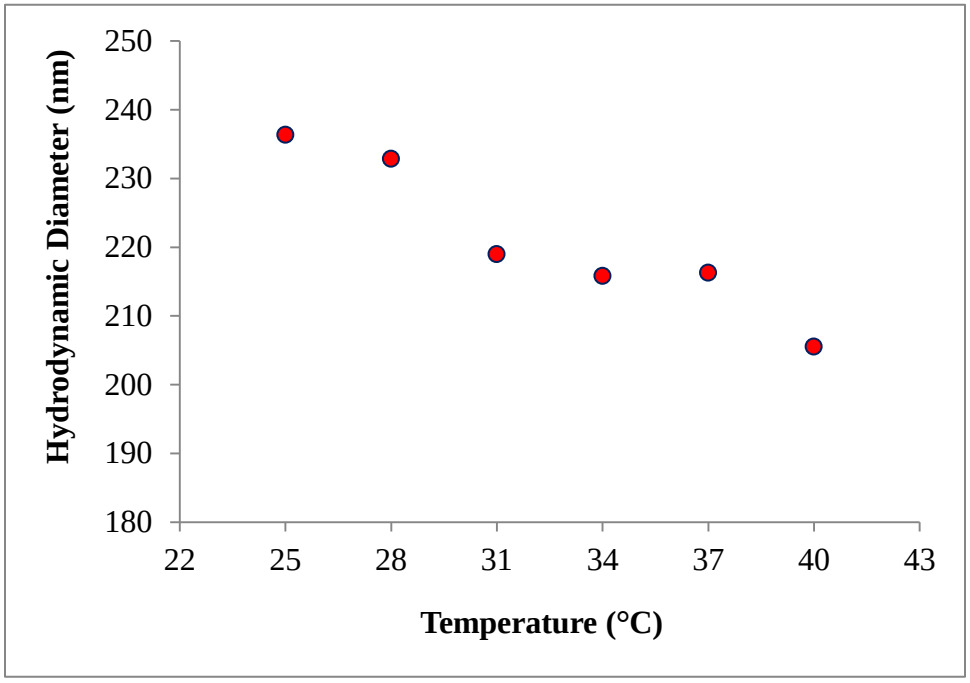

Figure 5.4 Hydrodynamic diameter temperature dependence of Fe_3O_4-PIA-b-PNIPAM nanoparticles.

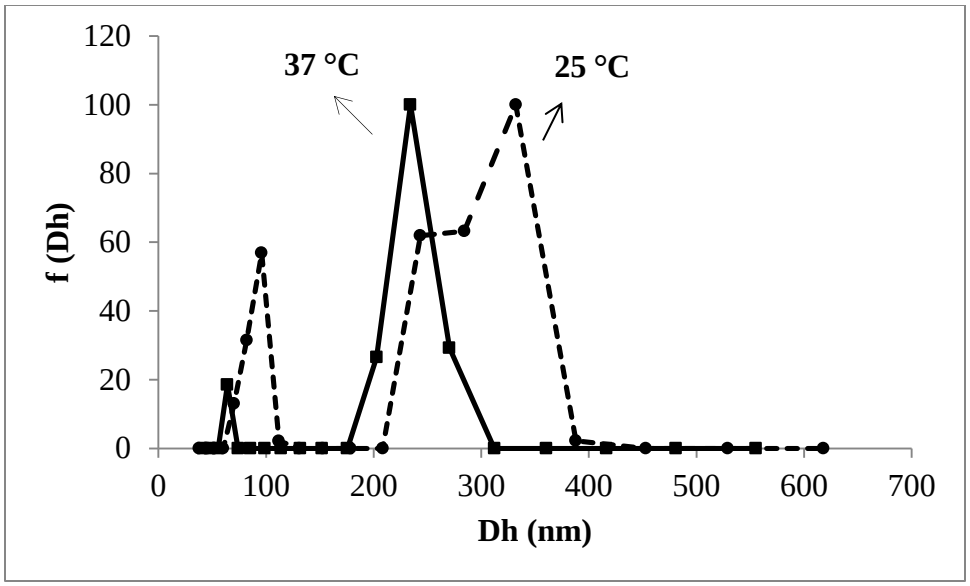

Figure 5.5 DLS size distribution curves of the Fe_3O_4-PIA-b-PNIPAM nanoparticles at 25 and 37 °C, below and above the LCST temperature (32 °C) of PNIPAM.

The thermogravimetric analysis (TGA) curves of the Fe_3O_4-PIA and Fe_3O_4-PIA-b-PNIPAM are shown in Fig. 5.6. The TGA curve of Fe_3O_4-PIA had two stages of weight loss with heating. First, a weight loss of around 7.7% occurred until 400 °C, and then another weight loss lasted until 800 °C at 10.5%. The first weight loss can be accounted for as the loss of the PIA while the second was for the aminosilane present on the iron oxide core. For Fe_3O_4-PIA-b-PNIPAM, three stages of the weight loss were observed by TGA curve. The slow transition between the stages can be due to the overlapping of decomposition temperatures of PIA and PNIPAM. As a result, the percentages of grafting can be calculated to be 10.5 wt.% and 13.9 wt.% for the Fe_3O_4-PIA and Fe_3O_4-PIA-b-PNIPAM nanoparticles, respectively.

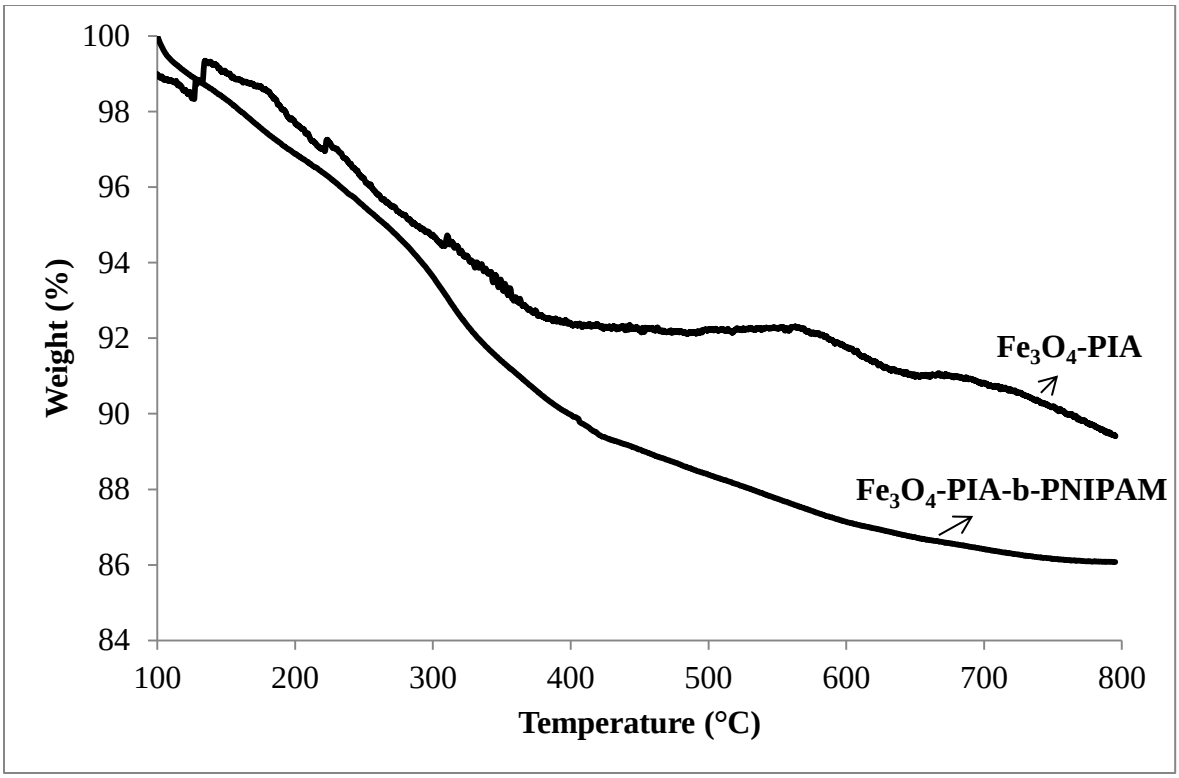

Figure 5.6 TGA curves of the Fe_3O_4-PIA and Fe_3O_4-PIA-*b*-PNIPAM nanoparticles. (Note the noise in the Fe_3O_4-PIA trace is likely due to the small sample size (~ 1 mg) available for this measurement.)

The morphology and size of the amine functionalized and polymer modified MNPs were determined by TEM. As the TEM image of the Fe_3O_4-NH_2 (Fig. 5.7a) shows clearly, the nanoparticles with a multi-domain core are roughly spherical in shape with a particle size of about 200 nm that was claimed by Chemicell. After the homopolymerization of itaconic acid on the surface of MNPs, the TEM image (Fig. 5.7b) show a large butterfly wing-shaped structure attached to one side of the MNPs that may be PIA. If so, this kind of structure may correspond to grafting can be associated with the low content of the initiating groups after the bromine initiation step. After the PIA modification, more well-dispersed and stable MNPs in water were observed, and they

could be separated by an external magnetic separator easily and quickly. Figure 5.7c,d show the TEM images of Fe_3O_4-PIA-b-PNIPAM nanoparticles at two different magnifications. The images show one giant MNP-polymer aggregate with a particle size of about 2 µm. Besides this aggregate, the small, well-dispersed nanoparticles were observed since all nanoparticles were not modified.

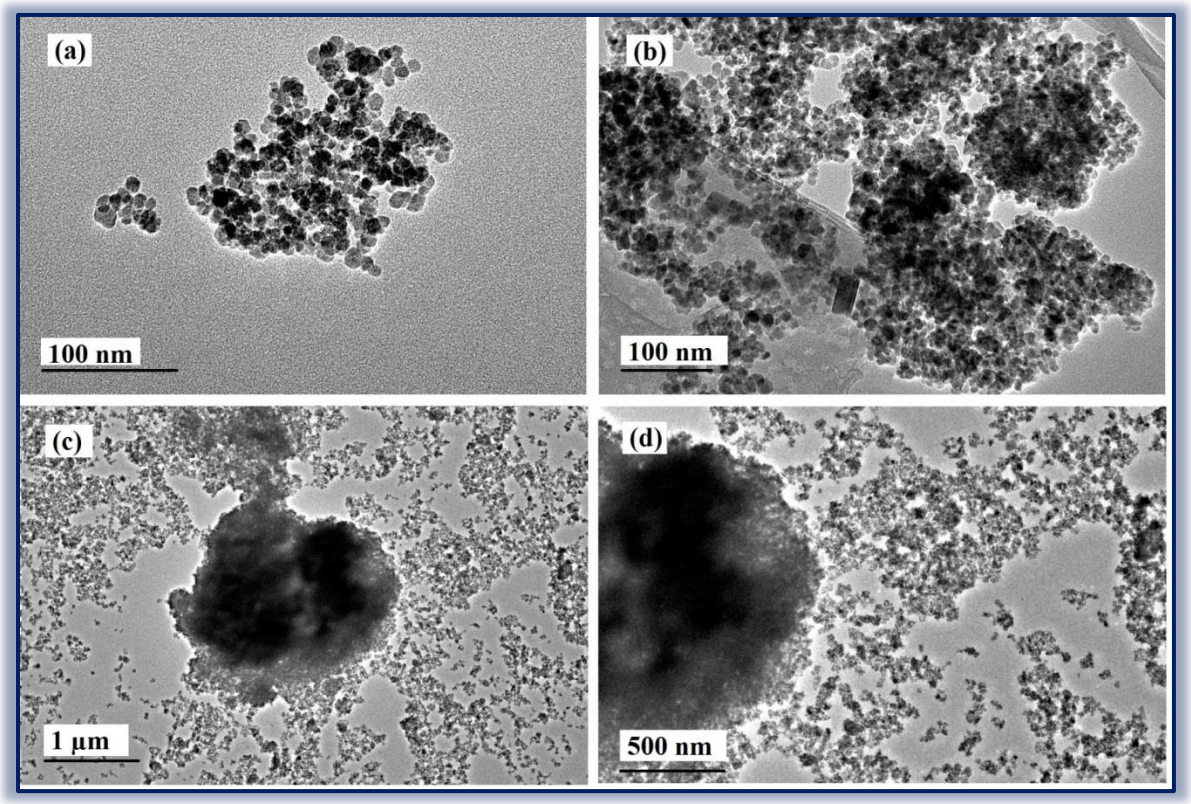

Figure 5.7 TEM images of the Fe_3O_4-NH_2 (a), Fe_3O_4-PIA (b), and Fe_3O_4-PIA-b-PNIPAM (c, d) nanoparticles.

5.5 Conclusions

A pH- and thermo-responsive block copolymer comprised of IA and NIPAM was successfully grown from the surface of iron oxide nanoparticles. TEM image showed that

the morphology of the PIA homopolymer was interesting like a butterfly wing. According to the TGA results, the percentages of grafting of the PIA and PIA-b-PNIPAM nanoparticles were found to be 10.5 wt.% and 13.9 wt.%, respectively. The presence of the weak acidic polyelectrolyte, PIA, could enhance the capability of magnetic nanoparticles in some applications such as controlled drug delivery, and in new biomedical applications as well. The modified MNPs were well-dispersed and stable in water as well as some organic solvents.

5.6 Acknowledgements

The Republic of Turkey's Ministry of National Education is acknowledged for financial support. The authors gratefully acknowledge Dr. I-Wei Chu for TEM imaging.

5.7 References

1. Poizot, P.; Laruelle, S.; Grugeon, S.; Dupont, L.; Tarascon, J. M., "Nano-sized transition-metal oxides as negative-electrode materials for lithium-ion batteries," *Nature*, **2000**, 407, 496-499.

2. Tari, A.; Chantrell, R. W.; Charles, S. W.; Popplewell, J., "The magnetic properties and stability of a ferrofluid containing Fe3O4 particles," *Physica B+C*, **1979**, 97, 57-64.

3. Mahmoudi, M.; Simchi, A.; Imani, M.; Stroeve, P.; Sohrabi, A., "Templated growth of superparamagnetic iron oxide nanoparticles by temperature programming in the presence of poly(vinyl alcohol)," *Thin Solid Films*, **2010**, 518, 4281-4289.

4. Boyer, C.; Whittaker, M. R.; Bulmus, V.; Liu, J.; Davis, T. P., "The design and utility of polymer-stabilized iron-oxide nanoparticles for nanomedicine applications," *NPG Asia Materials*, **2010**, 2, 23-30.

5. Qiu, J.; Charleux, B.; Matyjaszewski, K., "Controlled/living radical polymerization in aqueous media: homogeneous and heterogeneous systems," *Progress in polymer science*, **2001**, 26, 2083-2134.

6. Moad, G.; Solomon, D. H., *The chemistry of radical polymerization*. Elsevier Science Limited: 2006.

7. Werpy, T.; Petersen, G.; Aden, A.; Bozell, J.; Holladay, J.; White, J.; Manheim, A.; Eliot, D.; Lasure, L.; Jones, S. *Top Value Added Chemicals From Biomass. Volume 1-Results of Screening for Potential Candidates From Sugars and Synthesis Gas*; DTIC Document: 2004.

8. Willke, T.; Vorlop, K. D., "Biotechnological production of itaconic acid," *Appl Microbiol Biotechnol*, **2001**, 56, 289-295.

9. Marvel, C. S.; Shepherd, T. H., "Polymerization Reactions of Itaconic Acid and Some of Its Derivatives," *The Journal of Organic Chemistry*, **1959**, 24, 599-605.

10. Zhang, J. L.; Srivastava, R. S.; Misra, R. D. K., "Core−Shell Magnetite Nanoparticles Surface Encapsulated with Smart Stimuli-Responsive Polymer: Synthesis, Characterization, and LCST of Viable Drug-Targeting Delivery System," *Langmuir*, **2007**, 23, 6342-6351.

11. Reynolds, A. F.; Hilt, J. Z., "Poly(n-isopropylacrylamide)-based hydrogel coatings on magnetite nanoparticles via atom transfer radical polymerization," *Nanotechnology*, **2008**, 19, 175101.

12. Akiyama, Y.; Shinohara, Y.; Hasegawa, Y.; Kikuchi, A.; Okano, T., "Preparation of novel acrylamide-based thermoresponsive polymer analogues and their application as thermoresponsive chromatographic matrices," *Journal of Polymer Science Part A: Polymer Chemistry*, **2008**, 46, 5471-5482.

13. Aqil, A.; Vasseur, S.; Duguet, E.; Passirani, C.; Benoît, J.-P.; Jérôme, R.; Jérôme, C., "Magnetic nanoparticles coated by temperature responsive copolymers for hyperthermia," *Journal of Materials Chemistry*, **2008**, 18, 3352-3360.

14. Sankhe, A. Y.; Husson, S. M.; Kilbey, S. M., "Effect of Catalyst Deactivation on Polymerization of Electrolytes by Surface-Confined Atom Transfer Radical Polymerization in Aqueous Solutions," *Macromolecules*, **2006**, 39, 1376-1383.

CHAPTER VI

GRAFTING OF THERMO- AND PH-RESPONSIVE POLYMER BRUSHES FROM MAGNETIC NANOPARTICLES

6.1 Abstract

Superparamagnetic iron oxide nanoparticles were modified with thermoresponsive polymers, poly(N-isopropylacrylamide) (PNIPAM) and poly(2-(dimethylamino) ethyl methacrylate) (PDMAEMA), via surface-initiated aqueous atom transfer radical polymerization (SI-ATRP). Chemical analysis of these polymers was performed using ATR-FTIR. UV-Vis and DSC analyses were used to determine the cloud point. These magnetite hybrid nanoparticles can be used in targeted drug delivery, controllable release, and hyperthermia.

6.2 Introduction

Along with the remarkable development of nanotechnology in recent years, the core-shell nanoparticles have shown a tremendous promise in targeted delivery of drugs and genes in the body [1]. Stimuli-responsive polymers are 'smart' materials which show a measurable change in their properties with environmental stimuli such as temperature, pH, light, magnetic field, moisture, etc. This stimuli responsive behavior can be utilized in a wide range of applications, including "smart" drug delivery, biomedical materials, and even textiles. Moreover, in some cases, several stimuli have been combined to tune

the properties of the responsive polymers in manifold ways. Several biological stimuli including pH, temperature, and redox microenvironment can be exploited for targeted drug and gene delivery applications [2-6]. For instance, the extracellular pH tends to be significantly more acidic (~6.5) in solid tumors compared to the pH of the blood (7.4) at 37 °C [7].

Poly(N-isopropylacrylamide) (PNIPAM) is one of the most studied thermoresponsive polymers with a lower critical solution temperature (LCST) around 32 °C that makes it suitable to be used at the targeted and controlled release applications of drugs [8-9]. At temperatures lower than the LCST, PNIPAM is completely soluble in water. Above the LCST, the polymer become insoluble and aqueous solutions of PNIPAM become cloudy. It was reported that this phase transition is attributed to the interactions of hydrogen bonds between amide groups and water due to the increase molecular movements of water at higher temperatures [10-11]. The temperature of such a transition can be adjusted by copolymerization with another monomer. Another well-studied stimuli responsive polymer is poly(2-(dimethylamino)ethyl methacrylate) (PDMAEMA) that displays dual thermo- and pH-responsiveness. PDMAEMA also has been shown to have potential in antibacterial, hemostatic, and anticancer applications [12].

In this study, we present grafting of pH- and thermo-responsive polymers containing N-isopropylacrylamide (NIPAM) and 2-(dimethylamino)ethyl methacrylate (DMAEMA) from iron oxide (Fe_3O_4) magnetic nanoparticles (MNP) via aqueous SI-ATRP. Chemical composition, structure, and thermal behavior of the modified MNPs were analyzed by FTIR, DSC, and UV-Vis.

6.3 Experimental section

6.3.1 Materials

Magnetic iron oxide (Fe_3O_4) nanoparticles with a nominal diameter of 200 nm were purchased from Chemicell (Berlin, Germany) with amine group already present on the periphery. N-isopropylacrylamide (NIPAM) (Aldrich, ≥99%), 2-(dimethylamino)ethyl methacrylate (DMAEMA) (Aldrich, 98%), ethyl α-bromoisobutyrate (EBIB) (Aldrich, 98%), 2,2-bipyridyl (bpy) (Sigma-Aldrich, ≥99%), 2-bromopropionyl bromide (Aldrich, 97%), triethylamine (TEA) (Sigma-Aldrich, ≥99.5%), copper(I) bromide (Sigma-Aldrich, 98%), neutral alumina (Acros Organics), THF (anhydrous, Sigma-Aldrich, ≥99.9%), toluene (anhydrous, Sigma-Aldrich, 99.8%), 2-propanol (anhydrous, Sigma-Aldrich, 99.5%), diethyl ether (Fisher), petroleum ether (Sigma-Aldrich, ACS reagent), and water (HPLC grade) were used as received without further purification.

6.3.2 Methods

6.3.2.1 General procedure for immobilization of Br-initiator on magnetic nanoparticles

First, 1 mL aqueous solution of amine functionalized Fe_3O_4 nanoparticles (~25 mg) were added into a Schlenk flask, and then dried under vacuum. Under N_2 atmosphere, 5 mL of triethylamine (83.6 µl, 0.6 mmol)/anhydrous toluene solution was added into the Schlenk flask at ~ 0 °C. After 1-2 minutes, 5 mL of 2-bromopropionyl bromide (52.4 µL, 0.5 mmol)/anhydrous toluene solution was charged dropwise to the Schlenk flask, and the mixture was stirred at room temperature overnight under N_2 atmosphere. The bromine-initiated magnetic nanoparticles were then separated using a

1.32 T permanent magnet. After washing with ethanol and sonication three times, the Br-initiated MNPs were dried under vacuum at room temperature.

6.3.2.2 Surface-initiated polymerization of N-isopropylacrylamide (NIPAM)

First, the Schlenk flask containing the dried Br-initiated MNPs and a magnetic stir bar was purged with N_2. NIPAM (2.263 g, 20 mmol) and anhydrous 2-propanol/HPLC water (3:1, v/v, total volume 20 mL) were charged to the Schlenk flask. After three freeze-pump-thaw cycles, 2,2-bipyridyl (bpy) (31.2 mg, 0.2 mmol) and Cu(I)Br (14.3 mg, 0.1 mmol) were added quickly. The Schlenk flask was then degassed again with two additional freeze-pump-thaw cycles, followed by a sonication for 10 min. The mixture was stirred at room temperature for 24 h under inert atmosphere. The polymerization was allowed to proceed for the desired time and then the reaction was stopped by exposure air. The polymer-modified nanoparticles were separated using a permanent magnet. After washing with ethanol and then water at least three times to remove any catalyst, unreacted monomer and ungrafted polymers, the PNIPAM-grafted MNPs were dried under vacuum.

6.3.2.3 Surface-initiated polymerization of 2-(dimethylamino)ethyl methacrylate (DMAEMA)

The Schlenk flask containing the dried Br-initiated MNPs and a magnetic stir bar was purged with N_2. DMAEMA (3.37 mL, 20 mmol), 2,2-bipyridyl (bpy) (15.6 mg, 0.1 mmol) and anhydrous 2-propanol/HPLC water (3:1, v/v, total volume 20 mL) were charged to the Schlenk flask. After three freeze-pump-thaw cycles, EBIB (14.7 µL, 0.1 mmol) was added as a free initiator, and Cu(I)Br (14.3 mg, 0.1 mmol)/Cu(II)Br (2.2 mg, 0.01 mmol) were added quickly. The Schlenk flask was then degassed again with two

additional freeze-pump-thaw cycles, followed by a sonication for 10 min. The mixture was immersed into a pre-heated oil bath at 40 °C and stirred for 48 h under inert atmosphere. The polymerization was stopped by exposure the tube to air, and the polymer-grafted MNPs were removed by magnetic separation. After washing with THF at least three times to remove any catalyst, unreacted monomer and ungrafted polymers, the PDMAEMA-MNPs were dried under vacuum.

6.3.3 Characterization

The polymer modified-magnetic nanoparticles were characterized by ATR-FTIR spectroscopy using a dry air-purged Thermo Electron 6700 instrument with mercury-cadmium-telluride (MCT) detector and KBr beam splitter. A MIRacle-ATR (Pike Technologies) with ZnSe/diamond crystal was used to collect spectra over the wavenumber range of 800-4000 cm^{-1} with the resolution of 4 cm^{-1} and 256 scans. Samples were solution cast from THF onto the ZnSe/diamond crystal.

A TA Instruments Q-2000 modulated dynamic scanning calorimeter (mDSC) with the TA Universal Analysis 2000 software (v4.7A) was used for LCST determination of PDMAEMA-modified nanoparticles. Aqueous MNP solutions were placed in hermetically sealed pans. The samples were first held isothermally for 30 min and then heated from 3 to 80 °C at a rate of 3 °C/min under a 50 mL/min of nitrogen purge.

UV-Vis turbidimetry measurements were performed with a Shimadzu UV-Vis 2550 spectrophotometer coupled with a temperature controller using a 10 mm × 610 mm cell. The absorbances of the aqueous MNP solutions were recorded between wavelengths of 400 and 600 nm as the temperature was increased from 25 °C to 45 °C. Prior to each run, the sample solution was sonicated for 5 min and then equilibrated for 10 min at

controlled temperature. Afterwards, absorbances at a wavelength of 500 nm were analyzed as a function of temperature to determine the cloud point (LCST).

6.4 Results and discussion

The surface modification of the magnetic nanoparticles with PNIPAM was performed by surface-initiated ATRP (Figure 6.1), and was confirmed by FTIR. The ATR-FTIR spectra of the Fe_3O_4-NH_2 (as received) and Fe_3O_4-PNIPAM are shown in Fig. 6.2. The presence of aminosilane on the surface of the as received Fe_3O_4-NH_2 nanoparticles was confirmed by the absorption bands at 3389 cm^{-1} and 1095 cm^{-1} that correspond to the N-H stretching of the $–NH_2$ group and Si-O-Si stretching vibrations. The peaks at 1635 cm^{-1} and 1513 cm^{-1} in the Fe_3O_4-PNIPAM sample are characteristic for PNIPAM and correspond to the C=O stretching of amide secondary and N-H stretching of amide secondary, respectively.

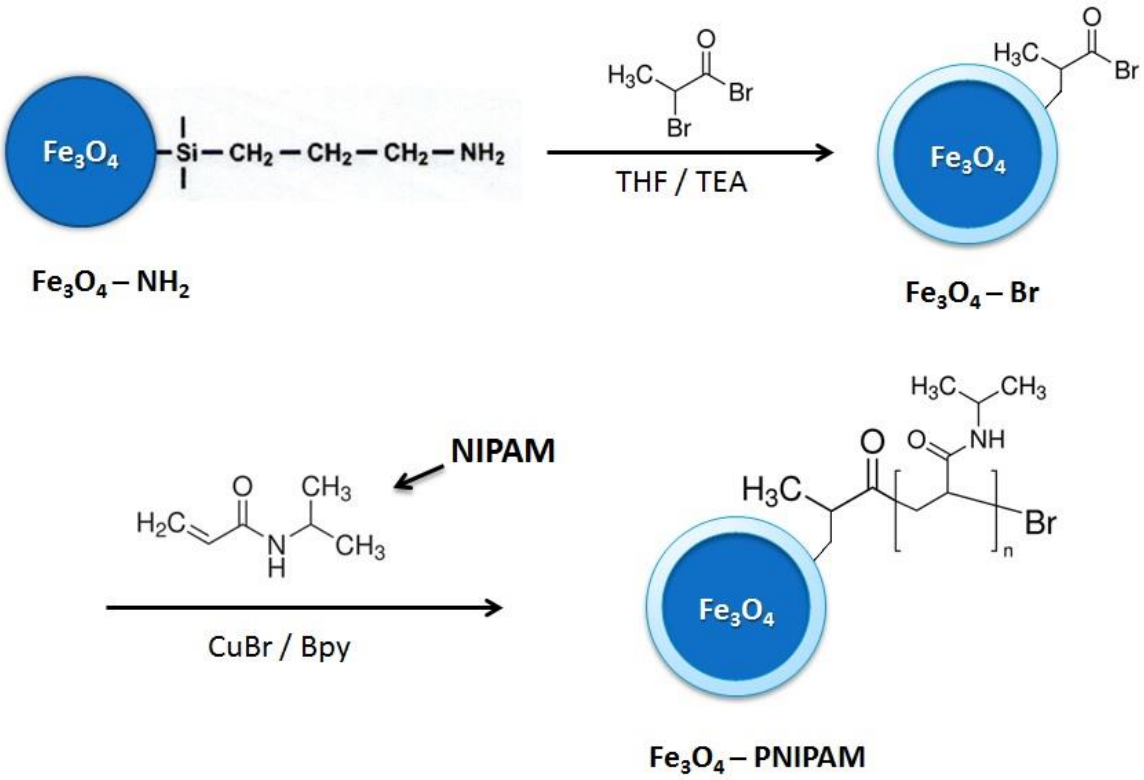

Figure 6.1 Schematic route for the synthesis of Fe_3O_4-PNIPAM nanoparticles.

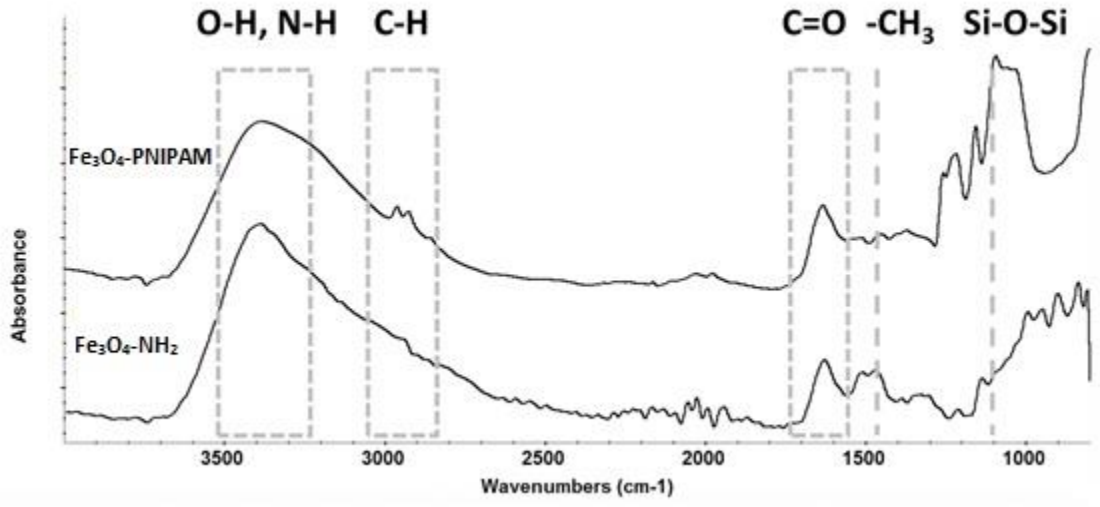

Figure 6.2 FTIR spectra of the Fe_3O_4-NH_2 and Fe_3O_4-PNIPAM nanoparticles.

The UV-Vis measurements were performed to determine LCST of PNIPAM-modified Fe_3O_4 in water. It is well known that the PNIPAM has a LCST at 32 °C [8-9]. It was reported that this phase transition is attributed to the interactions of hydrogen bonds between amide groups and water due to the thermal movement of water at higher temperatures [10]. Therefore to look for an apparent LCST in the Fe_3O_4-PNIPAM sample, UV-Vis measurements were collected from 25 °C to 45 °C. Fig 6.3 shows a sudden change around 37 °C in the absorbance of these nanoparticles as the temperature was increased. At temperatures above the LCST, PNIPAM became hydrophobic which results in the aggregation and eventually precipitation of the nanoparticles. A similar result was reported by Zhou et al. [13]. They obtained a LCST of PNIPAM around 37 °C in the UV-Vis spectra of an aqueous solution of Fe_3O_4@PNIPAM@Au nanocomposites. The observed LCST for PNIPAM shifts away from 32 °C based on the molecular weight and presence of other materials [13].

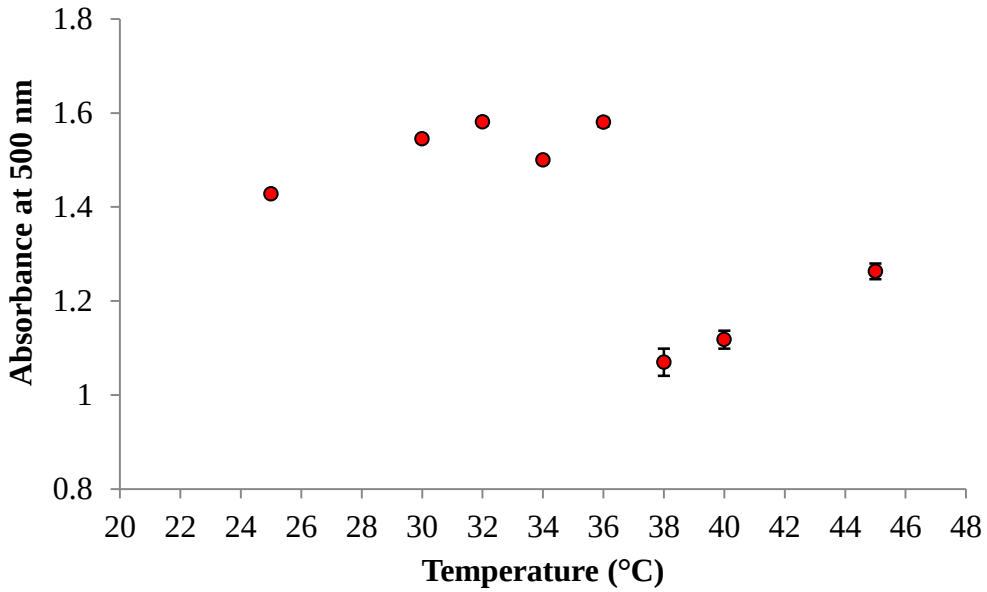

Figure 6.3 UV-Vis absorbance of Fe_3O_4-PNIPAM from 25 °C to 45 °C at a wavelength of 500 nm.

The surface modification of the magnetic nanoparticles with PDMAEMA was also confirmed by FTIR. The ATR-FTIR spectra of the Fe_3O_4-NH_2 (as received) and Fe_3O_4-PDMAEMA are shown in Fig. 6.4. Again, the presence of aminosilane on the surface of the Fe_3O_4 nanoparticles was confirmed by the absorption bands at 3389 cm^{-1} and 1095 cm^{-1} that correspond to the N-H stretching of the $–NH_2$ group and Si-O-Si stretching vibrations. The characteristic peak at 1728 cm^{-1} corresponds to the C=O stretching vibrations of ester in the PDMAEMA grafted onto the surface.

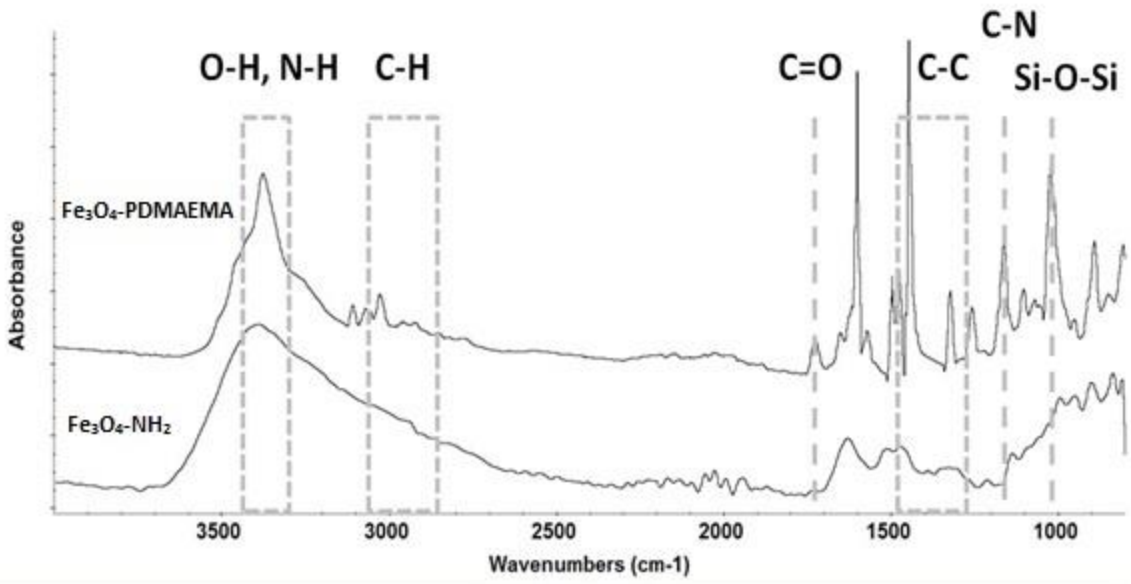

Figure 6.4 FTIR spectra of the Fe_3O_4-NH_2 and Fe_3O_4-PDMAEMA nanoparticles.

Poly(2-(dimethylamino)ethyl methacrylate) (PDMAEMA) is dual pH- and thermo-responsive polymer which has a LCST that is strongly dependent on pH. The LCST of PDMAEMA has been reported at 50 °C [14], with PDMAEMA hydrophobic above the LCST due to the presence of the dimethylamino (pendant) and ethyl (backbone) groups. Fig. 6.5 shows the DSC heating thermograms of PDMAEMA-Fe_3O_4 magnetic nanoparticles, showing an endothermic peak at 50.49 °C during heating. This value is close to the LCST reported for PDMAEMA in the literature [14]. The use of the nanoparticles with this LCST is generally not practical in biomedical applications, such as drug delivery. But might be useful in hyperthermic applications of magnetic nanoparticle where cell death is the goal [10].

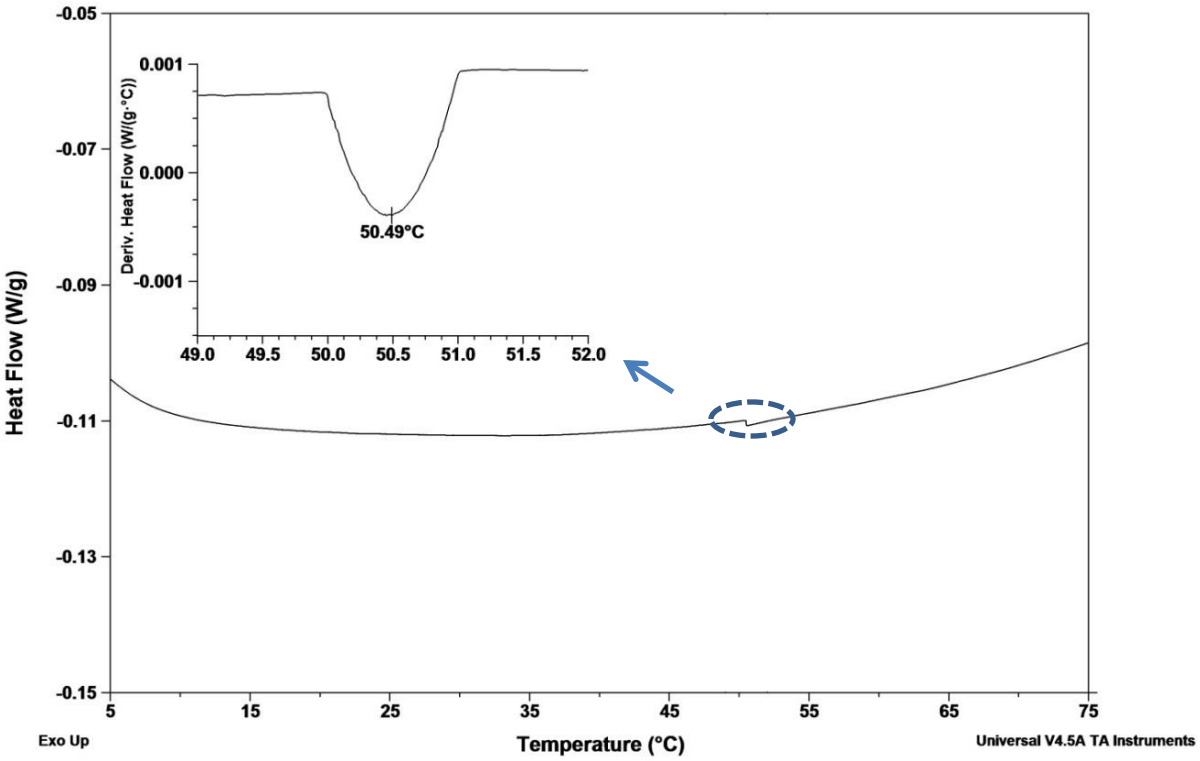

Figure 6.5 LCST determination of the Fe_3O_4-PDMAEMA nanoparticles by DSC.

6.5 Conclusions

Two thermo-responsive homopolymers, PNIPAM and PDMAEMA, were successfully polymerized from iron oxide nanoparticles. The polymers were characterized by FTIR, UV-Vis, and DSC. The LCST of polymers were varied with the polymer composition. In particular, these thermoresponsive polymers can be used in smart drug delivery devices and other biomedical applications that required a stimuli responsive behavior on a substrate surface.

6.6 Acknowledgements

The Republic of Turkey's Ministry of National Education is acknowledged for financial support. DSC, TGA, and DLS measurements were made possible by financial support by the National Science Foundation [CBET-0933493; EPS-1006883]. The authors gratefully acknowledge undergraduate researchers Jasmine Young and Jack Stogner for their assistance in the lab.

6.7 References

1. Couvreur, P.; Vauthier, C., "Nanotechnology: Intelligent Design to Treat Complex Disease," *Pharm Res*, **2006**, 23, 1417-1450.

2. Torchilin, V. P., "Targeted pharmaceutical nanocarriers for cancer therapy and imaging," *The AAPS journal*, **2007**, 9, E128-E147.

3. Shenoy, D.; Little, S.; Langer, R.; Amiji, M., "Poly(Ethylene Oxide)-Modified Poly(β-Amino Ester) Nanoparticles as a pH-Sensitive System for Tumor-Targeted Delivery of Hydrophobic Drugs: Part 2. In Vivo Distribution and Tumor Localization Studies," *Pharm Res*, **2005**, 22, 2107-2114.

4. Shenoy, D.; Little, S.; Langer, R.; Amiji, M., "Poly(ethylene oxide)-Modified Poly(β-amino ester) Nanoparticles as a pH-Sensitive System for Tumor-Targeted Delivery of Hydrophobic Drugs. 1. In Vitro Evaluations," *Molecular Pharmaceutics*, **2005**, 2, 357-366.

5. Shenoy, D. B.; Amiji, M. M., "Poly(ethylene oxide)-modified poly(ε-caprolactone) nanoparticles for targeted delivery of tamoxifen in breast cancer," *International Journal of Pharmaceutics*, **2005**, 293, 261-270.

6. Kommareddy, S.; Amiji, M., "Preparation and Evaluation of Thiol-Modified Gelatin Nanoparticles for Intracellular DNA Delivery in Response to Glutathione," *Bioconjugate Chemistry*, **2005**, 16, 1423-1432.

7. Vaupel, P.; Kallinowski, F.; Okunieff, P., "Blood flow, oxygen and nutrient supply, and metabolic microenvironment of human tumors: a review," *Cancer research*, **1989**, 49, 6449-6465.

8. Reynolds, A. F.; Hilt, J. Z., "Poly(n-isopropylacrylamide)-based hydrogel coatings on magnetite nanoparticles via atom transfer radical polymerization," *Nanotechnology*, **2008**, 19, 175101.

9. Zhang, J.; Srivastava, R.; Misra, R., "Core-shell magnetite nanoparticles surface encapsulated with smart stimuli-responsive polymer: Synthesis, characterization, and LCST of viable drug-targeting delivery system," *Langmuir*, **2007**, 23, 6342-6351.

10. Aqil, A.; Vasseur, S.; Duguet, E.; Passirani, C.; Benoît, J.-P.; Jérôme, R.; Jérôme, C., "Magnetic nanoparticles coated by temperature responsive copolymers for hyperthermia," *Journal of Materials Chemistry*, **2008**, 18, 3352-3360.

11. Akiyama, Y.; Shinohara, Y.; Hasegawa, Y.; Kikuchi, A.; Okano, T., "Preparation of novel acrylamide-based thermoresponsive polymer analogues and their application as thermoresponsive chromatographic matrices," *Journal of Polymer Science Part A: Polymer Chemistry*, **2008**, 46, 5471-5482.

12. Yancheva, E.; Paneva, D.; Maximova, V.; Mespouille, L.; Dubois, P.; Manolova, N.; Rashkov, I., "Polyelectrolyte Complexes between (Cross-linked) N-Carboxyethylchitosan and (Quaternized) Poly[2-(dimethylamino)ethyl methacrylate]: Preparation, Characterization, and Antibacterial Properties," *Biomacromolecules*, **2007**, 8, 976-984.

13. Zhou, L.; Zheng, L.; Yuan, J.; Wu, S., "Synthesis and characterization of thermo-sensitive magnetite-Au nanocomposites," *Materials Letters*, **2012**, 78, 166-169.

14. Cho, S. H.; Jhon, M. S.; Yuk, S. H.; Lee, H. B., "Temperature-induced phase transition of poly (N, N-dimethylaminoethyl methacrylate-co-acrylamide)," *Journal of polymer science Part B: Polymer Physics*, **1997**, 35, 595-598.

CHAPTER VII

CONCLUSIONS AND RECOMMENDATIONS

7.1 Conclusions

7.1.1 Properties of renewable bioplastics

Blend films of PLA with PTM with various ratios (5, 10, and 20 wt.%) were prepared via solvent casting. Partially miscible blends exhibited Young's modulus and elongation-to-break values that significantly extend the applications for PLA. For example, PLA with 10 wt.% PTM demonstrated tensile strength comparable to polyamide-imide, a Young's modulus that exceed polyamide-imide, and elongation-to-break greater than polypropylene, polycarbonate, and nylon 6 [1]. The macroscale Young's modulus values obtained by conventional tensile testing were compared to the nanoscale Young's modulus values from AFM PeakForce Quantitative Nanomechanical (QNM) mode. Young's modulus values from AFM were found to be 2.89 GPa and 7.21 GPa at 5 wt% and 10 wt% PTM. AFM Peak Force QNM mode is a powerful tool to estimate surface mechanical properties of materials, and examine micro- and nano-scale mechanical properties, in concert with topography and phase analyses. The second part of the bioplastics study involved hydrolytic degradation of two bioplastics, PTM and PTI, and subsequent nanomechanical testing of the degraded PTM and PTI. Young's modulus of the PTI decreased from 4.3 GPa to 1.8 GPa over 10,000 min degradation. DSC studies showed hydrolytic degradation induced crystallinity for PTI.

7.1.2 Synthesis of stimuli-responsive polymers via ATRP

Stimuli-responsive polymers were combined with magnetic nanoparticles to produce multifunctional pH-, thermo-, and magneto-responsive nanocomposites. Bromine-initiators were initially immobilized on the surfaces of the amine functionalized magnetite (Fe_3O_4) nanoparticles, and stimuli-responsive polymers including PNIPAM, PDMAEMA, and PIA were grafted via surface-initiated aqueous atom transfer radical polymerization (SI-ATRP). The thermo-responsiveness of the grafted polymers was investigated using DLS, UV-Vis, and DSC. To the author's knowledge, the grafting of PIA from the surface of magnetic nanoparticles was performed here for the first time. The PIA and PIA-*b*-PNIPAM-coated MNPs were well-dispersed and stable in water and propanol. PIA layers reached a thickness of 13 nm in 13 h of polymerization. The DLS size measurements for PNIPAM revealed a polymer thickness of approximately 23 nm that was reached after 6 h. In another study, a variety of stimuli-responsive bulk block copolymers were synthesized. In particular, these thermo-responsive polymers can be used in smart drug delivery devices, primarily as carrier particles for biomaterials such as cells, proteins, antigens, and DNA in magnetofection, and other biomedical applications that required a stimuli responsive behavior on a substrate surface.

7.2 Recommendations

7.2.1 Properties of renewable bioplastics

This research provided an understanding of the miscibility limits for blends of PLA with a novel bioplastic, PTM, with the goal of improving mechanical properties of PLA. The effects of hydrolytic degradation on the molecular weight and mechanical

properties were also described. Based on these results, the following are recommendations for future work.

1. PLA and PTI blends were briefly investigated studied. Alternative synthesis and blending methods could be used to prepare PLA/PTI nanocomposites with well-dispersed PTI.
2. Miscible PLA/PTM blend films were prepared via solvent casting as part of this research. In order to improve properties, copolymerization of these two polymers can be performed. Also, commercial block copolymers such as PS-*b*-PAA, PS-*b*-PEG, and PS-*b*-PMMA can be used as compatibilizer in the blends.
3. These polymers are bio-based plastics, and it is anticipated that they are biocompatible and non-toxic. However, a cell toxicity analysis should be carried out on these bioplastics and their blends.

7.2.2 Synthesis of stimuli-responsive polymers via ATRP

A preliminary investigation was performed to study the synthesis and responsiveness of the stimuli-responsive polymers as either bulk polymers or graft polymers on MNPs. In order to adapt them to the real applications, a more extensive investigation is necessary. The following recommendations as future work are presented.

1. Polymerization of itaconic acid was not complete, expanded study is needed to optimize catalyst/ligand/solvent combinations and temperatures. Polymerization kinetics can be monitored with GPC, DLS, and NMR to better understand the mechanisms. Its pH-responsiveness is needed to be fully investigated. The copolymers, hydrogels, and/or composites of PIA

with other sensitive polymers and grafting of it from a variety of substrates would provide well-designed/defined materials for many applications.

2. Phase transfer of thermo-responsive polymer-grafted MNPs between aqueous and organic phases can be studied. This would allow storing them in a desired solvent for a long time. UV-visible spectroscopy can be used to determine the concentration change of the particles in the solution during the transfer.
3. The findings and experience on ATRP synthesized stimuli-responsive polymers can be used to prepare/construct materials with required architecture and properties for specific applications, such as clean energy and hydrogen production/storage. The materials produced in this study also need to be tested for drug delivery.

7.3 References

1. Matweb: Material Property Data.
http://www.matweb.com/reference/tensilestrength.aspx (accessed June 19, 2013).

APPENDIX A

PROCEDURES

A.1 General polymerization procedure for bioplastics via polycondensation (adapted from [1])

A.1.1 Materials

- Alcohol monomer (1,3-propanediol 98%)
- Acid monomer (malonic acid 98% or itaconic acid 98%)
- Catalyst (aluminum chloride 99%)
- 1 x 100 mL round bottom flask with 24/40 neck
- 2 large septum for 24/40 necked flask
- 1 x 0.75” magnetic stir bar
- 1 silicone oil bath rated to at least 180 °C
- 3 barb to luer lock fittings
- 4 x 18 gauge needles
- Tubing rated for up to 200 °C and vacuum (at least 2 ft)
- 1 x 500 ml round bottom flask with 24/40 neck (condenser)
- 1 x 24/40 vacuum adapter
- 1 small insulated cooler for ice bath
- Liquid nitrogen
- Dual bank manifold set-up for vacuum and dry nitrogen
- Dry nitrogen gas cylinder
- 3 spatulas
- 1 disposable glass pipette and bulb
- 2 glass 100 mL beakers
- Denver APX-100 Analytical balance

- Weigh dishes

A.1.2 Procedure

Before starting the polymerization, calculate the amount of each monomer and catalyst used. This procedure was written for a 50 g charge of monomer. It can be scaled up.

1. Set oil bath at desired temperature.
2. Put liquid nitrogen into liquid nitrogen trap on vacuum manifold system.
3. Equip a 500 mL round bottom flask with a septum.
4. Immerse the 500 mL round bottom into ice bath.
5. Connect tubing to vacuum manifold.
6. Run tubing to condenser.
7. Put a male Luer lock fitting on the end of the tubing running from the vacuum manifold.
8. Put a 18 gauge needle on the end of tubing with Luer lock fitting.
9. Put the needle into the septum on top of 500 mL vacuum flask.
10. Take a second piece of tubing and put Luer lock fitting and 18 gauge needle on both ends and put one end into the 500 mL round bottom flask.
11. Weigh the 100 mL round bottom flask, stir bar, acid monomer, and alcohol monomer using the spatula and pipette with bulb.
12. Put stir bar, acid monomer, and alcohol monomer in flask.
13. Put a septum onto the 100 mL round bottom flask.

14. Connect the 100 mL round bottom flask to the other end of the piece of tubing running from the 500 mL flask.
15. Put a second needle into the 100 mL round bottom flask that vents to the atmosphere.
16. Purge the system with dry nitrogen for 5 min, while not in the oil bath.
17. Weigh out appropriate amount of catalyst with 5% extra to allow for deactivation during transfer to round bottom flask.
18. Turn off nitrogen purge, remove the 2nd needle in the 100 mL round bottom, and turn on vacuum. The reaction set-up should look like Figure A.1 after the 2nd needle is removed and vacuum is turned on.
19. Put catalyst into 100 mL round bottom flask and remove needle that vents to atmosphere.
20. Put flask under vacuum and place flask into oil bath.
21. Leave flask in oil bath for predetermined reaction time.
22. When reaction time is complete, remove flask from oil bath and remove needle that connects the flask to the vacuum system.
23. Place flask into ice water to cool for 10 min to quench the reaction.

A.1.3 General polymer purification procedure for bioplastics project

A.1.3.1 Materials

- Buchner funnel
- Erlenmeyer flask with 24/40 ground glass joint
- 24/40 vacuum adapter

- Grade 40 Whatman ashless filters of appropriate size to fit Buchner funnel
- Aspirator
- 500 mL Griffin beaker
- Reacted polymer in 100 mL round bottom flask
- 98%+ chloroform
- 98% diethyl ether
- Petri dish top and bottom
- Denver APX-100 Analytical balance
- Magnetic stir plate
- Vacuum system with liquid nitrogen trap
- Vacuum oven
- Spatulas

A.1.3.2 Procedure

1. Assemble Buchner funnel, Erlenmeyer, and vacuum adapter.
2. Connect to aspirator.
3. Weigh out 4 filters of appropriate size to fit Buchner funnel.
4. Weigh petri dish top and bottom separately.
5. Put 50 mL of chloroform into 100 mL round bottom flask that has polymer in it.
6. Allow to dissolve polymer.
7. Pour out chloroform into Griffin beaker.

8. Using a spatula, remove polymer still in round bottom flask.
9. If necessary, repeat steps 4-7 to remove all polymer.
10. Take stir bar from round bottom flask and put it into the Griffin beaker.
11. Once all polymer is out of round bottom flask, pour diethyl ether into Griffin beaker to make a 5:1 to 10:1 solution of diethyl ether to chloroform.
12. Place Griffin beaker on stir plate and stir vigorously for at least 10 min to allow for polymer to precipitate.
13. Put a filter into Buchner funnel.
14. Turn on water to aspirator.
15. Carefully pour diethyl ether/chloroform/polymer solution through filter.
16. Change filter as needed (it will normally take all 4 filters to filter once, but at times it will take up to 12, depending on polymer).
17. Keep filters separate from purified polymer as they have a tendency to become entrapped in polymer during drying.
18. Once the solution has been filtered, dispose of the solution in the harmful hazardous waste container.
19. Put the filters and purified polymer into vacuum oven.
20. Put liquid nitrogen into vacuum system liquid nitrogen trap.
21. Close the vacuum oven and turn on the vacuum.
22. Pull maximum vacuum.
23. Leave polymer in vacuum oven for at least 24 h at room temperature.

24. Increase temperature in vacuum oven to 40 °C and leave polymer under elevated temperature and vacuum for at least 24 h (this should be extended if there is more than 60 g of polymer in the vacuum oven at the same time or if the polymer appears to still be partially solubilized after 48 h. To determine if polymer is still losing solvent and needs to be dried longer, periodically weigh the petri dish with polymer and continue drying until the dish is losing minimal weight).
25. After polymer has had solvent removed, weigh petri dish with polymer.

A.2 Compression molding procedure for neat bioplastics and bioplastic blends (adapted from [1])

A.2.1.1 Materials

- Polymer
- Hot gloves
- Spatula
- Hammer (if needed)
- Knife or screwdriver (if needed)
- Shims or mold
- 2 x aluminum plates 12” x 12”
- Silicon release spray

A.2.1.2 Procedure

1. Turn on the power to the compression molder by switch on the wall to the right of the instrument.
2. Turn on the instruments main power with the red switch on the right hand side of the instrument.
3. Turn on the power to the hydraulic pumps by switching the right rocker switch on the instrument panel to on.
4. Turn on the power the heated platen by switching the left rocker switch on the instrument panel to on.
5. Set the temperature to the upper and lower platen use their individual controllers by pressing the right most button on each temperature controller once.
6. Use the up and down buttons to set the temperature.
7. Press the right most button again to confirm set point
8. To set pressure, switch to manual mode by pressing “man” on the right control panel.
9. Then press “set” 3 times to get to force setting in pounds.
10. Use the up and down arrows to select appropriate force.
11. Press “man” to confirm.
12. Allow platen and mold to come to equilibrium.
13. Place material in mold.
14. Allow the material to melt for 5 min (blends).

15. Press the two large green buttons at the same time and hold until pressure is reached.
16. Let press sit until time is complete.
17. Press red button and remove mold.
18. Turn on the water at the spigot on the right wall or the compressed air from back.
19. Cool the mold to room temperature (ice bath can be used to cool faster).
20. Carefully remove sample from mold once cooled (use hammer and knife/screwdriver if needed).

A.3 GPC procedure (adapted from [1])

Water GPC system with a Water 2414 refractive index detector, Waters 1515 isocratic HPLC pump, Waters 717plus autosampler, column heater, Waters Styragel HR 5E, 4E and guard column. The system is run at 0.3 mL/min of Optima tetrahydrofuran at 30 °C. The GPC should always be running in recycle mode at 0.1 mL/min of tetrahydrofuran (THF).

A.3.1 To start the GPC

1. Turn on the computer, auto-sampler (switch on front), column heater (switch on back), isocratic pump (switch on left side), and refractive index detector (RID) (switch on front).
2. Once the computer is on, start the Breeze software (it will take the software 5 min to start).

3. Turn on solvent recycle by pressing “shift” than “3/recycle” on the RID front control panel.
4. Set the temperature to 30 °C by pressing “Temp” on the RID control panel, and then type 30 in the cell for the detector and column heater.
5. On the Breeze software, open the correct experimental set-up by going to “View Method”. Then go to file menu and select open. Open the appropriate experimental file.
6. Set the flow rate to 0.1 ml/min by going to the panel on the screen that shows flow rate and pressure (this should always be on the screen). Click on the flow rate and set to 0.1 mL/min.
7. The system is now set in stand-by state.

A.3.2 Sample preparation

1. The GPC is setup to run THF, so the samples will be dissolved in Optima THF.
2. Weigh out 4 to 8 mg of sample (ask your supervisor which weight to weigh out because it will be sample dependent due to different Mw materials have different viscosity responses).
3. Add 4 mL of Optima THF to make the samples concentration to be between 1 and 2 mg/mL (if there is a small amount of material (~1mg), just add 1 mL of Optima THF).

4. Let the samples dissolve for 4 to 24h (Longer solution times are better. If the sample is not dissolving, put samples into sonication bath for extended period of time.).
5. Get a clean, 1 mL, snap vials (enough for all of your samples), a disposable needle (maybe pink one, thick), and a glass syringe for the next steps.
6. Get 2 beakers and put just enough Optima THF in one to rinse the syringe 3 times between each sample, and use the 2nd beaker for waste.
7. Put a clean needle on the syringe (be comfortable with holding the syringe before use).
8. Rinse the syringe and needle three times with Optima THF.
9. Draw your sample out of vial.
10. Carefully remove the needle from the syringe with the sample in the syringe.
11. Put a syringe filter on the syringe (repeat filtration three times if material may contain any catalyst).
12. Slowly depress the plunger to push the sample though the filter and into a clean vial.
13. Dispose of the filter and the needle (the needle goes into a sharp container).
14. Repeat steps 7 through 12 for each sample.

A.3.3 Running samples

1. Get the carousel out of the auto-sampler by opening the door on the front of the auto-sample and wait until the auto-sampler releases the carousel.
2. Put the 1 mL, snap vials into slots starting at 1, and keep track of which slot which sample is in the carousel.
3. Put the carousel back into the auto-sampler and close the auto-sampler's door.
4. Go to the Breeze program and open the "Sample Queue."
5. The first column is slot number, and the second column is sample name. Put your sample names into the second column.
6. The third column is function, select broad sample from the drop down list on this column.
7. Fourth column is the method, and select the correct method from the drop down menu on this column.
8. In the next 2 columns, set the run time to 32 min and the injection volume to 30 µL.
9. Set the first row to equilibrate the system for 60 min before running samples.
10. Once this is done for all samples, click on run in lower left hand corner.
11. The program will prompt for a set name, enter the sample sets name.
12. Click run.

13. Ensure that flow rate increases to 0.3 mL/min and that recycle turns off when the first blank runs. (This happens when the computer has been on too long).
14. If the flow rate does not increase and/or recycle does not turn off, click stop in the lower left hand corner and select stop immediately.
15. Save your sample set by going to the file menu and selecting "save sample set."
16. Close the program and turn off the GPC by switching the 4 switches on the GPC system to off.
17. Restart the GPC by following the "To start GPC procedure" above and then repeat the above steps except open your sample set by going to file menu and "open sample set".

A.3.4 Analysis of data

1. During or once the sample set is completed, go to "Find Data" window.
2. Go to channels tab and click "Update" on the top tool bar.
3. The completed runs should be showing, highlight the samples to be analyzed.
4. Right click and then click "Review" (this will take you to the "View Data" window).
5. To manually integrate the peaks, zoom in on the peak of interest by left clicking on the GPC trace and making a box around the peak of interest.
6. Left click at the start of the peak and drag to end of peak.

7. If more than one peak, repeat step 6 for multiple peaks.
8. To quantify the peak, go to the top tool bar and find the 8th button from the right. Click this button, and the peaks retention time will change to the molecular point.
9. To view Mw, Mn, and other properties, go to the 3rd button from the right on the top tool bar and click it.

A.3.5 Export data (Mw, Mn and other parameters)

1. Go to "Find Data."
2. Click on the "Results Tab."
3. Highlight the samples of interest
4. Right click and select "Export Data."
5. There are several export methods, select "Exporting 2."
6. The data will export to Eport file on the desktop
7. Open the file and copy-paste into an Excel file.

A.3.6 Export raw data (chromatogram)

1. Go to "Find Data."
2. Click on the "Channels" tab.
3. Highlight data of interest.
4. Click on "Database" on the file menu bar
5. Click "Export."

6. A window will appear and click “By-Pass Export Methods.”
7. Select a file to save the data to.
8. Click “Export.”
9. Open the file and copy-paste into an Excel file.

A.3.7 GPC calibration

This is a relative calibration using 10 polystyrene standards:

1. Prepare calibration standards by following “Sample Preparation” method above.
2. Run the samples following the “Running Samples” method above, except change function from broad sample to broad standard or narrow standard.
3. Once the standards have been run, got to “Find Data” and highlight the standards.
4. Right click on standards and select “Alter Sample” this will open the alter sample window.
5. Highlight the standards in the alter sample window.
6. Got to “Edit” in the tool bar above the samples and select “Components” and this will bring up the components editor window.
7. Click on “Current Sample” tab at the bottom of components editor widow.
8. Go to the “Moments” tab.
9. Enter the Mw, Mn, and Mp into the correct cells (the Mw, Mn, and Mp can be found on the standards) or only the Mp for narrow standards.

10. Once all of the standards components have been entered, click “Ok” at the bottom of the components editor window.
11. Click save in the alter sample window and then “Ok.”
12. Highlight the standards in the “Find Data” window.
13. Right click on the highlighted standards and select “Review.”
14. Manually integrate the peaks by left clicking start of the peak on the GPC trace and dragging to the end of the peak.
15. Then click the 7th button from the left on the upper tool bar (calibrate button)
16. Repeat for all standards.
17. To save the calibration, go to file menu then scroll over “Save” and click on “Calibration.”
18. The calibration is now complete and saved.

A.3.8 Trouble shooting procedures

Auto zero offset excessive (value out of range):

1. Press the DIAG key on the detector’s front panel.
2. Then, press 5 to access the other diagnostics.
3. Press 1 for Auto Zero offsets from the list.
4. Reset the auto zero offset to zero by pressing Cancel (Shift 0).
5. Then, press Home button.
6. To purge the detector, next to the pump flow rate there are three buttons, click the middle button.

7. Follow the directions given by the software.
8. Max flow rate is 0.5 mL/min for purging the auto-injector and RID.

A.4 MIRacle-ATR FTIR procedure (adapted from [1])

On a Thermo Electron corporation Nicolet 6700 FT-IR with a helium-neon laser, a mercury-cadmium-telluride (MCT) detector or a deuterated triglycine sulfate (DTGS) detector, a MIRacle-ATR (Pike Technologies) with ZnSe/diamond crystal using Omnic 8.1.10 software (copyright 1992-2009, Thermo Fisher Scientific Inc.).

A.4.1 Clearing water from drip leg

1. Ensure the wash sink is clear of glassware.
2. Get ear plugs for everyone in the lab
3. Go the yellow handle valve above the GPC that is on the main compressed airline for the lab.
4. Close the yellow handle valve.
5. Slowly open on the red handle valve directly below it.
6. Compressed air, with any water that had pooled in the drip leg, will now flow into the wash sink.
7. When the compressed air shows no indication of water, close off the red handled valve and open on the yellow handled valve.

A.4.2 Filling liquid nitrogen dewar on MCT detector

1. On the left side of the instrument, open the front most circular lid above where the detectors are located in the instrument.
2. Remove the black plug.
3. Put in the funnel with a metal stem and expanded polystyrene spacer gently into where the black plug was located.
4. Carefully pour a small amount of liquid nitrogen into the funnel and allow the funnel and dewar to cool for 2 min.
5. Gently pour liquid nitrogen into the dewar until it over flows.
6. Let the funnel warm up while in the dewar to avoid breaking it when taking it out.
7. Remove the funnel, and carefully replace black plug.
8. Gently replace lid to original position, but do not push down on the lid until the rubber gasket has come to room temperature.
9. Once rubber gasket is up to room temperature, press lid into place.

A.4.3 MIRacle-attenuated total reflectance - FTIR

1. Put the MIRacle-ATR accessory into the accessory bay on the FTIR with the removable flanges on the instrument in place where the IR beam enters and exits the sample chamber.
2. Plug in the purge line for the accessory into the back of the sample compartment.
3. Purge the FTIR for at least 20 min.

4. While FTIR purges, open Omnic program on the FTIR computer.
5. Go to collect on the upper menu and experimental setup
6. Click “open” in the experiment setup window to open saved experimental files.
7. If there is no saved experimental files for current sample set, go to the “Collect” tab.
8. Input number of scans, resolution, and set format to absorbance on the left side of the window.
9. In the file handling area of the same window on the upper right side, input your initials and check both “save automatically” and “save interferograms”
10. In the background handling section below file handling area, click on either “Collect background before every sample” or “Collect background after every sample.”
11. Go to bench tab in the experimental setup window.
12. Set “Sample Compartment” to Main
13. Set “Detector” to either “DTGS TEC” or “MCT High D*.”
14. Set “Beam Splitter” to “XT-KBr.”
15. Select appropriate source for your samples under “Source.” The standard choice is “IR.” The “IR - Turbo” should be avoided because it can significantly reduce the He-Ne laser’s life span, the “IR – Rest” is for when the instrument is not in use for extended periods of time, and “White light” is for probing low wavelengths.

16. Set “Accessory” to match the accessory in the accessory compartment.
17. Set the range of wavenumbers to be scanned (usually left at default values).
18. Adjust gain (1 to 8) and aperture (32 to 74) to obtain a signal between 5 and 8. If the signal values cannot be reduced to appropriate levels, put in a physical screen (A-D) on the inside of the left side of the sample chamber where the beam exits the sample chamber.
19. Before taking data, always go to the “Diagnostic” tab in the experimental setup window and click on the “Align” button to maximize signal.
20. Save the experimental file.
21. Close the experimental setup window.
22. Take a background with no sample by hitting “Ctrl + B.”
23. If background has a low concentration of water, save the background by going to file menu and save. The background needs to be retaken every 30 min to 1 hr.
24. Open the experimental setup window again.
25. Go to the collect tab, and under “Background Handling” click “Use specific background file:” and load the previously taken background.
26. Click “Save” and then “Ok.”
27. Gently place solid sample (or droplet of solution and allow solvent to evaporate) onto the crystal.
28. Take the sample spectrum by hitting “Ctrl + S”

29. If the sample has noticeable water interference, at the end of taking the spectrum, click “More Scans” and not “Add to Window” when prompted. If the spectrum is satisfactory, click “Add to Window” when prompted.

A.5 Simultaneous thermogravimetric analysis and differential scanning calorimetry (SDT) (adapted from [1])

Analysis was performed on a TA Instruments SDT Q600 using Advantage for Q series (Version 2.8.0.394, Thermal Advantage Release 5.1.2, copyright 2001-2009, TA Instruments-Waters LLC) and analysis was performed on TA Instruments Universal Analysis 2000 software for Windows 2000/XP/Vista (version 4.7A, build 4.7.0.2, copyright 1998-2009, TA Instruments-Waters LLC).

1. Open furnace by going to control panel on SDT, press furnace button, set to open, and hit apply.
2. Take two Pt pans and, carefully, put on cantilever balance. The rear pan is a reference and front pan is for the sample.
3. Close the furnace using the SDT control panel.
4. Open Q600 SDT controller by clicking on the Q600 SDT icon in the TA Instrument Explorer window.
5. Tare the weight of the pans by clicking on the tare button that looks like an old fashion counter weight balance button on the top tool bar.
6. Open the furnace using the SDT control panel.
7. Remove the front Pt pan.

8. Put it on the balance and tare the weight.
9. Weigh out ~5 mg of sample into pan.
10. Put the sample Pt pan back onto cantilever balance.
11. Close the furnace.
12. In the middle section, click on the summary tab.
13. Under Procedure Summary, set mode to SDT Standard and Test to Ramp.
14. In Sample Information, enter a sample name, Pan type to PT, enter any additional comments, set the data file name, and check network drive.
15. Go to the Procedure tab.
16. Under method, check Use Current.
17. Set final temperature to 300 ^{0}C.
18. Next add Ramp at 5 °C/min.
19. Go to Notes tab
20. Set Mass Flow Control Settings to #1-Nitrogen and a flow rate of 50 mL/min.
21. Click run in the upper left hand corner.

A.6 Modulated differential scanning calorimetry (DSC) (adapted from [1])

Analysis was performed on a TA Instruments DSC Q2000 using Advantage for Q series (Version 2.8.0.394, Thermal Advantage Release 5.1.2, copyright 2001-2009, TA Instruments-Waters LLC) and analysis was performed on TA Instruments Universal Analysis 2000 software for Windows 2000/XP/Vista (version 4.7A, build 4.7.0.2, copyright 1998-2009, TA Instruments-Waters LLC).

1. Weigh a T-Zero pan and lid.

2. Weigh out 5 mg of sample.
3. Put sample into T-Zero pan and put lid on pan.
4. Put the Black T-Zero cupped die into the upper part of the press.
5. Put the pan with sample and lid into the Black T-Zero lower die.
6. Put die into press.
7. Press the pan to seal pan.
8. Put pan into auto sampler of DSC
9. Open Q2000 DSC controller by clicking on the Q2000 DSC icon in the TA Instrument Explorer window.
10. In the middle section, click on the summary tab.
11. Under Procedure Summary, set mode to Standard and Test to Custom.
12. In Sample Information, enter a sample name, enter the pan number (position in auto sampler), set Pan type to Tzero Aluminum, check pan mass, enter a sample size and pan mass, enter any additional comments, set the data file name, and check network drive.
13. Go to the Procedure tab.
14. Under method, click on editor.
15. Add equilibrate at -90 °C
16. Next add Data storage On.
17. Next add Ramp at 5 °C/min to 220 °C.
18. Finally add Data storage Off.
19. Go to Notes tab

20. Set Mass Flow Control Settings to #1-Nitrogen and a flow rate of 50 mL/min.
21. To add another sample repeat steps 1-8, then append a new run in the left most window, and repeat steps 12 – 18.
22. Click run in the upper left hand corner.

A.7 X-Ray photoelectron spectroscopy (XPS) (adapted from [1])

This procedure is to be used for PHI 1600 ESCA with Perkin-Elmer dual anode source x-ray source, 04-548, Perkin-Elmer Omni III lens, 72-366S, Perkin-Elmer ion pump, Perkin-Elmer specimen manipulator, 10-325, Perkin-Elmer instrument console, 40-710, Perkin-Elmer dual x-ray source control, 32-096, Perkin-Elmer x-ray supply, 20-040, Perkin-Elmer DGC III digital gauge controller, and Perkin-Elmer spherical capacitor energy analyzer, 10-360, with PHI Surface Analysis Software for windows version 3.0 copyright 1994 Physical electronics Inc.

A.7.1 Sample preparation

1. Sample needs to be put under vacuum for an extended period of time to remove all solvents and volatiles from the sample.
2. If the sample is a polymer film or Si wafer, mount sample on sample puck using copper hold downs.
3. If sample is a powder, compress sample into a small disk and use sample covers to hold sample in place.

4. If sample is too small to use sample covers or hold downs, copper or carbon tape can be use to hold sample in place, but this is not recommended.

A.7.2 Sample loading into XPS main chamber

1. On sample entry chamber, close red and black valves.
2. Open green valve to bring chamber to atmospheric pressure.
3. Remove cover from sample entry chamber.
4. Using puck tongs, place sample puck into sample holder.
5. Replace cover and ensure it is seated properly.
6. Close green valve.
7. Turn on main roughing pump that is connected to the black valve.
8. Open black valve.
9. Using the Varian Multi Gauge on the right side of the XPS, pump the entry chamber to 2 x 10^{-2} Torr.
10. Once 2 x 10^{-2} Torr is reached, close black valve and open red valve.
11. Pump down entry chamber to 1 x 10^{-4} Torr and then wait 1 h.
12. After pumping down entry chamber, open gate valve separating entry chamber and main chamber of the XPS.
13. If main chamber increases above 1 x 10^{-7} Torr (seen on the Perkin-Elmer Digital Gauge Control III), immediately close gate valve and continue to pump down entry chamber. Otherwise proceed with steps below.
14. Slide the sample over sample hold in main chamber.

15. Align main chamber sample holder using X and Y controls on the right side of XPS main chamber.
16. Raise main chamber sample holder using Z control on the right side of the XPS main chamber.
17. Remove sample holding arm from main chamber by sliding it out.
18. Close gate valve.
19. Allow pressure in main chamber to go below 9 x 10^{-9} Torr before attempting to turn on X-ray beam.

A.7.3 Starting X-ray source

If at any time during the following procedure the pressure increases above 5 x 10^{-8} Torr, the XPS will interlock fault, and the procedure has to be restarted from the beginning.

1. Turn on the heat exchanger on the far right side of the XPS.
2. Turn on the power to the X-ray supply (bottom panel on right side of XPS).
3. Turn on the power to the X-ray source control (top panel on right side of XPS).
4. On the X-ray source control, select source 1 and switch to Int.
5. On the X-ray source control, under filament energize, push Mg button.
6. On the X-ray source control, under parameter display/control, push HV button.
7. Press large, red, high voltage button on X-ray source control panel.

8. On the X-ray supply panel, turn the high voltage control until the parameter display/control on the X-ray source control reads 0.5 kV.
9. Continue increasing voltage by 0.5 kV every 1 to 2 min until 8 kV is reached.
10. Once 8 kV is reached, increase voltage by 0.1 kV every 1 to 2 min until 8.5 kV is reached. At 8.3 kV, the instrument has reached a high enough voltage as to cause instant death if an electrical component is touched.
11. At 8.5 kV, increased voltage by 0.5 kV every 1 to 2 min until 12 kV is reached and stop increasing voltage.
12. On the X-ray source control panel, under parameter display/control, push the Mg button to bring display the current power.
13. Using the up and down arrows under the parameter display/control, increase the power by 1 W every 1 to 2 min until 8 W is achieved and the X-ray source is now active.
14. At 8 W, let the instrument rest for 5 min to allow the X-ray source to achieve equilibrium.
15. After 5 min, increase power by 1 W every 1 to 2 min until 12 W is achieved.
16. Once 12 W is achieved, increase power to 25 W and every 1 to 2 min increase by 25 W until 200 W is achieved.
17. Under parameter display/control on the X-ray source control panel, push the HV button.

18. Increase voltage by 0.5 kV until 15 kV is achieved, and the system is now at maximum working voltage.
19. Under parameter display/control on the X-ray source control panel, push the Mg button.
20. Increase power by 25 W every 1 to 2 min until 300 W is achieved.
21. X-ray source is now at working power and voltage, push the card rack power button the power control panel on the left side of the instrument.
22. Turn on Fostec light (white box on XPS desk).
23. Using the built in 10X microscope, using X, Y, and Z control bring the area of interest on the sample into focus.
24. Open PHI CMA XPS software on the computer.
25. Go to file menu and select dir.
26. Select directory and input a 5 character sample name.
27. Click ok.
28. Go to Acquire on the menu bar and select survey.
29. Specify upper binding energy and range (normally upper binding energy is 1100 eV and range is 1100 eV).
30. Set step size to 0.5 eV, time/step to 10 ms, and 10 repeats.
31. Got Execution on menu bar and select start acquisition.
32. Once data acquisition is complete, got to file menu and save file as ASCII.
33. Go to Acquire on the menu bar and select Multiplex.

34. Add regions such as C1, O1, and Si1 in reference to the chemical elements of interest from survey scan for high resolution scan. Adjust regions range as needed.
35. Set step size to 0.2 eV, time/step to 50 ms, and repeats to 15.
36. Got Execution on menu bar and select start acquisition.
37. Once data acquisition is complete, got to file menu and save file as ASCII.
38. Repeat steps 22-37 for additional spots and samples.
39. To turn off instrument, on the X-ray source control panel, switch Int switch to Ext.
40. Under parameter display/control on the X-ray source control panel, push HV button.
41. On the X-ray supply panel, turn the high voltage control left until 0 kV is read off of X-ray source control.
42. X-ray source is now off; push the card rack power button the power control panel on the left side of the instrument.
43. Turn off the X-ray source control, X-ray supply, and heat exchanger.
44. Open the gate valve between the entry chamber and the main chamber and remove the sample.
45. Using a Fat 16 formatted flash drive, transfer files to flash drive to analyze on CasaXPS.

A.7.4 Analysis with CasaXPS

This procedure is to be used with CasaXPS version (2.2.88), copyright 1999-2004 Neal Fairley.

1. Start CasaXPS software.
2. Under file menu, click on "Convert and Merge."
3. Select survey and high resolution scans to be analyzed.
4. For Survey Spectrum
5. Open "Element Library" by pressing F10.
6. Go to "Periodic Table" tab in element library window.
7. Select elements in the spectrum or click find peaks in periodic table tab.
8. Click on create regions in periodic table tab.
9. Open "Quantification Parameters" by pressing F7.
10. Under the "Regions" tab in the quantification parameters window, adjust R.S.F. to values for PHI 1600 XPS found in Moulder, J. F., Stickle, W. F., Sobol, P. E., Bomben, K. D., Handbook of X-Ray Photoelectron Spectroscopy, Perkin-Elmer Corporation, Eden Prairie, MN, 1992, 253.
11. Adjust regions on spectrum to each element.
12. For High Resolution Spectrum
13. For high resolution scans, open "Quantification Parameters" by pressing F7.
14. Click on create in the quantification parameters' "Regions" tab.
15. Under the regions tab in the quantification parameters window, adjust R.S.F. to values for PHI 1600 XPS found in Moulder, J. F., Stickle, W. F.,

Sobol, P. E., Bomben, K. D., Handbook of X-Ray Photoelectron Spectroscopy, Perkin-Elmer Corporation, Eden Prairie, MN, 1992, 253.

16. Adjust region on spectrum for to include the peaks for the element.
17. Click on the "Components" tab in the quantification parameters window.
18. Click on create to "Create" peaks under spectrum peak.
19. Unclick "Use RMS" under components tab.
20. Click on "Fit Components" button until Chi^2 does not change.
21. If the peaks full width, half max (FWHM) differ by more than 10%, constrain them by editing the fwhm Constr. cells and adjust the fwhm cells, normally to 1.5-1.8 or 1.6-2.0, to values that fall within the FWHM constraints.
22. If peaks are within 0.8 eV, either reduce the number of peaks present or constrain the peaks position by editing Pos. Constr. cells and adjust peak positions to fall within constraints.
23. Repeat fitting components, step 18, if steps 19 and/or 20 were followed.
24. Open "Processing" by pressing F8.
25. Go to "Smoothing" tab in spectrum processing window.
26. Click on apply 3 times (or more if necessary, peaks may be loss if repeated too many times).
27. Go to quantification parameters' "Components" tab and repeat step 18.
28. Peaks may need to be added or subtracted at this point based on fitting and literature values.

29. Repeat steps 19 through 25 until a reasonable fit is achieved based on literature and Chi^2.
30. Once an acceptable peak fitting is achieved, the spectrum may need to shifted to allow C 1s C-C/C-H peak to fall at 285 eV.
31. Shift the peaks by going to spectrum processing window's "Calibration" tab.
32. Put in measured value of reference peak and correct position of peak.
33. Under adjust in the same tab, check both "Regions" and "Components."
34. Click apply.
35. Record peak positions, FWHM, and area.

A.8 Freeze-pump-thaw

1. Fill liquid nitrogen dewar connected to manifold for vacuum.
2. Place a big beaker containing water onto heater for thaw
3. Fill liquid nitrogen dewar completely for freeze.
4. Be careful that the flask is not full more than half of the volume.
5. Immerse the flask into the LN2 dewar to freeze. Allow it to freeze completely.
6. Take it out and open the stopcock to pump it out.
7. Close the stopcock, and immerse the flask into water bath to thaw.
8. Check for the gas bubbles coming out.

Repeat steps (5) – (7) as needed. A minimum of three cycles.

A.9 References

1. Rowe, M. D. Development of renewable and hydrolytically degradable polymers from biomass-based monomers. Ph.D., Mississippi State University, Ann Arbor, 2010.

APPENDIX B

PLA/PTM BLENDS THERMAL ANALYSIS

B.1 Differential scanning calorimetry (DSC)

A TA Instruments Q-2000 modulated DSC (mDSC) was used for thermal analysis of PLA and PLA/PTM blend films with the TA Universal Analysis 2000 software (v4.7A). The blend film samples weighing 5 mg were first heated from 40 to 200 °C at a rate of 10 °C/min, and then held for 5 min to eliminate the thermal history. Subsequently, they were cooled to - 50 °C, and heated again from – 90 °C to 200 °C at a rate of 10 °C/min under 50 mL/min of nitrogen purge.

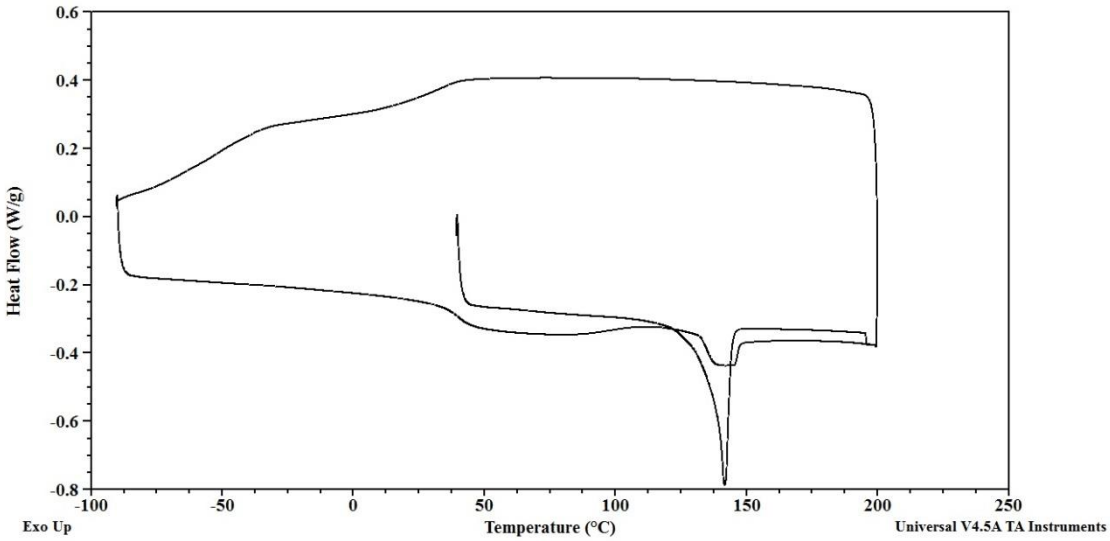

Figure B.1 DSC thermograms (heating-cooling-heating) of neat PLA.

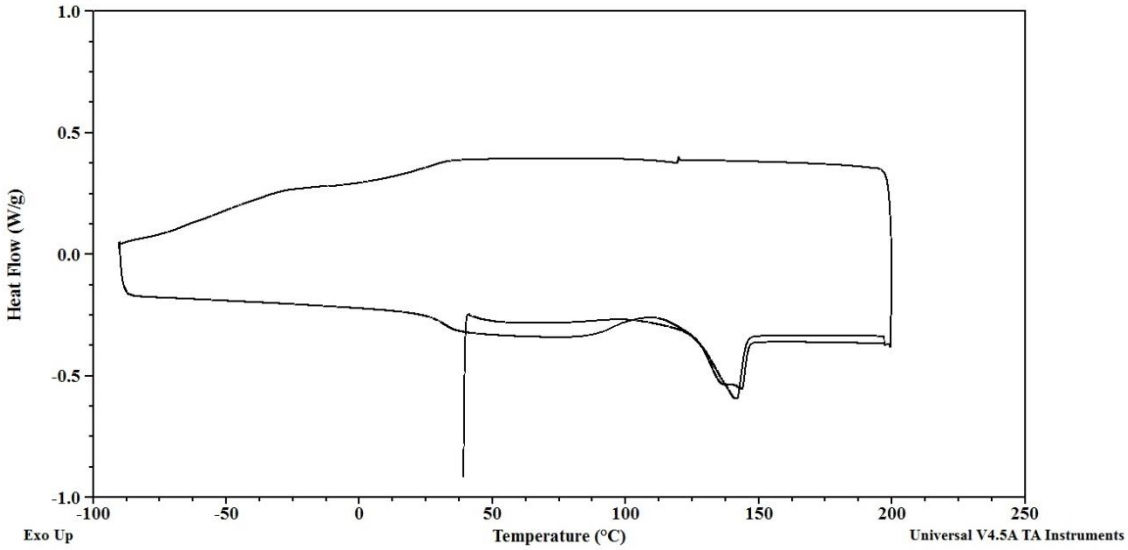

Figure B.2 DSC thermograms (heating-cooling-heating) of PLA95.

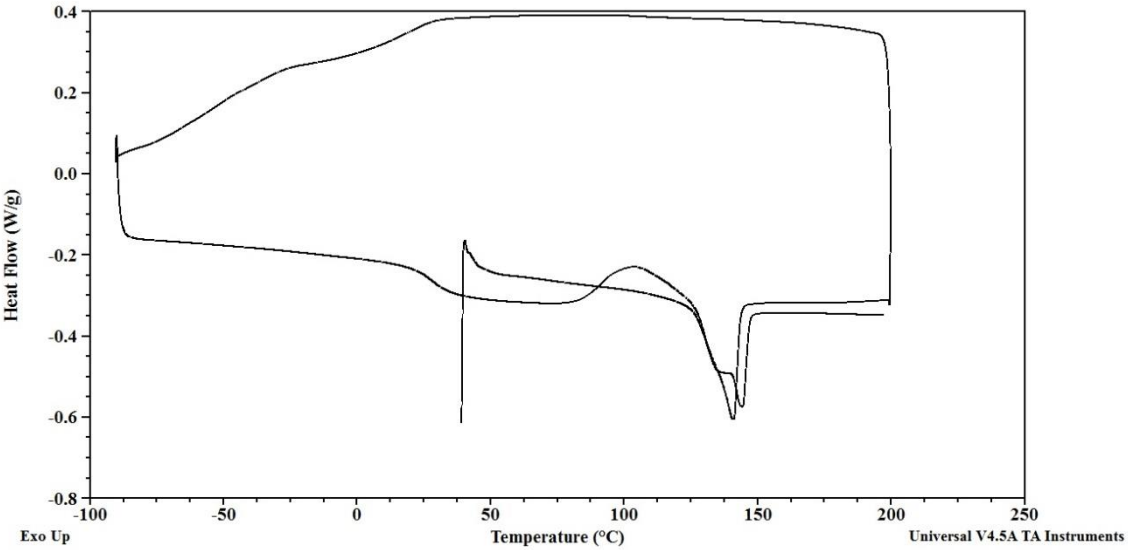

Figure B.3 DSC thermograms (heating-cooling-heating) of PLA90.

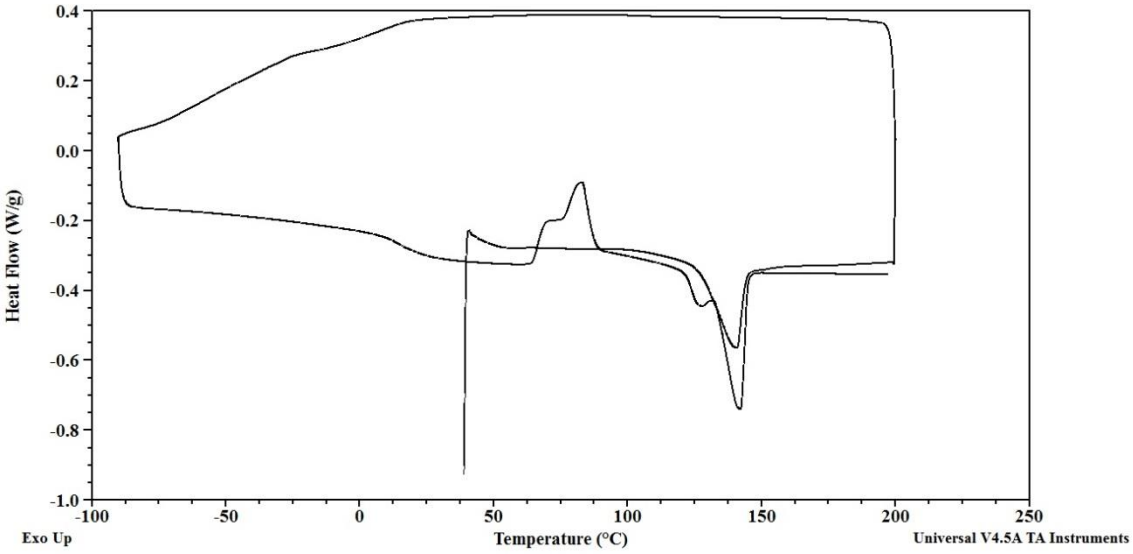

Figure B.4 DSC thermograms (heating-cooling-heating) of PLA80.

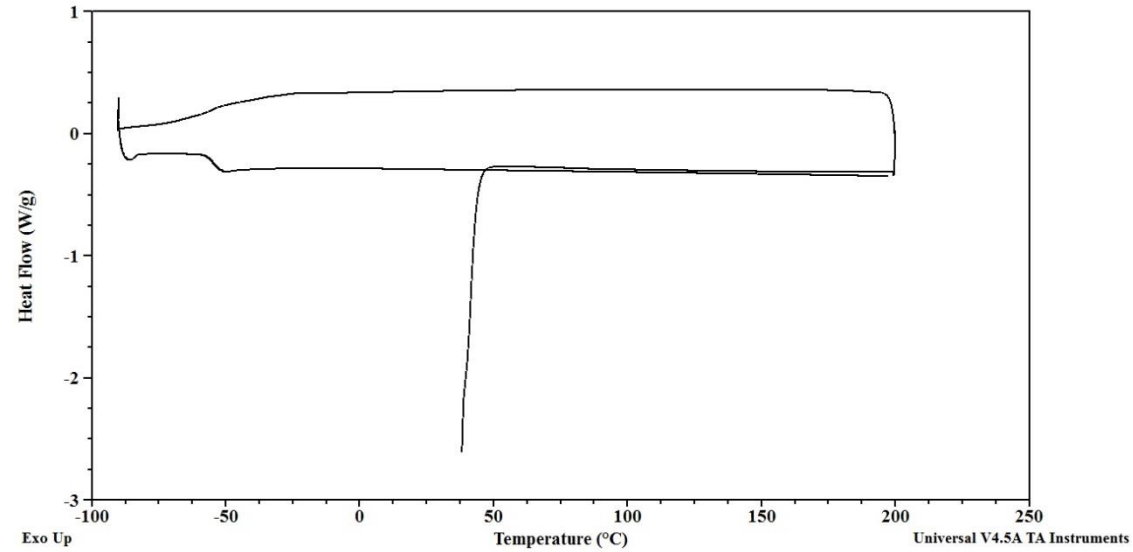

Figure B.5 DSC thermograms (heating-cooling-heating) of neat PTM.

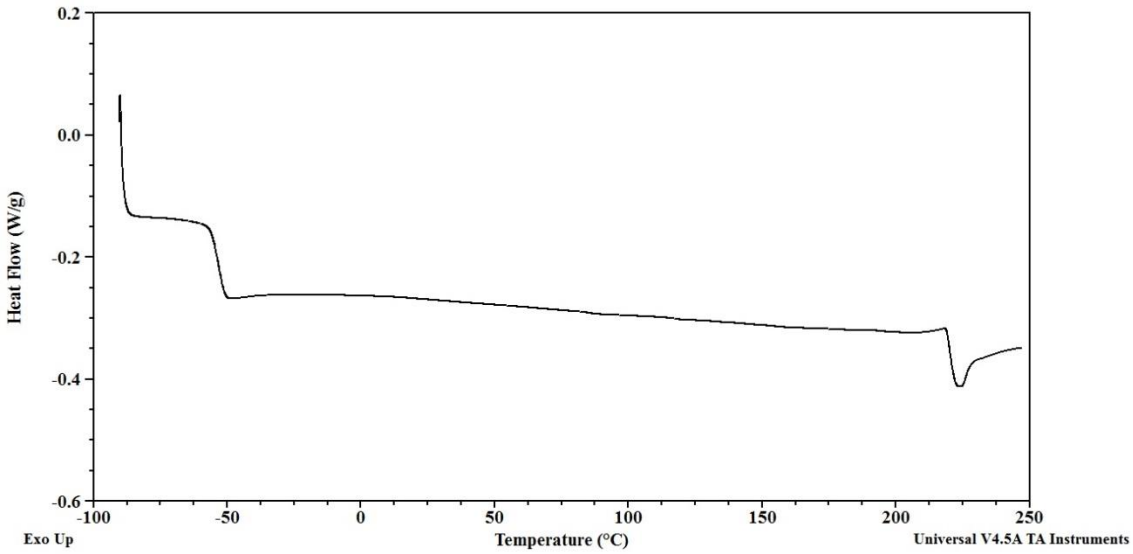

Figure B.6 DSC thermogram of 'as cast' neat PTM.

B.2 Thermogravimetric analysis (TGA)

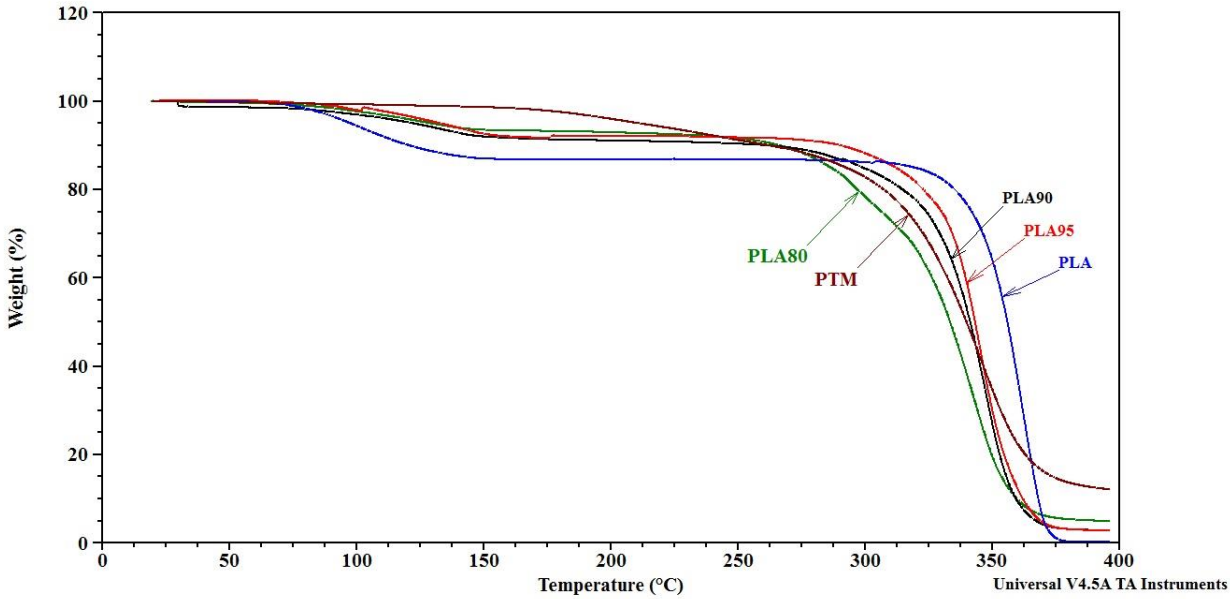

Figure B.7 TGA traces of PLA, PTM and PLA/PTM blend films.

APPENDIX C

PLA/PTM BLENDS DSC HEATING RATE STUDY

C.1 Differential scanning calorimetry (DSC)

A TA Instruments Q-2000 modulated DSC (mDSC) was used for thermal analysis of PLA and PLA/PTM blend films with the TA Universal Analysis 2000 software (v4.7A). The blend film samples weighing 5 mg were first heated from 40 to 200 °C at a rate of 10 °C/min, and then held for 5 min to eliminate the thermal history. Subsequently, they were cooled rapidly to 25 °C at a rate of 20 °C/min, and heated again from 25 °C to 200 °C at a rate of 3, 5, and 10 °C/min under 50 mL/min of nitrogen purge.

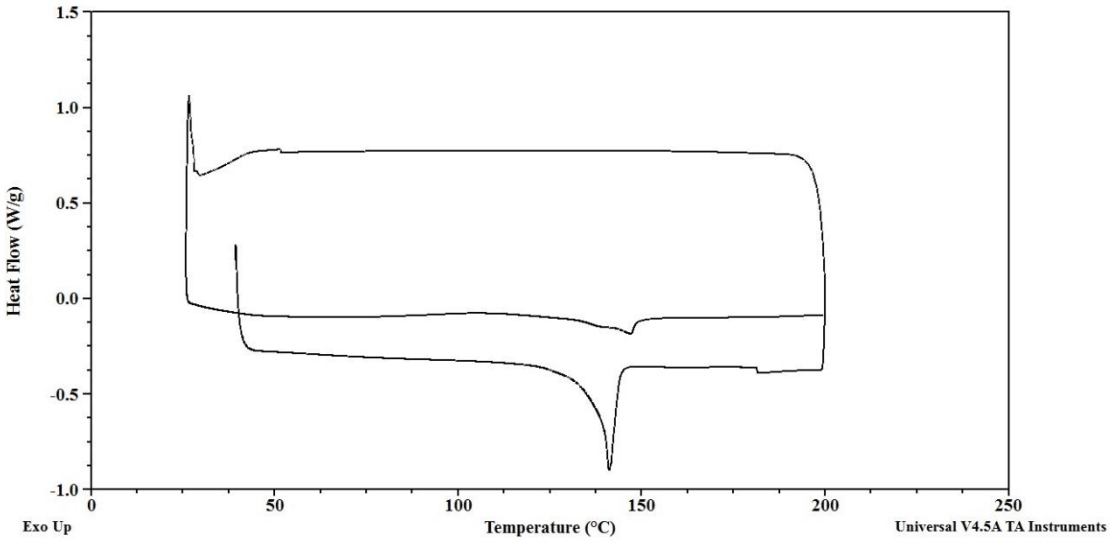

Figure C.1 DSC thermograms (heating-cooling-heating) of neat PLA with 3 °C/min second heating rate.

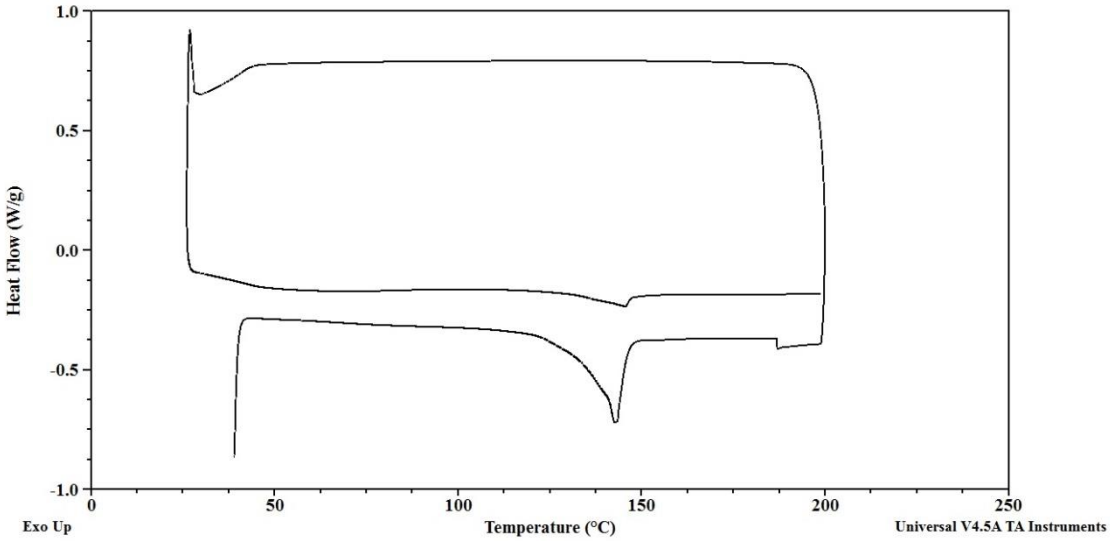

Figure C.2 DSC thermograms (heating-cooling-heating) of neat PLA with 5 °C/min second heating rate.

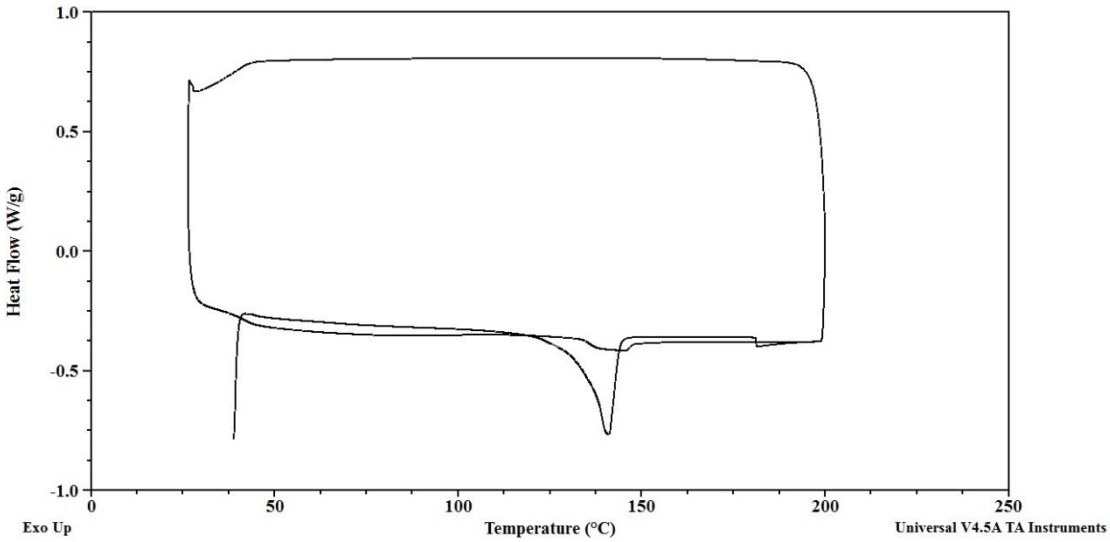

Figure C.3 DSC thermograms (heating-cooling-heating) of neat PLA with 10 °C/min second heating rate.

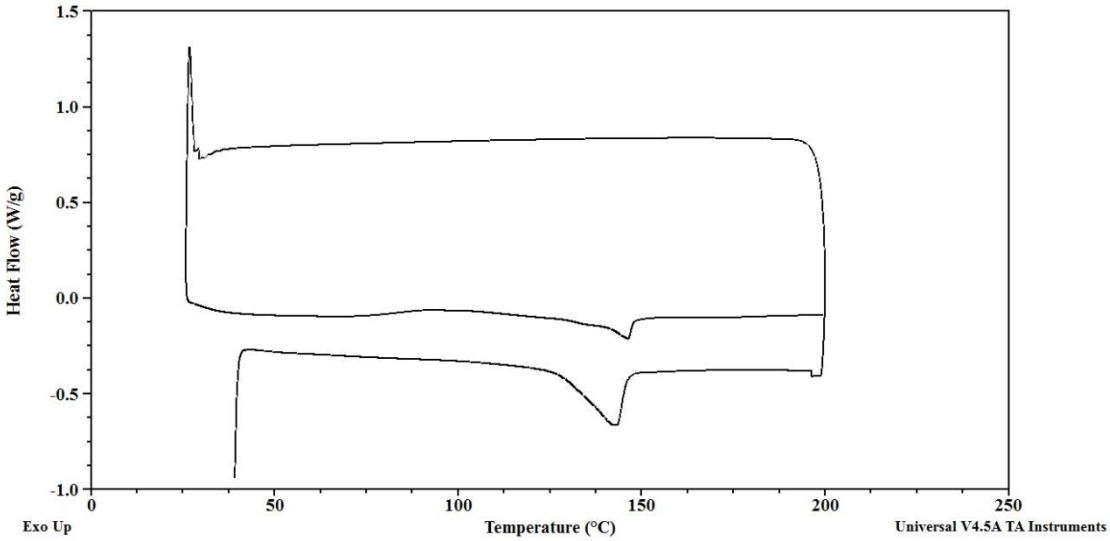

Figure C.4 DSC thermograms (heating-cooling-heating) of PLA95 with 3 °C/min second heating rate.

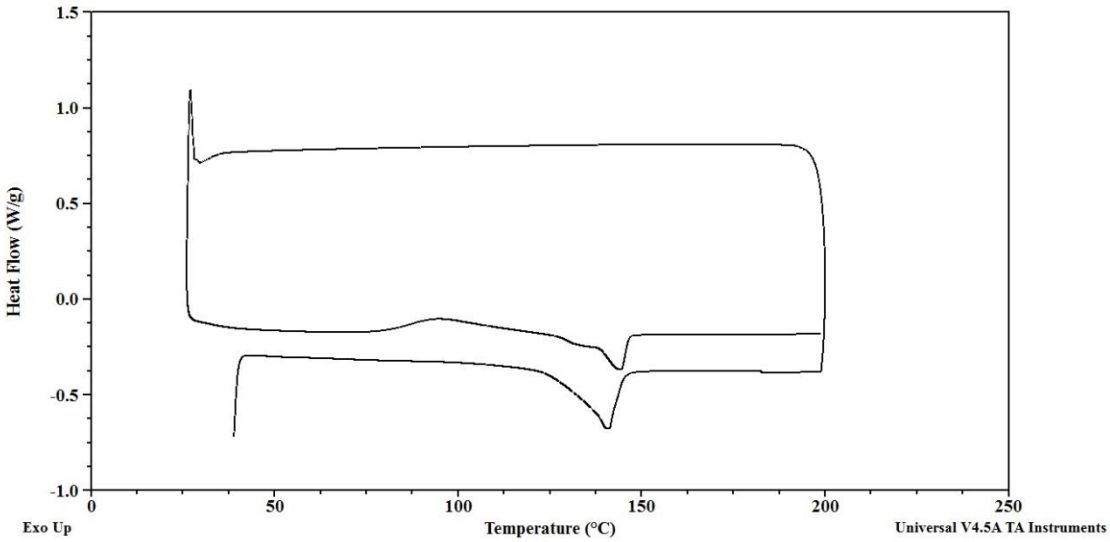

Figure C.5 DSC thermograms (heating-cooling-heating) of PLA95 with 5 °C/min second heating rate.

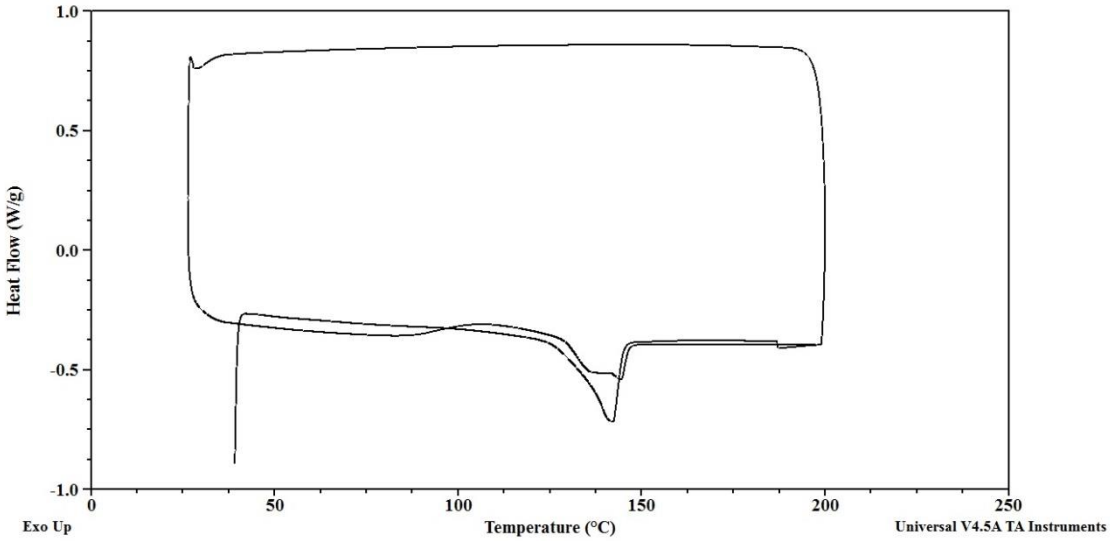

Figure C.6 DSC thermograms (heating-cooling-heating) of PLA95 with 10 °C/min second heating rate.

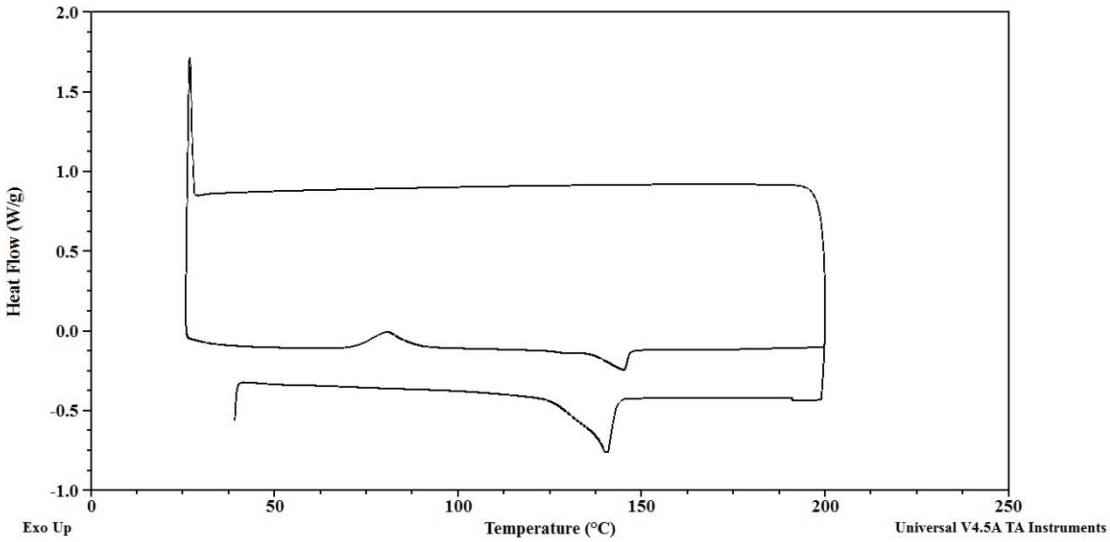

Figure C.7 DSC thermograms (heating-cooling-heating) of PLA90 with 3 °C/min second heating rate.

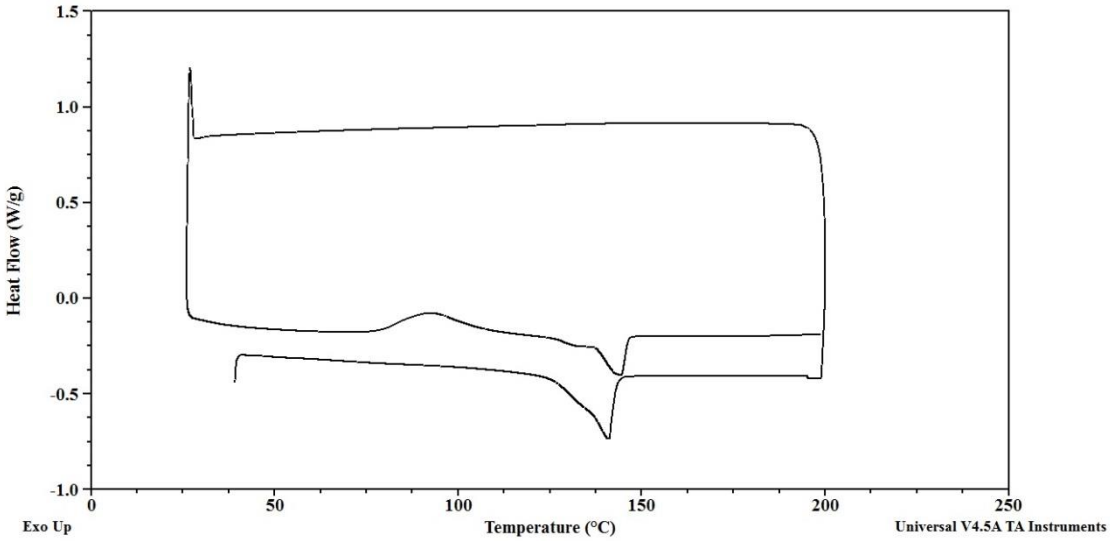

Figure C.8 DSC thermograms (heating-cooling-heating) of PLA90 with 5 °C/min second heating rate.

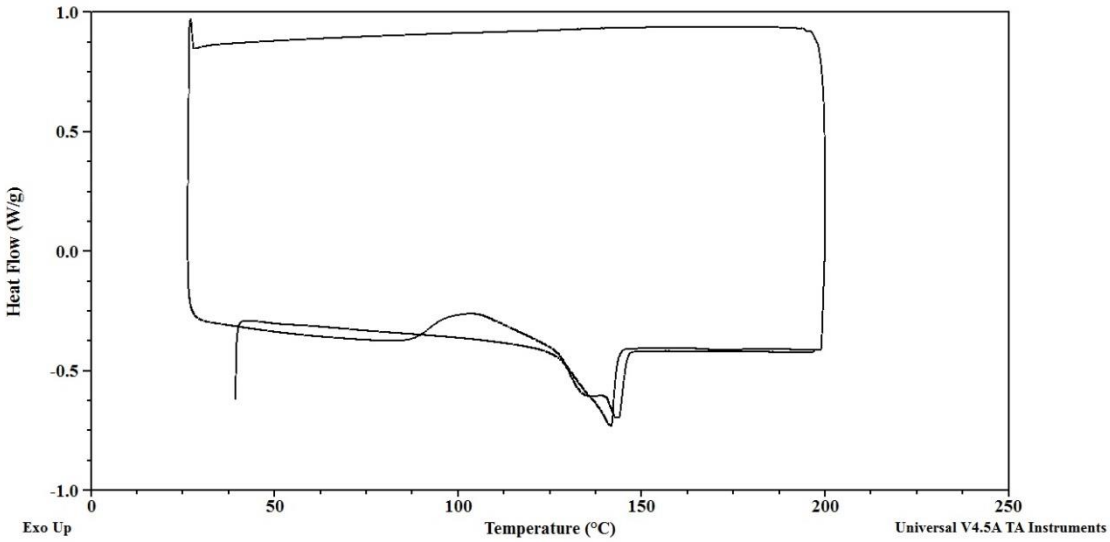

Figure C.9 DSC thermograms (heating-cooling-heating) of PLA90 with 10 °C/min second heating rate.

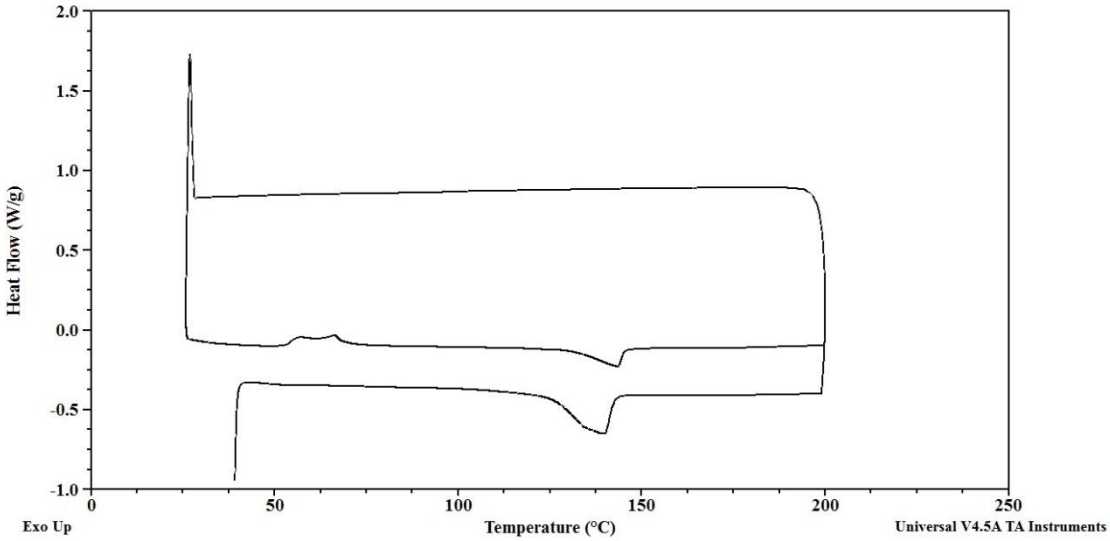

Figure C.10 DSC thermograms (heating-cooling-heating) of PLA80 with 3 °C/min second heating rate.

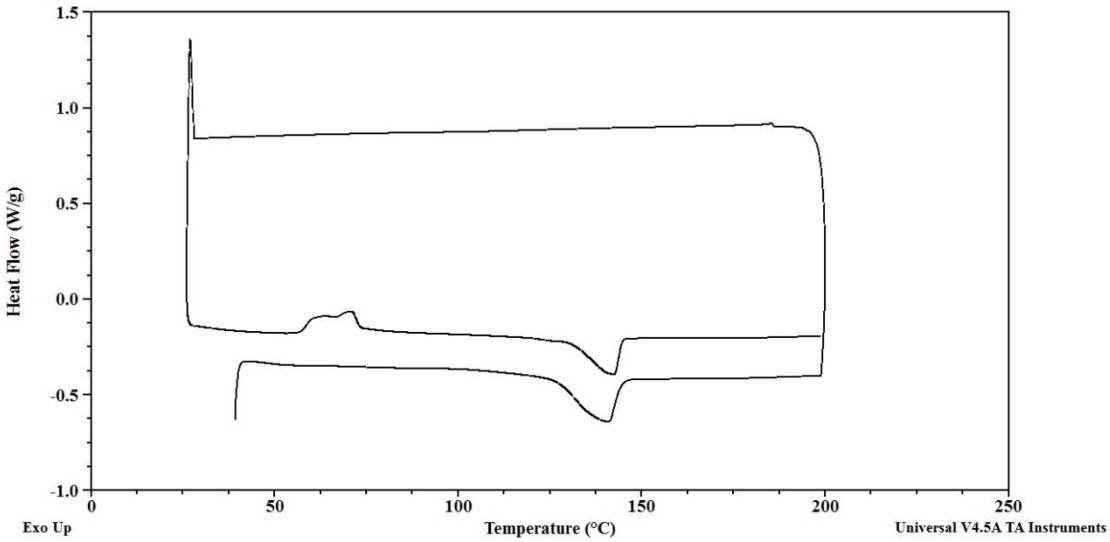

Figure C.11 DSC thermograms (heating-cooling-heating) of PLA80 with 5 °C/min second heating rate.

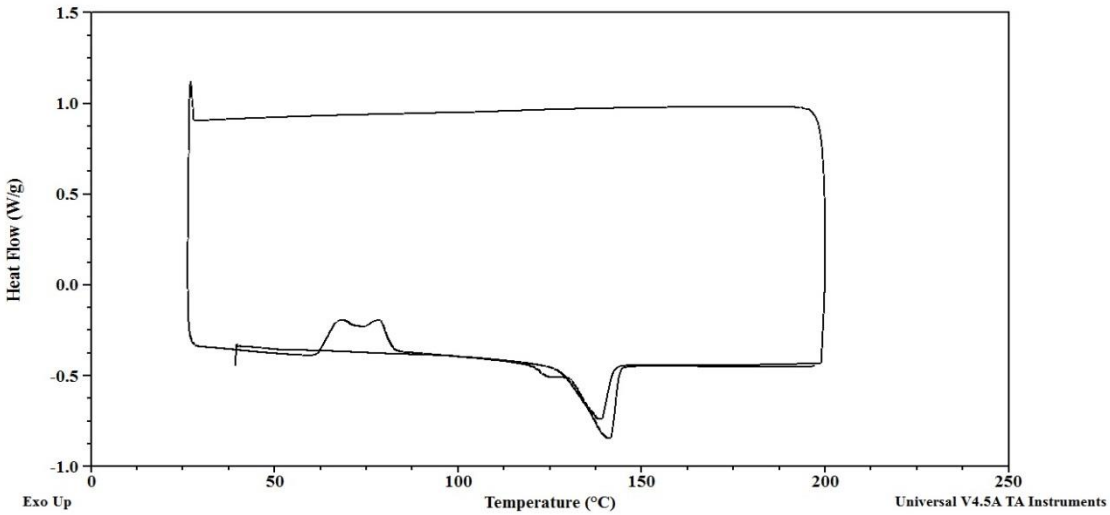

Figure C.12 DSC thermograms (heating-cooling-heating) of PLA80 with 10 °C/min second heating rate.

Table C.1 Thermal analysis data of PLA, PTM and PLA/PTM blend films with 3 °C/min second heating rate**.**

PLA Weight Fraction	Tg (◦C)	Tm1 (◦C)	Tm2 (◦C)	Tcc1 (◦C)	Tcc2 (◦C)	ΔHcc (J/g)	ΔHm (J/g)	Xm (%)	ΔHmf (J/g)	Xmf (%)
1.00	31	138	147	106	-	15	14	-	20	21.6
0.95	30	129	146	94	-	23	17	-	18	19.9
0.90	-	129	145	81	-	21	18	-	18	21.3
0.80	-	143	-	56	66	15	17	2.7	16	21.3

Table C.2 Thermal analysis data of PLA, PTM and PLA/PTM blend films with 5 °C/min second heating rate**.**

PLA Weight Fraction	Tg (◦C)	Tm1 (◦C)	Tm2 (◦C)	Tcc1 (◦C)	Tcc2 (◦C)	ΔHcc (J/g)	ΔHm (J/g)	Xm (%)	ΔHmf (J/g)	Xmf (%)
1.00	42	145	-	107	-	4.3	5.1	0.9	19.3	20.7
0.95	32	132	144	95	-	23.3	18.2	-	18.4	20.8
0.90	33	132	144	93	-	25.0	20.1	-	17.0	20.3
0.80	-	125	142	61	70.82	13.6	20.9	9.8	15.1	20.2

Table C.3 Thermal analysis data of PLA, PTM and PLA/PTM blend films with 10 °C/min second heating rate.

PLA Weight Fraction	Tg (◦C)	Tm1 (◦C)	Tm2 (◦C)	Tcc1 (◦C)	Tcc2 (◦C)	ΔHcc (J/g)	ΔHm (J/g)	Xm (%)	ΔHmf (J/g)	Xmf (%)
1.00	41	142	-	112	-	1.6	2.4	0.8	20.4	22.0
0.95	39	135	144	107	-	7.1	11.1	4.5	19.5	22.1
0.90	37	133	144	104	-	18.3	18.8	0.6	17.9	21.4
0.80	-	124	141	68	79	17.4	24.4	9.4	15.0	20.2

APPENDIX D

PTI DEGRADATION THERMAL ANALYSIS

D.1 Thermogravimetric analysis (TGA)

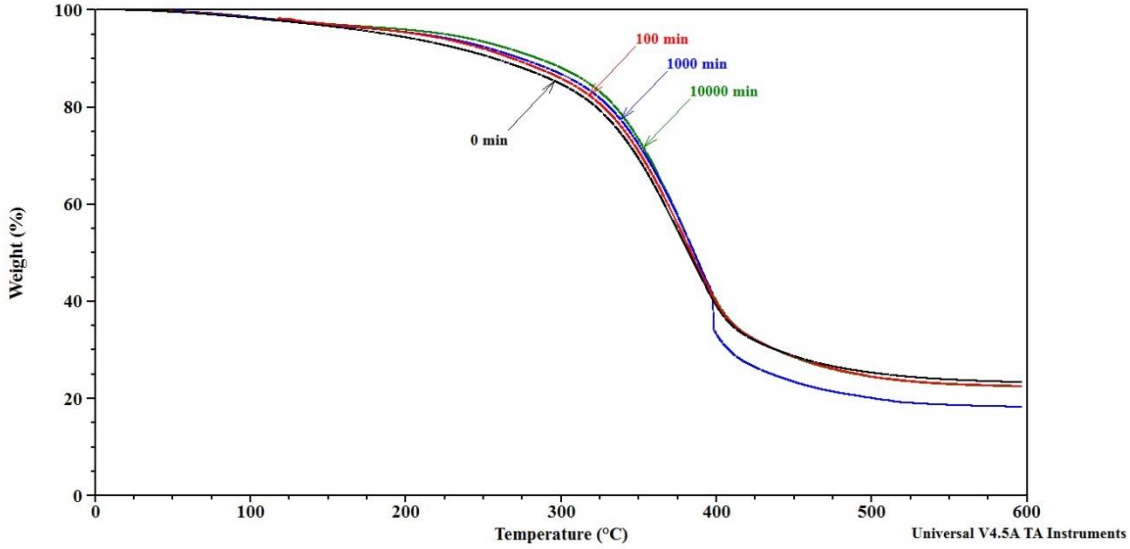

Figure D.1 TGA traces of PTI after 0, 100, 1000, and 10,000 min of degradation.